

https://dspace.org/

Assessing changes in internal bone architecture of the immature human pars basilaris and pars lateralis during the prenatal and postnatal stages of growth

Mendelow, Mira Grace

2025

University of the Witwatersrand, Johannesburg

https://hdl.handle.net/10539/48237

Mendelow, Mira Grace . (2025). Assessing changes in internal bone architecture of the immature human pars basilaris and pars lateralis during the prenatal and postnatal stages of growth [Master`s dissertation, University of the Witwatersrand, Johannesburg]. WIReDSpace. https://hdl.handle.net/10539/48237

Downloaded from a DSpace repository. https://dspace.org/

Assessing changes in internal bone architecture of the immature human pars basilaris and pars lateralis during the prenatal and postnatal stages of growth



UNIVERSITY OF THE
WITWATERSRAND,
JOHANNESBURG

Mira Grace Mendelow

A dissertation submitted to the Faculty of Health Sciences, University of the Witwatersrand, Johannesburg, in fulfilment of the requirements for the degree of Master of Science in Medicine in the field of anatomical sciences.

Johannesburg, 2025

Supervised by:

Professor Erin Hutchinson, MSc, PhD (Wits),

Dr Roxanne Thornton, MSc, PhD (Rhodes).

Declaration

I, Mira Mendelow declare that this dissertation is my own, unaided work. It is being submitted for the Degree of Master of Science in Medicine at the University of the Witwatersrand, Johannesburg. It has not been submitted before for any degree or examination at any other University.



9th day of June 2025 in Johannesburg

In loving memory of my grandmother

Judie Mendelow

1925-2024

Abstract

The internal architectural arrangement of bone serves as a reflection of bone adapting to the surrounding biomechanical environment, as well as the functional demands imposed on the bone. The pars basilaris and pars lateralis contribute significantly to the borders of the foramen magnum within the posterior cranial base, and as such, understanding the impact of the growth of the surrounding brain, neurovasculature, and muscles on these bones is important. Thus, the aim of the study was to investigate the internal structure of 84 pars basilari and 96 pars laterali during the prenatal and postnatal stages of growth. Skeletal elements were sourced from early prenatal (20-30 gestational weeks, n=34), late prenatal (30-40 gestational weeks, n=42) and postnatal (birth-7.5 months, n=30) individuals housed by the Johannesburg Forensic Paediatric Collection. Micro-computed tomography was used to assess bone volume fraction (BV/TV), bone surface area fraction (BS/BV), trabecular thickness (TbTh), trabecular number (TbN), trabecular separation (TbSp), degree of anisotropy (DA) and mean grey value (MGV) in 14 regions across both skeletal elements using multivariate analysis of variance within and between the age groups. Findings revealed that the late prenatal group generally had a higher BV/TV and TbTh but lower TbN compared to the early prenatal group, indicating that modelling is the primary mechanism of development. Limited differences between the late prenatal and postnatal groups indicate that the trabecular architecture of the posterior cranial fossa achieves stability postnatally. Variations between the regions within the age groups show that internal architecture is not uniform throughout the bones, reflecting functional regions within the bones.

Acknowledgments

I am immensely grateful to my supervisors, Professor Erin Hutchinson and Dr. Roxanne Thornton. Their unwavering guidance, support, and patience at every stage of this research have been invaluable. Thank you for your insightful feedback and for challenging me to think critically throughout this master's process.

I would like to extend my sincerest thanks to the team at NECSA, particularly Kobus Hoffman, Lunga Bam, and all those who took the time to teach me how to use the Micro-CT scanners and software. The insight into the technical aspects of this project has been a cornerstone of my research. My appreciation goes out to the School of Anatomical Sciences, University of Witwatersrand, Johannesburg. I would also like to thank Anteneh Yalew for his guidance in the statistical analysis of my data.

A special thanks to my fellow master's student, Gizelle Govender, for her camaraderie and help throughout this process. I also want to share my appreciation for my siblings, Ella and Max, and my boyfriend, Sean, for their humour, constant encouragement, and occasional proofreading. In addition, thank you to my parents for their unwavering support. I cannot thank you enough for being my foundation.

I would also like to acknowledge the prenatal and postnatal individuals whose skeletal remains formed the basis of this study. Their contribution is deeply valued and appreciated.

Table of contents

Declaration i

Abstract iii

Acknowledgments iv

Table of contents v

List of tables viii

List of figures x

List of abbreviations xi

Chapter 1: Literature review 1

1.1. Introduction 1

1.2. Anatomy of the pars basilaris and pars lateralis 4

1.2.1. Embryology 4

1.2.2. Anatomy of the pars basilaris 6

1.2.3. Anatomy of the pars lateralis 8

1.3. Trends in the ontogeny of trabecular bone 10

1.3.1. Modelling and remodelling 13

1.3.2. Predetermined trabecular template for early development 15

1.3.3. Role of mechanical loading in postcranial skeletal development 19

1.4. Biomechanical environment and development of the cranial base 21

1.5. Bone mineral density and mineralisation 26

1.6. Aim 28

1.7. Objectives 28

Chapter 2: Materials and methods 30

2.1. Sample 30

2.2. Methodology 32

2.3. Statistical analysis 41

Chapter 3: Results 43

3.1. Bone volume fraction, bone surface area fraction 44

3.1.1. Pars basilaris 44

3.1.2. Pars lateralis 62

3.2. Trabecular thickness, trabecular number, trabecular separation 72

3.2.1. Pars basilaris 72

3.2.2. Pars lateralis 80

3.3. Degree of anisotropy 91

3.3.1. Pars basilaris 91

3.3.2. Pars lateralis 96

3.4. Mean grey value 101

3.4.1. Pars basilaris 101

3.4.2. Pars lateralis 106

Chapter 4: Discussion and conclusions 112

4.1. Prenatal development....113

4.1.1. Trabecular organisation....118

4.1.2. Mineralisation and density....121

4.2. Postnatal development....122

4.3. Limitations....128

4.4. Conclusions....129

Chapter 5: References....131

Appendix A: Ethics certificate....147

Appendix B: Observer error....149

Appendix C: AI Statement....151

Appendix D: Turnitin report....152

List of tables

Table 1: Number of pars basilari and pars laterali per age group.....31

Table 2: Regions of interest selected on the pars basilaris and pars lateralis.....37

Table 3: Definitions and descriptions of trabecular bone morphometric indices 39

Table 4: Median values and pairwise comparisons of bone volume fraction and bone surface area fraction between the early prenatal, late prenatal and postnatal pars basilaris for each region of interest.....45

Table 5: Pairwise comparisons of bone volume fraction and bone surface area fraction between regions of interest within the early prenatal, late prenatal and postnatal pars basilaris 54

Table 6: Median values and pairwise comparisons of bone volume fraction and bone surface area fraction between the early prenatal, late prenatal and postnatal pars lateralis for each region of interest.....64

Table 7: Pairwise comparisons of bone volume fraction and bone surface area fraction between regions of interest within the early prenatal, late prenatal and postnatal pars lateralis 68

Table 8: Median values and pairwise comparisons of trabecular thickness, trabecular number and trabecular separation between the early prenatal, late prenatal and postnatal pars basilaris for each region of interest 73

Table 9: Pairwise comparisons of trabecular thickness, trabecular number and trabecular separation between regions of interest within the early prenatal, late prenatal and postnatal pars basilaris 78

Table 10: Median values and pairwise comparisons of trabecular thickness, trabecular number and trabecular separation between the early prenatal, late prenatal and postnatal pars lateralis for each region of interest 81

Table 11: Pairwise comparisons of trabecular thickness, trabecular number and trabecular separation between regions of interest within the early prenatal, late prenatal and postnatal pars lateralis 85

Table 12: Median values and pairwise comparisons of degree of anisotropy between the early prenatal, late prenatal and postnatal pars basilaris for each region of interest 92

Table 13: Pairwise comparisons of degree of anisotropy between regions of interest within the early prenatal, late prenatal and postnatal pars basilaris 95

Table 14: Median values and pairwise comparisons of degree of anisotropy between the early prenatal, late prenatal and postnatal pars lateralis for each region of interest 97

Table 15: Pairwise comparisons of degree of anisotropy between regions of interest within the early prenatal, late prenatal and postnatal pars lateralis 99

Table 16: Median values and pairwise comparisons of mean grey value between the early prenatal, late prenatal and postnatal pars basilaris for each region of interest 102

Table 17: Pairwise comparisons of mean grey value between regions of interest within the early prenatal, late prenatal and postnatal pars basilaris 104

Table 18: Median values and pairwise comparisons of mean grey value between the early prenatal, late prenatal and postnatal pars lateralis for each region of interest 107

Table 19: Pairwise comparisons of mean grey value between regions of interest within the early prenatal, late prenatal and postnatal pars lateralis 109

List of figures

Figure 1: Reference planes for the pars basilaris. 35

Figure 2: Reference planes for the pars lateralis. 36

Figure 3: Regions of Interest for the pars basilaris and pars lateralis 38

Figure 4: Regional variations of bone volume fraction and bone surface area fractions in the pars basilaris 46

Figure 5: Regional variations of bone volume fraction and bone surface area fractions in the pars lateralis 65

Figure 6: Regional variations of trabecular thickness, trabecular number and trabecular separation in the pars basilaris 74

Figure 7: Regional variations of trabecular thickness, trabecular number and trabecular separation in the pars lateralis.....82

Figure 8: Regional variations of the degree of anisotropy in the pars basilaris 93

Figure 9: Regional variations of the degree of anisotropy in the pars lateralis 98

Figure 10: Regional variations of the mean grey value in the pars basilaris.....103

Figure 11: Regional variations of the mean grey value in the pars lateralis. 108

List of abbreviations

BMD	Bone mineral density
BS/BV	Bone surface area fraction
BV/TV	Bone volume fraction
DA	Degree of anisotropy
IQR	Interquartile range
JFPC	Johannesburg Forensic Paediatric Collection
JFPS	Johannesburg Forensic Pathology Services
MANOVA	Multivariate analysis of variance
MGV	Mean grey value
Micro-CT	Micro-computed tomography
MRI	Magnetic resonance imaging
NECSA	South African Nuclear Energy Corporation
ROI	Region of interest
TbN	Trabecular number
TbSp	Trabecular separation
TbTh	Trabecular thickness

Chapter 1: Literature review

1.1. Introduction

The basicranium is considered the “keystone of the skull”, as it connects the facial skeleton, calvaria, inner ear and vertebral column, thus facilitating in integrated craniofacial growth (Lieberman et al., 2000; Jeffery, 2003; Nie, 2005; Weiss-Bilka et al., 2018). In addition, the basicranium houses the brain while providing adequate space for its expansion (Jeffery, 2003). The basicranium also serves as the transitional platform that transmits important neurovascular structures between the head and neck regions through foramina (Akbareian et al., 2015). Chief among these foramina is the foramen magnum, enclosed by the occipital bone (Akbareian et al., 2015; Cunningham et al., 2016). The immature occipital bone consists of four skeletal elements (the pars squama, the pars basilaris and two paired pars laterali) arranged around the foramen magnum (Cunningham et al., 2016). The pars squama forms the posterior portion of the occipital bone (Cunningham et al., 2016). The pars basilaris is the symmetrical, centrally located bone that forms the anterior border of the foramen magnum (Cunningham et al., 2016). The paired pars laterali form the lateral borders of the foramen magnum (Cunningham et al., 2016). The pars lateralis consists of a quadrilateral plate and a jugular and condylar limb that extend anteromedially from the posterolateral aspect of the foramen magnum border to form the hypoglossal canal (Cunningham et al., 2016). Within the occipital bone, the pars basilaris and pars lateralis undergo significant changes during prenatal and postnatal development (Thornton et al., 2023; 2024). Therefore, understanding the anatomy and development of the pars basilaris and pars lateralis is central to understanding the development of the basicranium as a whole.

The pars basilaris and pars lateralis have warranted significant attention across forensic and medical fields due to their unique characteristics and applications (Zdilla et al., 2022). Both bones undergo predictable changes in size and shape with age, thus providing reliable indicators of age in the immature skeleton (Scheuer & MacLaughlin-Black, 1994; Thornton et al., 2020). The pars basilaris is a robust bone and is resilient to taphonomic factors like decay and fragmentation (Scheuer & MacLaughlin-Black, 1994; Thornton et al., 2020). However, the pars lateralis is less frequently used to establish a biological profile, as it tends to get damaged at its border with the temporal part of the mastoid bone (Figueiro et al., 2022). Understanding the ontogeny of the internal architecture of these bones can serve as an indicator of age in juvenile remains in cases where the external shape of the bones is less informative due to damage or degradation.

Clinically, the pars basilaris and pars lateralis are important for understanding and treating conditions affecting the skull base and craniovertebral junction (Rai et al., 2018; Swan & Dunn, 2019). Disruptions in the normal anatomy of these structures due to congenital anomalies, trauma, or degenerative changes can lead to instability of the craniovertebral junction, which can lead to compression of the brainstem and spinal cord (Menezes, 1997; Swan & Dunn, 2019). Thus, understanding the biomechanics of this region, influenced by the internal architecture of the skeletal elements, is valuable for diagnosing instability and determining the appropriate treatment (Swan & Dunn, 2019). In addition, the pars basilaris may exhibit developmental bony discontinuities throughout the internal aspects of the bone, namely the clival canal and clival foramen (Zdilla, 2017; Malakhov et al., 2024). These channels connect the pharynx to the intracranial cavity, which creates a pathway for infections to ascend from

the pharynx to the brain and spinal cord (Zdilla, 2017; Emecen et al., 2019; Flynn et al., 2021; Singh et al., 2022). This is particularly relevant in paediatric populations and can lead to recurrent meningitis (Emecen et al., 2019; Flynn et al., 2021; Singh et al., 2022). Thus, understanding the normal internal structure of the bones can aid clinicians in identifying abnormalities or variations that may predispose individuals to infection.

Owing to the significance of the pars basilaris and pars lateralis across various fields, the study of the ontogeny of these bones during the prenatal and postnatal period has employed a wide range of techniques. These methods have included metric techniques that measure the dimensions of the bones (Redfield, 1970; Fazekas & Kosa, 1978; Scheuer & MacLaughlin-Black, 1994; Tocheri & Molto, 2002; Nagaoka et al., 2012; Olivares & Aguilera, 2017; Thornton et al., 2020; Smith et al., 2021; Figueiro et al., 2022; Zdilla et al., 2022). Some studies have expanded on this to include indices and regression equations for age estimation (Nagaoka et al., 2012; Olivares & Aguilera, 2017; Figueiro et al., 2022; Smith et al., 2021). Geometric morphometrics has been used for three-dimensional analysis of shape changes (Niel et al., 2019; Zdilla et al., 2022; Thornton et al., 2023; 2024). In addition, bone mineral density (BMD) studies have assessed the distribution of BMD on the surface of the bones (Thornton et al., 2023; 2024). Preliminary attempts of assessing bone configuration have involved observations of the morphological features on the surface of the bones such as the presence of striations, porosity, canals, ridges, tubercles, and facets (Zdilla, 2017; Thornton et al., 2023; Eggington et al., 2024). While the external anatomy of the pars basilaris and pars lateralis has contributed to understanding the structure of bone, there is a paucity of information that describes the internal anatomy of these bones.

1.2. Anatomy of the pars basilaris and pars lateralis

1.2.1. Embryology

The embryological origin of the pars basilaris and pars lateralis is the paraxial mesoderm (Pang & Thompson, 2011; Bernard et al., 2015). The mesoderm gives rise to somites, which are the segmented blocks of tissue that form along the neural tube (Pang & Thompson, 2011; Bernard et al., 2015). The first four somites are the occipital somites (Pang & Thompson, 2011; Bernard et al., 2015). Each somite differentiates into a dermatome, a myotome, and a sclerotome (Pang & Thompson, 2011; Bernard et al., 2015). The majority of the pars basilaris develops from the fusion of two parachordal cartilages, which are derived from the first two occipital sclerotomes (Müller & O'Rahilly, 1994; 2003; Pang & Thompson, 2011). The third occipital sclerotome contributes to the jugular limb and quadrilateral plate of the pars lateralis (Müller & O'Rahilly, 1994; 2003). The fourth occipital sclerotome, known as the proatlas, fuses with the first three occipital sclerotomes and contributes to the borders of the foramen magnum, the occipital condyles of the pars lateralis and the posterior tubercles of the pars basilaris, (Muhleman et al., 2012; Bernard et al., 2015).

The pars squama develops through intermembranous ossification, making it distinct from the pars basilaris and the pars lateralis (Cunningham et al., 2016). The pars basilaris and pars lateralis develop through endochondral ossification, where a cartilaginous precursor is replaced by bone tissue (Nemzek et al., 2000; Mackie et al., 2008). The cartilaginous anlages are derived from the sclerotomes and form around neurovascular structures that have already commenced development, resulting in specific positioning of foramina prior to ossification (Di Ieva et al., 2014). The cartilages closely resemble the shape of the future pars basilaris and

pars lateralis and act as a model for ossification (Mowbray, 2005; Mackie et al., 2008). Chondrocytes near the centre of the bony model begin to hypertrophy and secrete collagen X and fibronectin, which causes the extracellular matrix of the model to calcify (Mackie et al., 2008). The calcification of the matrix hinders the diffusion of nutrients, causing apoptosis of the hypertrophic chondrocytes (Mackie et al., 2008). Blood vessels invade the cavities left by the chondrocytes and carry in osteogenic cells that differentiate into osteoblasts (Mackie et al., 2008). The osteoblasts deposit osteoid bone matrix on the calcified cartilage scaffold (Mackie et al., 2008). The central aspect of the bone where ossification commences is the primary ossification site (Mackie et al., 2008). The primary ossification sites are apparent between 8 and 10 weeks for the pars lateralis and between 11 and 12 weeks for the pars basilaris (Badiu et al., 2019; Grzonkowska et al., 2021). While ossification occurs at the central aspect of the bone, cartilage continues to proliferate at the periphery of the pars basilaris and pars lateralis, causing the radial expansion of the bones (Mackie et al., 2008).

In addition to depositing osteoid, the osteoblasts also regulate the mineralisation of the osteoid (Ecarot-Charrier et al., 1988). Mineralisation is the process by which minerals, primarily calcium and phosphate, get incorporated into the organic matrix of bone, which transforms osteoid into hard, rigid bone tissue that can support weight while resisting mechanical stresses (Kovacs, 2014). Osteoblasts secrete vesicles containing calcium and phosphate ions (Ecarot-Charrier et al., 1988). These vesicles are released into the extracellular matrix surrounding the osteoid (Ecarot-Charrier et al., 1988). This localised release increases the concentration of calcium and phosphate ions in the immediate vicinity of the osteoid, creating a favourable environment for mineral deposition (Ecarot-Charrier et al., 1988).

1.2.2. Anatomy of the pars basilaris

The pars basilaris is medially wedged between the left and right petrous parts of the temporal bone at the inferior petrosal fissure, which contains the inferior petrosal sinus (Balboni et al., 2005; Cunningham et al., 2016; Charbonneau et al., 2024). The anterior-most part of the pars basilaris is flattened for the articulation with the basisphenoid at the spheno-occipital synchondrosis (Cunningham et al., 2016). The spheno-occipital synchondrosis is a cartilaginous joint similar to a "mirrored image" of a long bone growth plate (Nie, 2005; Hallett et al., 2022). The spheno-occipital synchondrosis has a central resting zone of chondrocytes flanked by mirrored proliferative and hypertrophic zones on either side (Nie, 2005; Hallett et al., 2022). This arrangement allows the spheno-occipital synchondrosis to expand bidirectionally, therefore contributing to the overall lengthening of the cranial base (Nie, 2005; Hallett et al., 2022).

The pars basilaris has two lateral angles on the posterolateral aspects of the bone, with facets for the condylar and jugular limbs of the pars lateralis (Cunningham et al., 2016; Thornton et al., 2024). The lateral angles deepen with age, which facilitates the transition from the narrow and elongated shape of the early prenatal pars basilaris to the hexagonal shape of the postnatal pars basilaris (Thornton et al., 2024). On the extracranial surface of the pars basilaris, there are two projections on either side of the foramen magnum where the occipital condyles of the pars lateralis articulate (Thornton et al., 2024).

The posterior border of the foramen magnum is curved to form the anterior boundary of the foramen magnum (Cunningham et al., 2016). The atlantooccipital membrane and superficial

anterior atlantooccipital ligament insert onto the medial aspect of the foramen magnum on the extracranial (inferior) surface of the pars basilaris (Fiester et al., 2021). The apical and cruciform ligaments insert onto the anterior margin of the foramen magnum at the basion inferior to the atlantooccipital membrane and superficial anterior atlantooccipital ligament (Fiester et al., 2021). The structures attached at the border of the foramen magnum function to maintain cervical vertebra stability at the atlantooccipital joint during head and neck movements (Fiester et al., 2021).

The pharyngeal raphe attaches to the extracranial surface of the pars basilaris, anterior to the edge of the foramen magnum and along the midline of the bone at the pharyngeal tubercle (Krmpotić-Nemanić et al., 2006; Eggington et al., 2024). The pharyngeal raphe is a fibrous band of tissue that acts as the origin and insertion for the pharyngeal constrictors, which constrict the pharynx to allow for swallowing and breathing (Shimada & Gasser, 1987). Lateral and posterior to the pharyngeal tubercle is a crest that serves as the insertion point for the rectus capitis anterior muscle (Rhoton, 2000; Krmpotić-Nemanić et al., 2006; Eggington et al., 2024). The longus capitis muscle inserts on the posteromedial portion of the pars basilaris (Rhoton, 2000; Krmpotić-Nemanić et al., 2006; Eggington et al., 2024). Both sets of muscles function to flex the head (Rhoton, 2000; Kennedy et al., 2017).

The intracranial surface of the pars basilaris is slightly concave to support the anterior medulla oblongata (Rhoton, 2000). The subarachnoid space, which contains cerebrospinal fluid, is located between the medulla oblongata and the skeletal pars basilaris are the medullary and pontine cisterns (Altafulla et al., 2019). Dura mater adheres to the bony part of the

intracranial pars basilaris, and the tectorial membrane blends with the dura mater (Tubbs et al., 2007a; Fiester et al., 2021). The basilar plexus overlies the tectorial membrane and covers the whole intracranial surface of the pars basilaris (Tubbs et al., 2007b). The intracranial surface of the pars basilaris commonly presents with nutrient foramina (Zdilla, 2017; Eggington et al., 2024). These foramina allow for the passage of blood vessels that supply the bone (Eggington et al., 2024). The number of veins in the basilar plexus decreases as it travels down the pars basilaris (Tubbs et al., 2007b). The pharyngeal venous plexus may communicate with the basilar plexus through clival foramen within the pars basilaris (Zdilla, 2017).

1.2.3. Anatomy of the pars lateralis

The curved medial border of the paired pars laterali forms the lateral borders of the foramen magnum (Cunningham et al., 2016; Thornton et al., 2023). The jugular and condylar limb of the pars lateralis extend anteromedially from the posterolateral aspect of the foramen magnum border (Cunningham et al., 2016; Thornton et al., 2023). During postnatal life, the ends of the limbs fuse to create the hypoglossal canal, which transmits the hypoglossal nerve (cranial nerve XII) and the meningeal branch of the ascending pharyngeal artery (Rhoton, 2000; Coqueugniot & Le Minor, 2002; Wysocki et al., 2004; Cardoso et al., 2013; Charbonneau et al., 2024). The hypoglossal canal fuses with the posterolateral aspects of the pars basilaris at the anterior interoccipital synchondrosis during postnatal development (Coqueugniot & Le Minor, 2002; Wysocki et al., 2004; Cardoso et al., 2013; Cunningham et al., 2016).

The quadrilateral plate of the pars lateralis is thickened on its posterior border where it articulates with the pars squama of the occipital bone at the posterior interoccipital synchondrosis (Coqueugniot & Le Minor, 2002; Cardoso et al., 2013; Cunningham et al., 2016). The lateral border of the pars lateralis articulates with the mastoid part of the temporal bone at the occipitomastoid suture (Cunningham et al., 2016; Charbonneau et al., 2024). In the prenatal and early postnatal pars lateralis, the corner where the lateral and posterior borders of the pars lateralis meet is open to the mastoid fontanelle, which ossifies within the first year of life (Cunningham et al., 2016).

The occipital condyle on the condylar limb articulates with superior articular facets of the atlas vertebra at the atlantooccipital joint (Rhoton, 2000; Charbonneau et al., 2024). On the medial aspect of each condyle is a small tubercle, which is the attachment site of the alar ligaments, which limits rotation and lateral flexion of the cervical vertebrae (Rhoton, 2000; Cunningham et al., 2016; Fiester et al., 2021; Charbonneau et al., 2024). The condylar fossa is the impression behind each condyle that accommodates the posterior margin of the atlas during extension of the head (Rhoton, 2000; Tuli et al., 2008; Kavitha & Anand, 2013; Cunningham et al., 2016; Smith et al., 2022). In a proportion of the condylar fossa, there is a posterior condylar canal that transmits a sigmoid emissary vein that connects the occipital sigmoid and suboccipital venous plexuses. (Rhoton, 2000; Tuli et al., 2008; Kavitha & Anand, 2013; Smith et al., 2022; Charbonneau et al., 2024). Lateral to the occipital condyle is the jugular process (Rhoton, 2000; Cunningham et al., 2016; Murakami et al., 2023; Charbonneau et al., 2024). The jugular process forms the posteroinferior margin of the jugular foramen, which transmits the glossopharyngeal (cranial nerve IX), vagus (cranial nerve X), and accessory cranial nerves

(cranial nerve XI) (Rubinstein et al., 1995; Rhoton, 2000; Charbonneau et al., 2024). The rectus capitis lateralis muscle inserts onto the extracranial surface of the jugular process and contributes to the stabilisation of the atlantooccipital joint (Rhoton, 2000; Murakami et al., 2023; Charbonneau et al., 2024). The intracranial surface of the pars lateralis is covered in dura mater and provides a platform to support the cerebellum (Thornton et al., 2023).

1.3. Trends in the ontogeny of trabecular bone

Skeletal tissue is composed of an external layer of cortical bone and an internal network of trabecular bone (Cunningham et al., 2016). Cortical bone is characterised by low porosity, giving bones their stiff and strong outer structure (Cunningham et al., 2016). The internal architecture of bone tissue is comprised of trabeculae. Trabecular tissue is a lattice-like arrangement of interconnected struts that provides a lightweight yet strong internal framework for the bone, which contributes to the strength and stability of the bone while also allowing for efficient load distribution (Oftadeh et al., 2015; Kivell, 2016). Bouxsein et al. (2010) outlined bone volume fraction (BV/TV), trabecular thickness (TbTh), trabecular number (TbN) and trabecular separation (TbSp) as the minimal set of variables that should be reported when describing trabecular bone morphology. Bone volume fraction (BV/TV) refers to the volume occupied by trabecular bone relative to the total volume of the region of interest (Bouxsein et al., 2010). A higher BV/TV generally corresponds to a denser and stronger bone structure (Bouxsein et al., 2010; Oftadeh et al., 2015; Kivell, 2016). Osteoblasts deposit new bone matrix, leading to increases in TbTh and potentially TbN, thus contributing to a higher BV/TV (Oftadeh et al., 2015). Osteoblasts indirectly affect TbSp as increased bone deposition could potentially lead to a reduction in TbSp if the rate of new bone formation outpaces the

rate of resorption in the space between trabeculae (Oftadeh et al., 2015). Osteoclasts resorb existing bone tissue, which can lead to decreases in TbTh and TbN and subsequently decreased BV/TV (Oftadeh et al., 2015). Osteoclasts directly affect TbSp by resorbing bone tissue in the spaces between trabeculae (Oftadeh et al., 2015). This resorption can lead to wider gaps between trabeculae, therefore increasing TbSp (Oftadeh et al., 2015). Osteoclast activity is important for removing old or damaged bone, regulating calcium homeostasis, and shaping trabecular architecture (Oftadeh et al., 2015). Moreover, some TbSp is necessary for the effective distribution of forces and nutrient diffusion within the bone tissue (Oftadeh et al., 2015).

The trabecular architecture of the skeleton is shaped by the confluence of hormonal, nutritional, and genetic factors (Kivell, 2016). In addition, the loading environment and biomechanical requirements of a bone also shape its trabecular structure (Bouxsein et al., 2010; Oftadeh et al., 2015; Kivell, 2016). Wolff's law states that bone adapts its structure to the loads placed on it (Wolff, 1892; Frost, 2004; Robling & Turner, 2009). Thus, the trabecular architecture within bones is influenced by mechanical stresses applied to the bone (Robling & Turner, 2009; Oftadeh et al., 2015; Kivell, 2016). Frost (1987; 2003) proposed the mechanostat principle which describes how bone senses and responds to mechanical loads. The mechanostat is a feedback loop that keeps bone strain within a physiologically safe range (Frost, 1987; 2003; Robling & Turner, 2009). When bone is loaded, the mechanostat signals osteoblasts to add bone mass, which increases BV/TV (Frost, 1987; 2003; Robling & Turner, 2009). The mechanostat also signals osteoclasts to remove bone from areas that are not loaded, which decreases BV/TV (Frost, 1987; 2003; Robling & Turner, 2009). This means that

bone mass is regulated to meet the mechanical demands placed on the skeleton (Frost, 1987; 2003; Robling & Turner, 2009).

In addition, degree of anisotropy (DA) significantly contributes to explaining the mechanical properties of a 3D structure (Bouxsein et al., 2010; Oftadeh et al., 2015). In the context of osteology, DA quantifies the preferential alignment of trabeculae along specific directions (Bouxsein et al., 2010; Oftadeh et al., 2015). Isotropy refers to a property of bone tissue where its mechanical and physical structure are uniform (Bouxsein et al., 2010; Oftadeh et al., 2015). Isotropic bone has evenly distributed trabeculae that are oriented in various directions (Bouxsein et al., 2010; Oftadeh et al., 2015). Anisotropic bone consists of trabeculae aligned in a specific direction (Bouxsein et al., 2010; Oftadeh et al., 2015). When bone is loaded in a particular direction, the mechanostat signals osteoblasts to align trabeculae along that direction, which increases DA (Robling & Turner, 2009; Oftadeh et al., 2015). Thus, a higher DA indicates a more anisotropic structure with trabeculae aligned in the direction of the stress to resist predictable loads, while a lower DA suggests a more isotropic arrangement adapted for minimal or multidirectional forces (Robling & Turner, 2009; Oftadeh et al., 2015).

The factors that affect the adult skeleton, such as biomechanics, hormones, nutrition, and genetics, also have an impact on the immature skeleton (Gkiatas et al., 2015; Reid et al., 2023). However, this impact is amplified during growth due to a confluence of developmental factors (Gkiatas et al., 2015). The physiology, growth and motor milestones of childhood generate far more dynamic and transient biomechanical forces compared to adulthood (Abel & Macho, 2011; Reid et al., 2023). Moreover, the ossification processes and complex developmental

interactions further contribute to the overall size and shape of the juvenile skeleton (Saers et al., 2020; Wiles et al., 2024). Given the significant impact development has on shaping the immature skeleton, an understanding of the ontogenetic development of trabecular architecture is important for understanding the relationship between form and function in the cranial base. Yet, there are limited studies that assess the development of trabecular architecture in the cranial base (Sips et al., 2008; Zdilla, 2017). However, assessments of the juvenile postcranial skeleton have revealed several trends that can help shape the approach to understanding the trabecular ontogeny of the pars basilaris and pars lateralis.

1.3.1. Modelling and remodelling

Frost (1990) differentiated between “modelling” and “remodelling”. Modelling involves uncoupled bone formation and resorption where the activity of osteoblasts and osteoclasts do not necessarily act in the same location or at the same time, leading to changes in bone size and shape (Frost, 1990; Robling & Turner, 2009). Remodelling is a sequential process where osteoclasts resorb old or damaged bone, followed by osteoblasts filling the resorption cavities with new bone for repair and maintenance of bone tissue (Frost, 1990; Robling & Turner, 2009).

Reissis and Abel (2012) used micro-computed tomography (micro-CT) to examine the humerus and femur of 38 human fetuses aged 4 to 9 gestational months and noted that trabeculae became thicker and less numerous as the fetuses developed and the bones increased in size. Wiles et al. (2024) also examined trabecular architecture in the femora and humeri of 35 human fetal skeletons aged between 4 and 9 months of gestation using high-

resolution 3D micro-CT and observed that TbTh increased with increasing fetal age in both the femora and humeri. The overall increase in bone size and TbTh observed by Reissis and Abel (2012) and Wiles et al. (2024) suggests that bone deposition is occurring, which is characteristic of bone modelling as the bone deposition leads to size changes (Salle et al., 2002; Robling & Turner, 2009). This observation is supported by Salle et al. (2002), where histological investigations of 35 prenatal and neonatal proximal femora showed that indices of bone resorption i.e., fraction of eroded bone surface, fraction of osteoclasts surface on bone surface, and number of osteoclasts on the bone perimeter were relatively low. Thus, suggesting that high rates of bone deposition and low rates of resorption were occurring in these prenatal bones and that modelling is likely the primary mechanism of bone development during prenatal growth in the humerus and femur (Salle et al., 2002; Robling & Turner, 2009).

Observations of the surface morphology of the pars basilaris and pars lateralis also suggest that modelling is occurring (Thornton et al., 2023; Eggington et al., 2024). Eggington et al. (2024) made observations about the microporosity and bone formation on the extracranial surface of 199 pars basilari aged between 36 gestational weeks to 3.5 years from European archaeological sites and found a decrease in microporosity with age, while the bones grew bigger. These observations suggest that bone deposition is rapidly occurring as the initial microporosity of the pars basilaris is gradually filled in during development, contributing to bone growth (Eggington et al., 2024). These results are consistent with bone deposition via modelling (Salle et al., 2002; Robling & Turner, 2009).

Thornton et al. (2023) used stereomicroscopy to make observations of the surface of the pars lateralis of 103 immature South African individuals from a forensic collection and noted longitudinal striations and trabeculae near the borders of the pars lateralis, and a porous appearance over the bone's surfaces. In addition, Thornton et al. (2023) used geometric morphometrics and observed changes in bone size and shape with age. The presence of these features indicates that bone deposition is actively contributing to the growth and shaping of the pars lateralis (Salle et al., 2002; Thornton et al., 2023). The observations made by Thornton et al. (2023) and Eggington et al. (2024) are indicative of modelling. However, further investigations into the internal architecture of the pars basilaris and pars lateralis are needed to understand how changes in trabecular structure and mineralisation patterns contribute to the overall process of bone shaping and growth.

1.3.2. Predetermined trabecular template for early development

Several studies have suggested that early trabecular development follows a predetermined blueprint (Cunningham & Black, 2009a; 2009b; Abel & Macho, 2011; Saers et al., 2020). Cunningham and Black (2009a; 2009b) used micro-CT and radiographic techniques to study the trabecular structure of 28 human neonatal ilia and found organised trabecular patterns which closely resembled the patterns seen in adult ilia despite the absence of weight-bearing loads in newborns. Similar results were observed by Abel and Macho (2011), where 2D image analysis of radiographs of 73 immature human pelvic bone showed that trabecular features like the sacro-pubic and ilio-ischial bundles, which are implicated in load transfer during bipedalism, are present in the youngest individuals before the onset of walking. In addition, micro-CT analysis of 35 postnatal human calcanei revealed dense trabecular structures in

regions of the calcaneus subjected to high compressive loads during walking in individuals less than one year old before the typical onset of walking (Saers et al., 2020). The early appearance of organised trabecular patterns in the pelvic bones and calcaneus before the onset of significant loading suggests that there is a predetermined trabecular template that is driven by factors beyond mechanical stimuli that play a role in the development (Saers et al., 2020).

Multiple studies have highlighted the role of vascularisation in the development of the trabecular architecture contributing to the predetermined template (Cunningham & Black, 2009a; 2009b; Maclean et al., 2014; Reid et al., 2024). Cunningham and Black (2009a; 2009b) used a combination of radiography and micro-CT to examine the internal structure of 28 human neonatal ilia and observed a distinct pattern of thickened trabeculae surrounding a "vascular collar" originating from the nutrient foramen. Cunningham and Black (2009a; 2009b) proposed that the invasion of the nutrient artery during endochondral ossification influences the spatial arrangement of trabeculae as they develop around the existing vascular structures, contributing to an adult-like distribution of trabeculae before the onset of walking. Maclean et al. (2014) support this finding by using macro-radiography and colour-mapping to analyse the development of the trabecular architecture of 55 immature human ischia and identified a region of lower bone density inferior to the acetabular rim in individuals under 6 months old. Maclean et al. (2014) attributed the regions of lower bone density to vascular pores in regions where the nutrient foramen was present. Thus, showing that the initial structure of the trabecular network is influenced by vascular cues before mechanical loading from walking begins.

The predetermined template observed in the pelvic bones and calcaneus has not been observed in all immature skeletal elements (Reid et al., 2023; 2024). Reid et al. (2023; 2024) used radiographic investigations to examine the development of the human tibia and talus. Reid et al. (2024) observed a rudimentary pattern in the perinatal talus that shared similarities with the adult structure. However, Reid et al. (2023) did not observe adult-like trabecular patterns in the tibia until after the onset of walking. The radiographic investigations of the postnatal talus showed the presence of numerous vascular foramina in the talar neck, coinciding with areas of lower BMD, which suggests that the invasion of vessels during endochondral ossification may contribute to determining the trabecular pattern in the developing bones (Reid et al., 2023; 2024). However, the tibia, which did not resemble the adult structural organisation, exhibited a simpler vascularisation pattern (Reid et al., 2023; 2024). Reid et al. (2024) suggested that the spatial arrangement of blood vessels, particularly the nutrient artery and its branches, may act as a blueprint that guides the formation and arrangement of trabeculae during bone development.

The role of vascularisation in pars basilaris development has also been explored by Zdilla (2017) where the dorsal surfaces of 104 prenatal and neonatal pars basilari were categorised based on the presence and distribution of vascular pits and foveae. The findings by Zdilla (2017) suggest that both clival canals and foramina form around vascular structures, particularly veins connecting the basilar plexus with other venous plexi. The presence of clival canals in prenatal individuals indicates that vascularisation influences bone development from a very early stage within the basicranium (Zdilla, 2017). To further explore the relationship between vascularisation and basicranial development, a micro-CT study would allow for a

more detailed three-dimensional visualisation of the vascular channels and trabecular architecture.

Moreover, the developmental trajectory of the trabeculae has been hypothesised to be related to the ossification process of the bones (Wiles et al., 2024). Wiles et al. (2024) compared the development of trabecular architecture in 35 prenatal human humeri and femora using micro-CT. While both bones reach complete chondrification and develop primary ossification centres around the same time (8-9 weeks), the femur exhibited a larger size, thicker trabeculae, and greater BV/TV compared to the humerus (Wiles et al., 2024). Wiles et al. (2024) proposed that the larger femoral cartilage anlage could explain the larger size and greater BV/TV observed in the femur (Wiles et al., 2024). Thus, emphasising the role of the initial cartilage template in determining the size and structure of trabecular bone, even before significant mechanical loading begins (Wiles et al., 2024). Thus, the distinctive cartilaginous precursors of the pars basilaris and pars lateralis may play a role in the trabecular development of the bones.

In addition to the cartilage anlage, the pattern of ossification has also been suggested to play a role in the pattern of trabecular development (Saers et al., 2020; Wiles et al., 2024). Wiles et al. (2024) observed a high degree of anisotropy (DA) in both the humerus and femur throughout gestation. The persistently high DA means the trabeculae are highly aligned in a specific direction, which may reflect the anisotropic organisation of the underlying cartilage model due to the columnar arrangement of the cartilage of the long bones (Wiles et al., 2024). Conversely, micro-CT analysis of postnatal calcanei showed that immature human calcaneal

trabecular bone structure is isotropic (low DA), which is attributable to the radial ossification pattern of the bone from a central ossification centre (Saers et al., 2020). The radial ossification pattern creates a more symmetrical distribution of trabeculae, without a dominant orientation, leading to a lower DA (Saers et al., 2020). These findings suggest that the anisotropy of the initial cartilage template, dictated by the ossification pattern, plays a significant role in determining the initial DA of the developing trabecular bone (Saers et al., 2020; Wiles et al., 2024). The pars basilaris and pars lateralis also exhibit a radial ossification pattern, which may also influence the alignment of the trabeculae (Mackie et al., 2008).

1.3.3. Role of mechanical loading in postcranial skeletal development

Micro-CT analysis of the prenatal human vertebrae (Nuzzo et al., 2003; Acquaah et al., 2015), femur (Reissis & Abel, 2012; Wiles et al., 2024), humerus (Reissis & Abel, 2012; Wiles et al., 2024) and calcaneus (Saers et al., 2020) presented a dense and relatively isotropic trabecular structure during fetal development. This isotropic arrangement, with numerous thin, closely packed trabeculae, is not typically observed in bones adapting to directional loading (Reissis & Abel, 2012; Acquaah et al., 2015). Thus, suggesting that the bones are likely not adapting to biomechanical forces (Reissis & Abel, 2012; Acquaah et al., 2015). The lack of adaptation is attributable to the intrauterine environment, which restricts fetal movement, therefore limiting the magnitude and consistency of mechanical forces that could influence trabecular development (Acquaah et al., 2015). Moreover, while fetal movements like kicking and punching do occur, they might not generate sufficient strain to induce significant architectural changes (Acquaah et al., 2015; Saers et al., 2020).

The development of trabecular bone architecture has been shown to be influenced by biomechanical factors, particularly during postnatal locomotor development (Ryan & Krovitz, 2006; Gosman & Ketcham, 2009; Colombo et al., 2019). Colombo et al. (2019) investigated the trabecular microarchitecture of 8 distal radii in human juveniles aged 0 to 3 years using micro-CT and found that the trabecular structure was most robust during crawling, with a higher BV/TV and TbTh and became less robust with the transition to walking, showing decreased BV/TV and increased TbSp (Colombo et al., 2019). Colombo et al. (2019) suggested that this pattern of change is likely due to the significant biomechanical loads experienced by the wrist during crawling, which diminish with the transition to walking.

Furthermore, the onset of walking has been shown to influence the trabecular development of the femur (Ryan & Krovitz, 2006) and tibia (Gosman & Ketcham, 2009). Ryan and Krovitz (2006) used micro-CT to study the human proximal femur and observed a decrease in BV/TV, TbN and DA before the age of 12 months, followed by an increase in BV/TV, TbTh and DA as gait develops. Similarly, Gosman and Ketcham (2009) observed changes in the trabecular architecture of the tibia in a prehistoric population using micro-CT. Gosman and Ketcham (2009) found that BV/TV and DA were at a maximum at birth and decreased until 1 year of age and then increased until between 6 and 8 years of age, where these values reached adult range (Gosman & Ketcham, 2009). Moreover, they found that TbN was at a maximum at birth and decreased until skeletal maturity, while TbTh was at its lowest at birth and increased until skeletal maturity (Gosman & Ketcham, 2009). The pattern observed in the femur and tibia suggests that an initially dense bone structure is remodelled and optimised in response to the weight-bearing demands of bipedalism (Ryan & Krovitz, 2006; Gosman & Ketcham, 2009).

Postcranial studies have focused on weight bearing elements, where the effects of discrete milestones such as walking and crawling offer distinct benchmarks to analyse the effects of biomechanics on development (Ryan & Krovitz, 2006; Gosman & Ketcham, 2009; Colombo et al., 2019). The pars basilaris and pars lateralis are not weight-bearing; however, they are subject to mechanical stresses from the developing brain surrounding muscles and neurovasculature (Richards & Jabbour, 2011; Edamoto et al., 2018). Moreover, other key postnatal milestones such as the development of posture and independently holding up the head on the neck may also contribute to the biomechanical stresses that influence the growth, modelling and remodelling of the pars basilaris and pars lateralis (Krmpotić-Nemanić et al., 2006; Richards & Jabbour, 2011; Eggington et al., 2024). Thus, these biomechanical stresses may affect the trabecular bone structure in these regions. Therefore, it is necessary to review the growth patterns and biomechanical environment of the occipital bone in order to establish a foundational understanding of their typical developmental trajectory. Thus, allowing for a more comprehensive assessment of how localised functional demands and growth patterns may differentially affect trabecular microarchitecture within the skeletal elements.

1.4. Biomechanical environment and development of the cranial base

Moss (1962) proposed the functional matrix hypothesis, which suggests that the morphological development of craniofacial bones is driven by the stresses and strains from the surrounding soft tissues rather than by genetics alone (Moss, 1962; Richards & Jabbour, 2011; Kaur et al., 2021). A matrix refers to the soft tissue structures or functional systems that influences the development of bones or structures (Kaur et al., 2021). Richards and Jabbour (2011) extended the functional matrix hypothesis to the development of the foramen

magnum by using metric and shape analysis to study 470 prenatal (n=28), juvenile (n=419) and mature (n=23) crania. The foramen magnum was observed to be predominantly elongated and oval shaped prenatally and broader with a more variable shape postnatally (Richards & Jabbour, 2011). Richards and Jabbour (2011) observed that the long, elongated shape of the foramen magnum prenatally was associated with the growth of the pars lateralis, which coincides with the rapid development of neurological structures such as the brainstem, meninges, neurovascular structures, and cerebrospinal fluid during prenatal development. The broader, more variable shape of the foramen magnum postnatally was associated with the development of the pars basilaris, which coincides with the development of upright head posture and secondary cervical curvature (Richards & Jabbour, 2011). Thus, the development of the foramen magnum was proposed to be shaped by two functional matrices, namely the ventral matrix, which involves musculature that primarily influences the development of the pars basilaris and the dorsal matrix, which includes neurological structures that primarily contribute to the development of the pars lateralis (Richards & Jabbour, 2011). The differential growth of the matrices was attributed to the distinct roles and developmental timings of the soft tissues and skeletal units comprising each matrix (Richards & Jabbour, 2011). Thus, morphological development of the region has been shown to have a relationship to the surrounding soft tissues and anatomy.

The relationship between brain and cranial base development has been examined by Delteil et al. (2021), where magnetic resonance imaging (MRI) was used to measure various parameters of the infant brain and cranial base in 47 infants aged between 0 and 24 months. Delteil et al. (2021) found that transverse cerebellar diameter strongly correlates with the

maximum length and width of the pars basilaris. This correlation suggests that the growth of the cerebellum may influence bone growth in the pars basilaris, leading to an increase in its length and width (Delteil et al., 2021). In addition, Kranioti et al. (2009) mapped the remodelling activity on the endocranial surface of the occipital bone of 10 immature human crania aged between 4 and 8 years using a reflected light microscope and found a shift in the remodelling pattern of the cerebral fossae that coincided with the completion of cerebral development. While the study by Kranioti et al. (2009) only focused on an older age range and the squamous part of the occipital bone, the findings of the study suggested that brain growth may have an influence on the remodelling patterns of the occipital bone. Specific analysis of the trabecular architecture of the pars basilaris and pars lateralis may help elucidate the underlying relationship between brain growth and the development of the occipital bone during early development.

In addition, Edamoto et al. (2018) focused on the postnatal development of pars basilaris in mice using histological and finite element analysis. Histological analysis found that the endocranial surface of the pars basilaris was predominantly populated by osteoclasts (Edamoto et al., 2018). This finding correlates with finite element analysis results, which indicated that the stress exerted on the endocranial surface by the brain is compressive and promotes resorption (Edamoto et al., 2018). In contrast, histology showed that the exocranial surface of the pars basilaris was primarily populated by osteoblasts (Edamoto et al., 2018). Finite element analysis in the exocranial region demonstrated that the stress generated by the muscles associated with the extracranial surface is tensile, which suggests that tensile stress promotes bone formation in the pars basilaris (Edamoto et al., 2018). The interplay between

the compressive stress from the brain causing resorption by osteoclasts on the intracranial surface and the tensile stress from muscles causing bone formation by osteoblasts on the extracranial surface contributed to the downward sloping morphology of the pars basilaris (Edamoto et al., 2018). Thus, the results of the study by Edamoto et al. (2018) suggests that both brain growth and muscle activity contribute to the development of the pars basilaris. However, the study does not fully address how compressive and tensile mechanical forces may influence the internal trabecular architecture of the pars basilaris.

The role of the pharynx in the prenatal development of the cranial base was explored by Jeffery (2005). High-resolution MRI scans of 40 human fetal specimens showed correlations between oropharyngeal size and angle of basicranial retroflexion, suggesting a link between these structures during prenatal development (Jeffery, 2005). Understanding the microarchitecture of the cranial base may help elucidate how biomechanical and developmental forces, such as those from the pharynx and brain, influence ossification patterns and cranial base morphology.

In addition to the influence of the brain and pharynx, the muscles of the pars basilaris and pars lateralis are thought to influence the morphology of the bone (Krmpotić-Nemanić et al., 2006; Murakami et al., 2023). Krmpotić-Nemanić et al. (2006) conducted a study examining the age-related changes of the osseous epipharynx using 60 human crania, encompassing adults, elderly individuals, and children aged 1 to 5 years. Krmpotić-Nemanić et al. (2006) observed that the longus capitis muscles were attached to a prominent bony crest of the pars basilaris crest in children. However, the longus capitis muscles were attached to a bony fossa

of the pars basilaris in adult crania (Krmpotić-Nemanić et al., 2006). The differences in the attachment site with age suggested that the continuous pull of the longus capitis muscles during head flexion may contribute to the remodelling of the pars basilaris over time, resulting in changes in the morphology of the bone (Krmpotić-Nemanić et al., 2006). Krmpotić-Nemanić et al. (2006) also observed that the attachment site of the rectus capitis anterior muscles on the pars basilaris was less prominent in children compared to adults. Younger individuals have limited head movement requiring the longus capitis and rectus capitis anterior muscles compared to older individuals (Krmpotić-Nemanić et al., 2006). Thus, the postural changes and the development of specific movements associated with muscle activity might influence the morphology of muscle attachment sites on the pars basilaris (Krmpotić-Nemanić et al., 2006). A limitation of the study by Krmpotić-Nemanić et al. (2006) is that it only focuses on individuals in older and broader age groups and, therefore, does not account for the impact of development changes in prenatal and the first year of life.

Murakami et al. (2023) studied the development of the rectus capitis lateralis muscles on the pars lateralis using histological analysis of paraffin-embedded sections of 22 midterm and late-term human fetuses. Murakami et al. (2023) observed that the rectus capitis lateralis muscle was wrapped around the cartilaginous jugular process in midterm fetuses (Murakami et al., 2023). However, in more mature fetuses, the jugular process was lengthened and was bony rather than cartilaginous (Murakami et al., 2023). Murakami et al. (2023) suggested that the pull of rectus capitis lateralis during development may have contributed to the elongation of the jugular process, ultimately contributing to the complete fusion of the occipital and temporal bones (Murakami et al., 2023). The findings by Krmpotić-Nemanić et al. (2006) and

Murakami et al. (2023) demonstrate how the surrounding musculature can shape the development of the pars basilaris and pars lateralis. However, to fully understand how the surrounding musculature influences the development of the pars basilaris and pars lateralis, it is necessary to examine the trabecular architecture of these bones, particularly within the attachment sites of the associated muscles.

1.5. Bone mineral density and mineralisation

While trabecular architecture provides information about bone structure, investigating BMD is important for understanding bone quality and strength (Beltrand et al., 2008). The degree and distribution of mineralisation can provide further insights into bone growth and development, particularly in the context of mechanical loading and its impact on bone health (Beltrand et al., 2008). Sips et al. (2008) used micro-CT to study the 3D architecture and mineralisation of trabecular bone in six fetal and postnatal porcine pars basilari using a peeling algorithm to determine the degree of mineralisation in each voxel layer. Sips et al. (2008) found a gradient of increasing mineralisation from the surface to the centre of individual trabeculae within the pars basilaris. Similar studies have also observed a gradient of increasing mineralisation from the surface to the centre of trabeculae in both the anterior and posterior regions of the fetal and postnatal porcine mandibular condyle and the mandibular corpus (Mulder et al., 2005; 2006). These animal studies suggest that trabecular elements grow due to the surface apposition of new bone (Mulder et al., 2005; 2006; Sips et al., 2008).

The literature also suggests that the distribution of mineralisation within a bone can reflect the mechanical stresses experienced by the bone (Hutchinson et al., 2017). Hutchinson et al.

(2017) assessed the BMD of the immature human mandible using micro-CT and found that BMD was significantly higher on the internal lingual surface of the mandible compared to the external buccal and labial surfaces. This higher BMD on the lingual surface of the mandible was associated with the biomechanical demands of the tongue (Hutchinson et al., 2017). In addition, the buccal and labial surfaces, which are primarily influenced by dental development, displayed BMD changes that mirrored the progression of tooth formation and eruption (Hutchinson et al., 2017). These findings highlight the interplay between functional demands and developmental processes in shaping the bone mineral density of the growing mandible (Hutchinson et al., 2017).

In contrast to the mandible, micro-CT analysis by Thornton et al. (2023; 2024) found that BMD was uniform across the surface of the pars basilaris and pars lateralis despite variations in the morphology of human individuals aged between 20 gestational weeks to 7.5 postnatal months. Moreover, Thornton et al. (2023; 2024) did not observe significant differences in the BMD of the pars basilaris and pars lateralis between different age groups. Similarly, Sips et al. (2008) did not observe significant differences in the degree of mineralisation with age in both the central aspect and the cortex of porcine pars basilaris. Thornton et al. (2023; 2024) hypothesised that the distribution of BMD across the cranial elements is uniform to support brain development in the prenatal and postnatal periods. Thornton et al. (2023; 2024) also emphasised the importance of form over mineralisation in the development of the pars basilaris and pars lateralis. A limitation of the studies by Thornton et al. (2023; 2024) is that they assessed the BMD on the surface of the bones, which may not reflect variations in internal bone architecture. Surface measurements overlook differences in mineralisation

within the trabeculae of bones (Lerebours et al., 2020). A more comprehensive analysis, including internal BMD, would provide a better understanding of cranial bone growth and its biomechanical properties (Lerebours et al., 2020).

1.6. Aim

The above review of the literature has shown that the development of the trabecular architecture of the immature skeleton is influenced by various developmental factors. Assessment of the functional environment of the pars basilaris and pars lateralis has shown that mechanical loading from the developing brain, muscles and adjacent bones does impact the bone structure and morphology of the pars basilaris and pars lateralis throughout development (Krmpotić-Nemanić et al., 2006; Kranioti et al., 2009; Richards & Jabbour, 2011; Edamoto et al., 2018; Delteil et al., 2021; Murakami et al., 2023). However, the nature of the impact of development on trabecular architecture in the prenatal and postnatal pars basilaris and pars lateralis remains underexplored. Therefore, this study aims to investigate changes in the internal architecture of the early prenatal, late prenatal, and postnatal human pars basilaris and pars lateralis.

1.7. Objectives

Objective 1: Evaluate the changes in bone volume of the various regions of the early prenatal, late prenatal, and postnatal pars basilaris and pars lateralis.

Objective 2: Assess variations in the trabecular number, spacing and thickness throughout the early prenatal, late prenatal, and postnatal pars basilaris and pars lateralis.

Objective 3: Assess the changes in trabecular anisotropy of the various regions of the early prenatal, late prenatal, and postnatal pars basilaris and pars lateralis

Objective 4: Evaluate the changes in bone density throughout the early prenatal, late prenatal, and postnatal pars basilaris and pars lateralis

Chapter 2: Materials and methods

2.1. Sample

The human pars basilaris and pars lateralis skeletal elements were sourced from 106 South African prenatal and postnatal individuals that were previously collected for the purposes of Dr Roxanne Thornton's PhD study (Thornton, 2018) and form part of the Johannesburg Forensic Paediatric Collection (JFPC). The JFPC is an initiative of the Department of Forensic Medicine and Pathology of the University of the Witwatersrand, Johannesburg, which aims to preserve and safeguard unclaimed and unidentified immature skeletal remains admitted to the Johannesburg Forensic Pathology Services (JFPS).

The JFPS is designated as the authority for the remains of abandoned fetal and postnatal individuals in accordance with the Births and Deaths Registration Act no. 51 of 1992, section 12, and the Criminal Procedure Act no. 57 of 1977, section 239. The donation of unclaimed forensic remains from such an authority for medical research is permitted under Chapter 8 of the National Health Act 61 of 2003, section 64. Data made available to the investigators included age, sex and circumstance of death. An ethical clearance certificate was granted by the University of the Witwatersrand, Johannesburg's Human Research Ethics Committee (Medical) (HREC: M230943, Appendix A).

Individuals were categorised into an early prenatal (20–30 gestational weeks, n=31), late prenatal (30–40 gestational weeks, n=45), or postnatal (birth–7.5 months, n=30) group, based on the dental and skeletal age estimations (Thornton, 2018). These groupings were

consistent with those used in previous studies on the pars basilaris and pars lateralis from the JFPC and allows for a substantive number of bones in each age group while still reflecting meaningful age differences (Thornton et al., 2020; 2023; 2024). Biological age was previously established based on digital radiological images of the anterior and lateral mandible taken on a Nomad portable X-ray unit (Aribex, Charlotte, NC, USA). Dental aging was based on The London Atlas of Human Tooth Development and Eruption (AlQahtani et al., 2010). In cases where the dentition could not be used, anthropometric criteria were employed on the left femur, where linear regression equations were used to predict crown-heel length from the diaphyseal width and length (Schaefer et al., 2009; Thornton, 2018).

All skeletal elements of an individual were excluded in cases of apparent abnormal development or pathology. Specific elements were excluded where that element showed evidence of significant post-mortem damage. Of the 106 individuals, 84 pars basilari and 96 pars laterali were included in the sample (Table 1).

Table 1: Number of pars basilari and pars laterali per age group

Age group	Pars basilari (n)	Pars laterali (n)
Early prenatal	28	30
Late prenatal	31	37
Postnatal	25	29
Total	84	96

Early prenatal: 20–30 gestational weeks. Late prenatal: 30–40 gestational weeks. Postnatal: birth–7.5 months.

The left and right pars laterali tend to be highly symmetrical (Figueiro et al., 2022). Therefore, the convention of analysing the left bone was employed. In cases where the left pars lateralis was absent or excluded, the right bone was used (Thornton et al., 2023).

2.2. Methodology

Micro-CT scans of all included skeletal elements were collected at the MIXRAD facility of the South African Nuclear Energy Corporation (NECSA) using a Nikon XTH 225L micro-focus CT X-ray unit (Nikon Metrology, Leuven, Belgium). For each scan, the pars basilari and pars laterali from two individuals were secured in a single block of OASIS floral foam (OASIS Floral Products, Gauteng, South Africa). OASIS foam has a very low density and is, therefore, non-attenuating while ensuring no movement of the bones during the scanning process (Bouxsein et al., 2010). A plastic peg of uniform composition was used for density calibration between scans to ensure consistency.

The pars basilari were orientated vertically, with the spheno-occipital synchondrosis region lodged into the foam and the anterolateral maxima facing upwards. The pars laterali were positioned so that the temporal mastoid aspects were wedged in the foam and the condylar and jugular limbs were aligned with the vertical axis of the scanner. A single spherical piece of Prestik mounting putty (Bostick, Gauteng, South Africa) was placed on one side of the peg for identification purposes.

The mounted bones were placed on the rotating sample manipulator, which facilitated scanning across 360^0. X-ray source scanning parameters were set to a voltage of 100 kV and current of 100 µA. The rotating sample manipulator was positioned to produce an isotropic voxel size of 100 μm^3. A 0.1 mm thick aluminium filter was used to correct for beam hardening artefacts resulting from the polychromatic nature of the x-ray beam by absorbing the lower-

density photons (Bouxsein et al., 2010). One thousand 2D angle images were obtained within an optimised time to produce a resolution ranging between 0.023 and 0.050 µm.

The raw angle data, consisting of the 2D angle images, was reconstructed into a 3D volume file using NIKON CTPro software version 4.4.3 (Nikon Metrology, Leuven, Belgium). Reconstruction was based on the Feldkamp filtered back-projection algorithm, built into the software (du Plessis et al., 2017). Corrections to beam hardening, noise reduction, and mild image enhancement were employed to ensure accurate and clear volumes for further analysis.

Subsequent to volume construction, VGStudio Max version 2.2 (Volume Graphics GmbH, Heidelberg, Germany) was used for further digital processing and analysis of the study sample volumes. Each skeletal element was isolated from the background and other bones using software-specific tools and subjected to a surface determination analysis. A surface determination analysis identifies and segments the surfaces of trabecular bone from the surrounding bone tissue, thus defining the boundaries from which measurements are calculated (Volume Graphics GmbH, 2013).

The orientation of the volumes was standardised by aligning each slice to a transverse reference plane to ensure consistency in analysis across different samples (Figure 1 and Figure 2). The bulk of the pars lateralis and pars lateralis is anatomically situated within the transverse plane, and thus a transverse reference plane provides consistent and relevant anatomical

references for orientation. The reference planes were established based on distinct morphological landmarks that are present across the age categories. The reference planes that were established on each pars basilaris are illustrated in the transverse (Figure 1a), sagittal (Figure 1b) and coronal (Figure 1c) views in Figure 1. The landmarks used to establish the reference plane for the pars basilaris included the horns for the occipital condyle on the extracranial surfaces of the left and right posterior-most projections of the pars basilaris, i.e., the anterolateral maxima of the foramen magnum (landmarks 1 and 2; Figure 1d-e), the left and right anterior-most projections on the extracranial surface of the spheno-occipital synchondrosis (landmarks 3 and 4; Figure 1e-f), and the midline point on the extracranial border of the spheno-occipital synchondrosis (landmark 5, Figure 1f).

The reference planes that were established on each pars laterali are illustrated in the coronal (Figure 2a) and transverse views (Figure 2b). The reference plane of the pars lateralis was established between the following landmarks: the posterior border of the jugular limb (landmark 1; Figure 2c-d), the angle on the medial border of the pars lateralis corresponding with the lateral borders of the foramen magnum (landmark 2; Figure 2c-d), the primary ossification site on the intracranial surface (landmark 3; Figure 2d), the posterior-most corner on the medial border of the pars lateralis (landmark 4; Figure 2c-e), the midline point on the mastoid temporal border (landmark 5; Figure 2d-e) and the immature jugular process (landmark 6; Figure 2d-e).

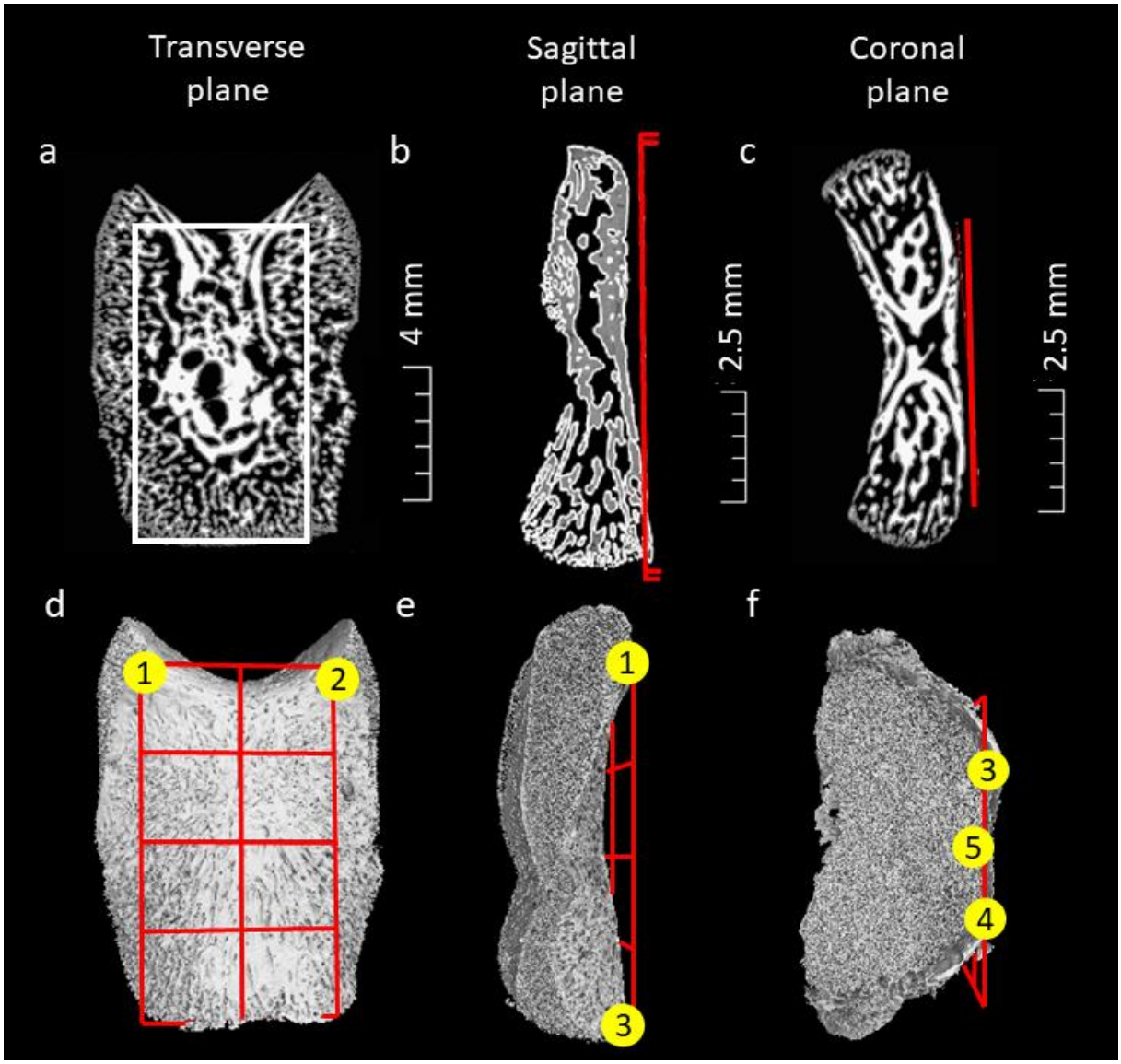


Figure 1: Reference planes for the pars basilaris: (a) Transverse view: white border represents reference plane. (b) Sagittal view: red line represents reference plane. (c) Coronal view: red line represents reference plane. (d) 3D reconstruction of the extracranial aspect of the early prenatal pars basilaris. (e) 3D reconstruction of lateral aspects of early prenatal pars basilaris. (f) 3D reconstruction of the spheno-occipital region of the early prenatal pars basilaris. Yellow circles represent landmarks: (landmarks 1 and 2): horns for the occipital condyle on the extracranial surfaces of the left and right posterior most projections of the pars basilaris. (landmarks 3 and 4): left and right anterior most projections on the extracranial surface of the spheno-occipital synchondrosis. (landmark 5): midline point on the extracranial spheno-occipital border. Images were generated using VGStudio Max V2.2 software (Volume Graphics GmbH, Heidelberg, Germany).

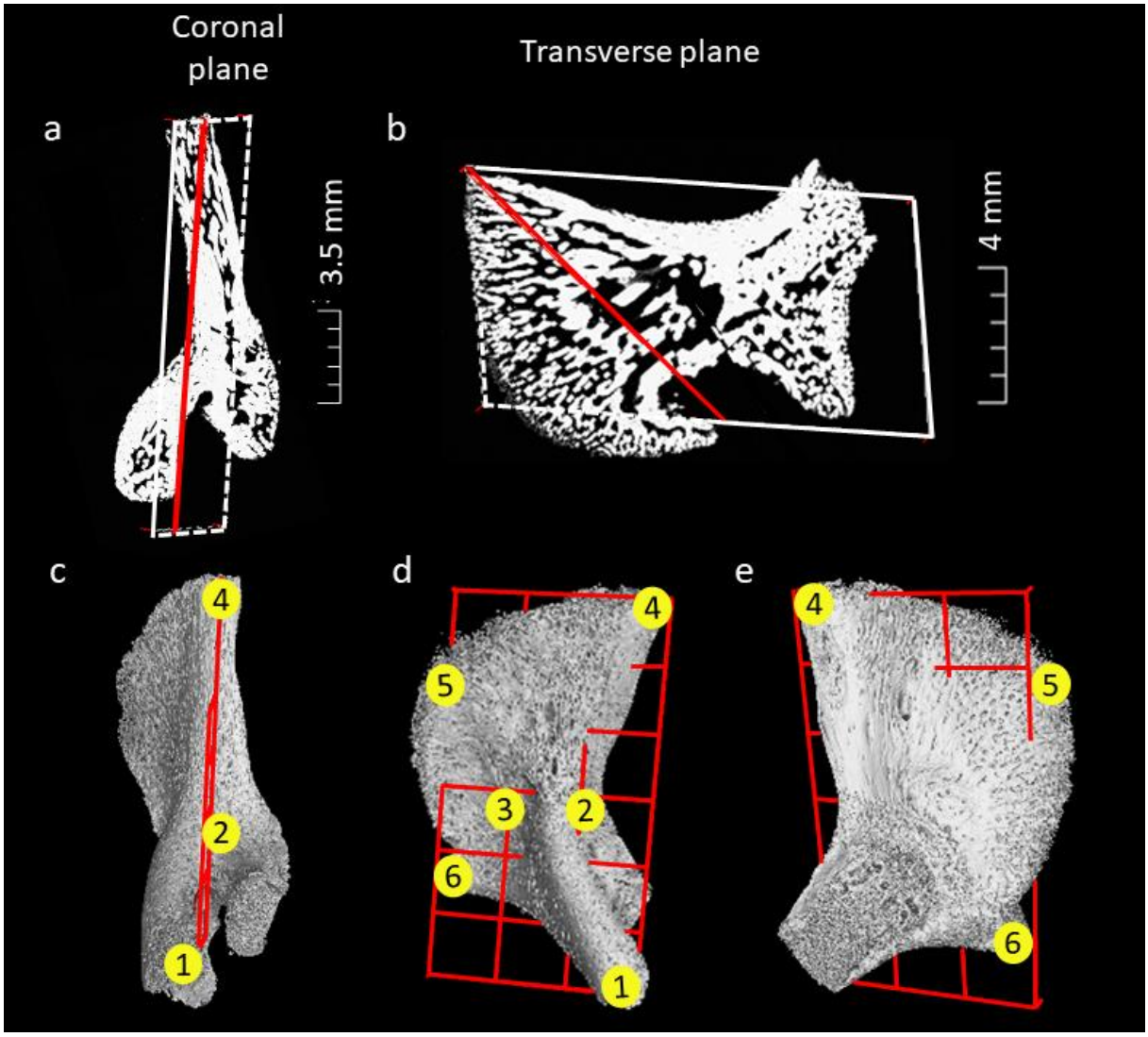


Figure 2: Reference planes for the pars lateralis: (a) Coronal view: white border and red line represent reference plane. (b) Transverse view: white border and red line represent reference plane. (c) 3D reconstruction of the hypoglossal region of the early prenatal pars lateralis. (d) 3D reconstruction of the intracranial aspect of the early prenatal pars lateralis. (e) 3D reconstruction of the extracranial aspect of the early prenatal pars lateralis. Yellow circles represent landmarks: (landmark 1): posterior border of the jugular limb. (landmark 2): angle on the medial border of the pars lateralis corresponding with the lateral borders of the foramen magnum. (landmark 3): primary ossification site on the intracranial surface. (landmark 4): posterior most corner on the medial border of the pars lateralis. (landmark 5): midline point on the mastoid temporal border. (landmark 6): immature jugular process. Images were generated using VGStudio Max V2.2 software (Volume Graphics GmbH, Heidelberg, Germany).

To assess the internal architecture within the various areas of each skeletal element, seven regions of interest (ROIs) were selected across each pars basilaris (Table 2, Figure 3a-c) and pars lateralis (Table 2; Figure 3d-f). The ROIs were positioned and sized so that there was no overlap between neighbouring ROIs and each ROI was made to fit entirely within the

trabecular structure of the bone. Owing to the size differences between the age groups, a range of ROI sizes was used to represent the relative area of each ROI. The radius of each ROI ranged between 0.5-1.25mm and the thickness ranged between 0.5-1.0mm. The primary ossification site (ROI 5) of the pars lateralis was excluded in cases where the posterior condylar canal was present such that the trabecular network could not be assessed in that region (n=13).

Table 2: Regions of interest selected on the pars basilaris and pars lateralis

ROI	Pars basilaris	Pars lateralis
1	Right anterolateral maxima of the foramen magnum border (right posterior most angle of the pars basilaris)	Jugular limb
2	Left anterolateral maxima of the foramen magnum border (left posterior most angle of the pars basilaris)	Condylar limb
3	Anterior foramen magnum border (angle on the posterior border of the pars basilaris)	Lateral foramen magnum border (angle on the medial border of the pars lateralis)
4	Primary ossification site	Posteromedial corner
5	Right lateral angle	Primary ossification site*
6	Left lateral angle	Jugular process
7	Spheno-occipital synchondrosis	Mastoid temporal border

*Excluded if posterior condylar canals obscured trabecular network in the region

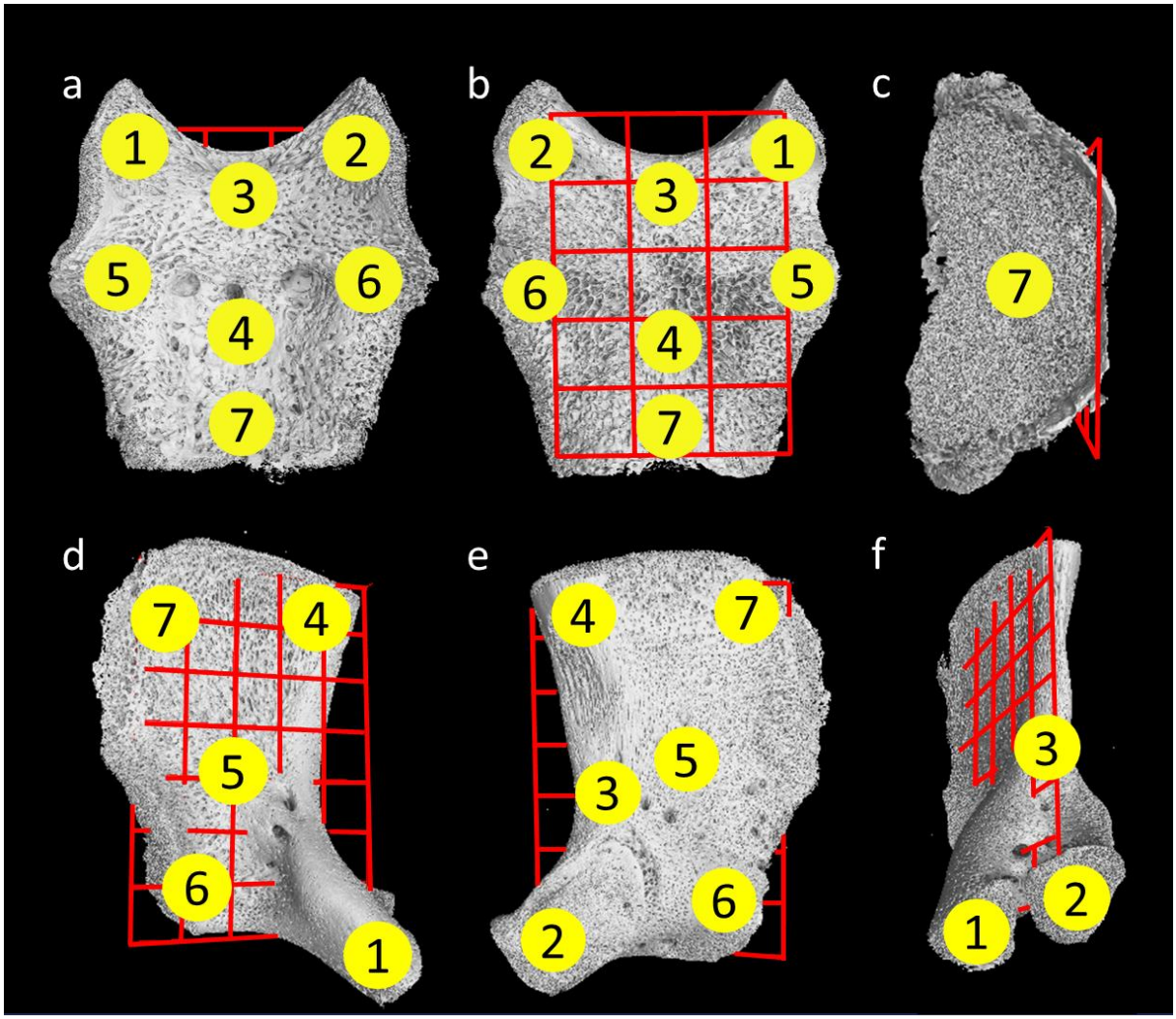


Figure 3: Regions of Interest (ROI) for the pars basilaris and pars lateralis. Pars basilaris: (a) 3D reconstruction of the intracranial aspect of the late prenatal pars basilaris. (b) 3D reconstruction of the extracranial aspect of the late prenatal pars basilaris. (c) 3D reconstruction of the spheno-occipital region of the late prenatal pars basilaris. Pars basilaris regions of interest: (ROI 1): right anterolateral maxima of the foramen magnum (right posterior most angle of the pars basilaris). (ROI 2): left anterolateral maxima of the foramen magnum (left posterior most angle of the pars basilaris). (ROI 3): anterior foramen magnum border (angle on the posterior border of the pars basilaris). (ROI 4): primary ossification site. (ROI 5): right lateral angle. (ROI 6): left lateral angle. (ROI 7): spheno-occipital synchondrosis. **Pars lateralis:** (d) 3D reconstruction of the intracranial aspect of the late prenatal pars lateralis. (e) 3D reconstruction of the extracranial aspect of the late prenatal pars lateralis. (f) 3D reconstruction of the hypoglossal region of the late prenatal pars lateralis. Pars lateralis regions of interest: (ROI 1): jugular limb. (ROI 2): condylar limb. (ROI 3): lateral foramen magnum border (angle on the medial border of the pars lateralis). (ROI 4): posteromedial corner. (ROI 5): primary ossification site. (ROI 6): jugular process. (ROI 7): mastoid temporal border. Images were generated using VGStudio Max V2.2 software (Volume Graphics GmbH, Heidelberg, Germany).

The investigation of the internal architecture required a comprehensive analysis of each ROI for each pars basilaris and pars lateralis element. A series of internal architectural parameters were generated using functions built into the VGstudio Max software (Volume Graphics GmbH, Heidelberg, Germany) (Table 3). The trabecular architectural parameters included bone volume fraction (BV/TV), bone surface area fraction (BS/BV), trabecular thickness (TbTh), trabecular number (TbN), trabecular separation (TbSp), mean grey value (MGV), and degree of anisotropy (DA) (Bouxsein et al., 2010) (Table 3).

Table 3: Definitions and descriptions of trabecular bone morphometric indices (adapted from Bouxsein et al., 2010)

Abbreviation	Variable	Description	Unit
BV/TV	Bone volume fraction	Ratio of bone volume within an ROI to the total volume of ROI, including both bone and non-bone elements	-
BS/BV	bone surface area fraction	Ratio of the surface area of segmented bone within an ROI to the bone volume within the ROI	mm^2/mm^3
TbTh	Trabecular thickness	Average thickness of trabeculae	mm
TbN	Trabecular number	Average number of trabecular per millimetre	mm^{-1}
TbSp	Trabecular separation	Average distance between trabeculae	mm
DA	Degree of anisotropy	Degree of preferential alignment of trabeculae in a specific direction. 0=completely isotropic (uniform structure with no directional dependence). 1=completely anisotropic (non-uniform structure, with significant directional dependence)	-
MGV	Mean grey value	The sum of the grey values of all the voxels within an ROI divided by the total number of voxels in that ROI	-

- Unitless measurement

Isotropy refers to a property of bone tissue where its mechanical and physical structure are uniform (Bouxsein et al., 2010; Oftadeh et al., 2015). Anisotropic bone consists of trabeculae aligned in a specific direction (Bouxsein et al., 2010; Oftadeh et al., 2015). Isotropic bone has evenly distributed trabeculae that are oriented in various directions (Bouxsein et al., 2010; Oftadeh et al., 2015). Trabeculae tend to become more anisotropic when adapting to mechanical loads in a specific direction and less anisotropic when the mechanical load is reduced or becomes more evenly distributed. Degree of anisotropy (DA) is a value ranging between 0 and 1 that describes the degree to which trabeculae are aligned in a specific direction (Bouxsein et al., 2010). A value of 0 is completely isotropic, i.e. the structure is uniform with no directional dependence (Bouxsein et al., 2010). A value of 1 denotes a completely anisotropic structure where the trabeculae are aligned in the direction of the mechanical strain (Bouxsein et al., 2010).

The digital volumes used to analyse each skeletal element consist of discrete voxel units. Voxels are analogous to pixels but exist in 3D and are cubic (Bouxsein et al., 2010; Volume Graphics GmbH, 2013; du Plessis et al., 2017). Each voxel holds a position in the 3D space and is assigned a single colour value on the grey spectrum ranging from 0–65535 (Volume Graphics GmbH, 2013; du Plessis et al., 2017). The colour value, known as the grey value, represents the density of that region (Volume Graphics GmbH, 2013; du Plessis et al., 2017). During micro-CT scanning, denser regions were more attenuating and, therefore, absorbed more X-rays, resulting in a lower voxel intensity (Volume Graphics GmbH, 2013; du Plessis et al., 2017). During reconstruction, the values were inverted so that the densest regions are represented by the brightest voxels, i.e., the voxels with the highest grey values (Volume Graphics GmbH,

2013; du Plessis et al., 2017). The mean grey value (MGV) takes the average grey value of all the voxels within an ROI and thus represents the overall density of the entire ROI (Volume Graphics GmbH, 2013; du Plessis et al., 2017).

2.3. Statistical analysis

All data was analysed using RStudio developed for R software version 4.2.1 (R Studio Core Team, Boston, MA, USA). Owing to the large number of variables assessed, a Hense-Zirkler multivariate normality test was used to test the normality of the sample (Henze & Zirkler, 1990). Where the data was parametric, descriptive statistics included the means and standard deviations. Non-parametric data was assessed using medians and interquartile ranges (IQR).

A multivariate analysis of variance (MANOVA) was used to ascertain the relationship between each age category (early prenatal, late prenatal and postnatal) and the trabecular parameters. Where significant results were found, a Dunn's post hoc test was used for pairwise comparisons of each architectural variable (Dunn, 1964). Corresponding ROIs were compared between the early prenatal and late prenatal groups and between the late prenatal and postnatal groups. Comparisons were not made between the early prenatal and postnatal groups due to the large age gap between them, which would overlook important developmental changes occurring in the late prenatal stage. An additional set of MANOVAs with Dunn's post hoc tests was conducted between different ROIs within each age group for each architectural variable. For all MANOVAs and post-hoc tests, $p \leq 0.05$ was considered statistically significant. This approach allowed for detailed comparisons of the trabecular architecture within and across different age groups.

Intra-observer repeatability was measured by having the primary investigator place ROIs on a subset of 12 pars basilari and 12 pars laterali, and then repeat the placement on the same bones after a suitable time interval to avoid recall bias. The trabecular parameters from both sessions were then compared using Lin's concordance correlation (Allan, 1982). Inter-observer reproducibility was assessed by having an independent observer place ROIs on the same subset 12 pars basilari and 12 pars laterali, using the same anatomical landmarks and guidelines. The primary investigator then repeated the placement independently. Trabecular parameters from both observers were compared to determine the level of agreement using a Lin's concordance correlation (Allan, 1982). For both the Inter- and intra-observer error tests a value between 81 – 100% was indicative of a high level of repeatability (Allan, 1982).

Chapter 3: Results

The Henze-Zirkler test for multivariate normality indicated that the data was not normally distributed (HZ = 9.71, $p \leq 0.01$) and therefore, medians and interquartile ranges (IQR) have been used to represent that data. Given the broad developmental range encompassed by the early prenatal, late prenatal and postnatal groups, outliers were retained in the analysis as they were considered representative of variability within developmental stages rather than data entry or measurement errors.

The Inter-observer error repeatability for the combined pars lateralis and pars basilaris ranged between 70% and 99% (Appendix B). Intra-observer error repeatability ranged between 70% and 99%. Mean grey value (MGV) was the parameters with the highest degree of repeatability (99%), whereas trabecular thickness (TbTh) had the lowest degree of repeatability (70% - 97%) (Appendix B). For both inter- and intra-observer error of the pars basilaris, the highest repeatability was observed in the anterolateral maxima (ROI 1 and ROI 2, 93% - 99%) (Appendix B). The lowest level of repeatability occurred at the primary ossification site (ROI 4, 70% - 99%) and the lateral angles (ROI 5 and 6, 75% - 99%) (Appendix B). For both inter- and intra-observer error of the pars lateralis, the highest repeatability was observed in the posterior-most corner (ROI 4, 82% – 99%) (Appendix B). The lowest level of repeatability occurred at the condylar limb (ROIs 2, 71% - 99%) and jugular process (ROI 6, 71% - 99%) (Appendix B).

3.1. Bone volume fraction (BV/TV), bone surface area fraction (BS/BV)

3.1.1. Pars basilaris

The median BV/TV ranged between 0.39 (0.30-0.46) and 0.58 (0.46-0.67) within the early prenatal pars basilaris, 0.45 (0.41-0.62) and 0.73 (0.64-0.81) within the late prenatal pars basilaris , and 0.40 (0.32-0.54) and 0.77 (0.70-0.80)within the postnatal group (Table 4, Figure 4a). The highest median BV/TV was observed in the anterior foramen magnum border (ROI 3) in the early prenatal (Median: 0.58, IQR: 0.46–0.67), late prenatal (Median: 0.73, IQR: 0.64–0.81), and postnatal (Median: 0.77, IQR: 0.70–0.80) pars basilaris (Table 4, Figure 4a). Within the early prenatal pars basilaris, the lowest median BV/TV was observed in the right lateral angle (ROI 5) (Median: 0.39, IQR: 0.32–0.47), left lateral angle (ROI 6) (Median: 0.39, IQR: 0.34–0.51), and spheno-occipital synchondrosis (ROI 7) (Median: 0.39, IQR: 0.30–0.46) (Table 4, Figure 4a). Within the late prenatal pars basilaris, the lowest median BV/TV was observed in the right lateral angle (ROI 5) (Median: 0.45, IQR: 0.41–0.62) and left lateral angle (ROI 6) (Median: 0.48, IQR: 0.42–0.66) (Table 4, Figure 4a). Within the postnatal pars basilaris, the lowest median BV/TV was observed in the right lateral angle (ROI 5) (Median: 0.45, IQR: 0.31–0.52) and left lateral angle (ROI 6) (Median: 0.40, IQR: 0.32–0.54) (Table 4, Figure 4a).

Table 4: Median values and pairwise comparisons of bone volume fraction (BV/TV) and bone surface area fraction (BS/BV) between the early prenatal, late prenatal and postnatal pars basilaris for each region of interest (ROI)

Variable	ROI	Median (Q_1-Q_3)			Group comparisons (p<0.05)	
		Early prenatal (n=28)	Late prenatal (n=31)	Postnatal (n=25)	Early prenatal vs. late prenatal	Late prenatal vs. postnatal
BV/TV	1	0.42 (0.37-0.47)	0.54 (0.44-0.66)	0.52 (0.46-0.57)	0.00*	1.00
	2	0.42 (0.37-0.49)	0.60 (0.44-0.66)	0.53 (0.46-0.59)	0.00*	0.85
	3	0.58 (0.46-0.67)	0.73 (0.64-0.81)	0.77 (0.70-0.80)	0.00*	0.32
	4	0.51 (0.40-0.61)	0.59 (0.50-0.70)	0.53 (0.42-0.61)	0.06	0.56
	5	0.39 (0.32-0.47)	0.45 (0.41-0.62)	0.45 (0.31-0.52)	0.04*	0.42
	6	0.39 (0.34-0.51)	0.48 (0.42-0.66)	0.40 (0.32-0.54)	0.03*	0.04*
	7	0.39 (0.30-0.46)	0.51 (0.45-0.77)	0.51 (0.42-0.55)	0.00*	0.60
BS/BV (mm^2/mm^3)	1	24.41 (21.02-26.42)	17.66 (11.96-21.19)	18.41 (15.61-19.64)	0.00*	1.00
	2	23.65 (20.54-27.37)	15.62 (11.39-20.10)	18.03 (15.24-20.07)	0.00*	1.00
	3	10.15 (9.05-14.50)	6.03 (4.86-7.19)	5.95 (4.41-7.38)	0.00*	0.39
	4	13.38 (10.79-18.30)	9.58 (7.06-12.66)	10.82 (9.19-13.46)	0.00*	1.00
	5	26.10 (20.70-29.85)	17.37 (12.12-21.30)	17.97 (14.55-20.12)	0.00*	1.00
	6	25.02 (20.27-28.84)	16.80 (12.29-20.68)	18.92 (15.32-21.25)	0.00*	0.61
	7	28.16 (22.62-32.05)	17.83 (8.86-22.74)	20.65 (17.63-23.60)	0.00*	0.71

Early prenatal: 20–30 gestational weeks. Late prenatal: 30–40 gestational weeks. Postnatal: birth–7.5 months. Pars basilaris regions of interest: (ROI 1): right anterolateral maxima of the foramen magnum. (ROI 2): left anterolateral maxima of the foramen magnum. (ROI 3): anterior foramen magnum border. (ROI 4): primary ossification site. (ROI 5): right lateral angle. (ROI 6): left lateral angle. (ROI 7): spheno-occipital synchondrosis. *Significant value (p≤0.05). Values <0.01 are represented as 0.00.

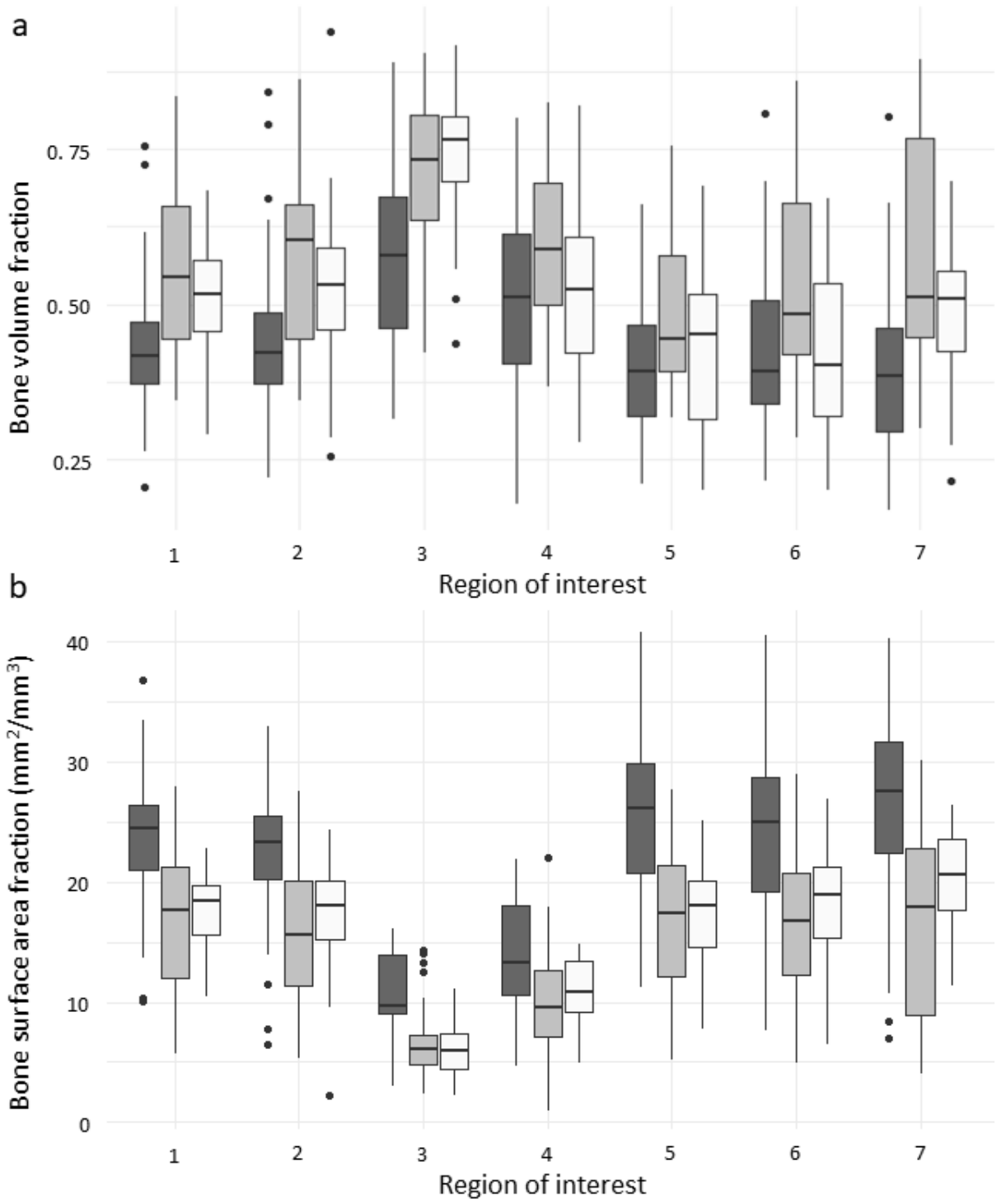


Figure 4: Regional variations of (a) bone volume fraction (BV/TV) and (b) bone surface area fractions (BS/BV) in the pars basilaris. Dark grey: early prenatal (20–30 gestational weeks, n=28). Light grey: late prenatal (30–40 gestational weeks, n=31). White: postnatal (birth–7.5 months, n=25). Dots represent outliers. Pars basilaris regions of interest: (ROI 1): right anterolateral maxima of the foramen magnum. (ROI 2): left anterolateral maxima of the foramen magnum. (ROI 3): anterior foramen magnum border. (ROI 4): primary ossification site. (ROI 5): right lateral angle. (ROI 6): left lateral angle. (ROI 7): spheno-occipital synchondrosis. Graphs were created in RStudio using ggplot2 (Wickham, 2016).

The median BS/BV ranged between 10.15 (9.05-14.50) and 28.16 (22.62-32.05) within the early prenatal pars basilaris, 6.03 (4.86-7.19) and 17.83 (8.86-22.74) within the late prenatal pars basilaris , and5.95 (4.41-7.38) and 20.65 (17.63-23.60) within the postnatal group (Table 4, Figure 4b). The highest median BS/BV was observed in the spheno-occipital synchondrosis (ROI 7) in the early prenatal (Median: 28.16 mm^2/mm^3, IQR: 22.62–32.05), late prenatal (Median: 17.83 mm^2/mm^3, IQR: 8.86–22.74), and postnatal (Median: 20.65 mm^2/mm^3, IQR: 17.63–23.60) age groups (Table 4, Figure 4b). The lowest median BS/BV was observed in the anterior foramen magnum border (ROI 3) within the early prenatal (Median: 10.15 mm^2/mm^3, IQR: 9.05–14.50), late prenatal (Median: 6.03 mm^2/mm^3, IQR: 4.86–7.19), and postnatal (Median: 5.95 mm^2/mm^3, IQR: 4.41–7.38) pars basilaris (Table 4, Figure 4b)

Comparisons between age groups

The BV/TV of the late prenatal pars basilaris was significantly greater than the early prenatal group in all regions (ROI 1, $p \leq 0.01$; ROI 2, $p \leq 0.01$; ROI 3, $p \leq 0.01$; ROI 5, $p \leq 0.04$; ROI 6, $p \leq 0.03$; ROI 7, $p \leq 0.01$), except the primary ossification site (ROI 4, $p > 0.05$) which did not significantly differ between the prenatal age groups (Table 4, Figure 4a). The right lateral angle (ROI 6) of the pars basilaris had a significantly lower BV/TV ($p \leq 0.04$) in the postnatal group compared to the late prenatal group (Table 4, Figure 4a). None of the other ROIs significantly differed in BV/TV ($p > 0.05$) between the late prenatal and postnatal age groups (Table 4, Figure 4a).

The late prenatal pars basilaris had a significantly lower BS/BV compared to the early prenatal pars basilaris across all seven regions (ROI 1, $p \leq 0.01$; ROI 2, $p \leq 0.01$; ROI 3, $p \leq 0.01$; ROI 4, $p \leq 0.01$; ROI 5, $p \leq 0.01$; ROI 6, $p \leq 0.01$; ROI 7, $p \leq 0.01$) (Table 4, Figure 4b). No significant

differences ($p \leq 0.05$) in BS/BV were observed between the late prenatal and postnatal pars basilaris (Table 4, Figure 4b).

Comparisons within age groups

Within the early prenatal pars basilaris, the anterior foramen magnum border (ROI 3) had a significantly higher BV/TV compared to the anterolateral maxima (ROI 1, $p \leq 0.01$ and ROI 2, $p \leq 0.02$), lateral angles (ROI 5, $p \leq 0.01$ and ROI 6, $p \leq 0.01$), and spheno-occipital synchondrosis (ROI 7, $p \leq 0.01$) (

Table 5, Figure 4a). In addition, the primary ossification site (ROI 4) had a significantly higher BV/TV ($p \leq 0.05$) compared to the spheno-occipital synchondrosis (ROI 7) within the early prenatal pars basilaris (

Table 5, Figure 4a).

No significant differences in BV/TV ($p>0.05$) were observed between the anterior foramen magnum border (ROI 3) and the primary ossification site (ROI 4) within the early prenatal pars basilaris (

Table 5, Figure 4a). In addition, no significant differences in BV/TV ($p>0.05$) were observed between the anterolateral maxima (ROI 1 and ROI 2), primary ossification site (ROI 4), and lateral angles (ROI 5 and ROI 6) within the early prenatal pars basilaris (

Table 5, Figure 4a). Furthermore, no significant differences in BV/TV ($p>0.05$) were observed between the anterolateral maxima (ROI 1 and ROI 2), lateral angles (ROI 5 and ROI 6) and spheno-occipital synchondrosis (ROI 7) within the early prenatal pars basilaris (

Table 5, Figure 4a).

Table 5: Pairwise comparisons of bone volume fraction (BV/TV) and bone surface area fraction (BS/BV) between regions of interest (ROI) within the early prenatal, late prenatal and postnatal pars basilaris

ROI comparisons	BV/TV			BS/BV (mm^2/mm^3)		
	Early prenatal (n=28)	Late prenatal (n=31)	Postnatal (n=25)	Early prenatal (n=28)	Late prenatal (n=31)	Postnatal (n=25)
1 vs 2	1.00	1.00	1.00	1.00	1.00	1.00
1 vs 3	0.01*	0.00*	0.00*	0.00*	0.00*	0.00*
2 vs 3	0.02*	0.01*	0.00*	0.00*	0.00*	0.00*
1 vs 4	0.67	1.00	1.00	0.00*	0.00*	0.00*
2 vs 4	1.00	1.00	1.00	0.00*	0.02*	0.00*
3 vs 4	1.00	0.07	0.00*	1.00	0.26	0.83
1 vs 5	1.00	1.00	0.26	1.00	1.00	1.00
2 vs 5	1.00	0.85	0.20	1.00	1.00	1.00
3 vs 5	0.00*	0.00*	0.00*	0.00*	0.00*	0.00*
4 vs 5	0.09	0.27	0.08	0.00*	0.00*	0.00*
1 vs 6	1.00	1.00	0.22	1.00	1.00	1.00
2 vs 6	1.00	1.00	0.16	1.00	1.00	1.00
3 vs 6	0.00*	0.00*	0.00*	0.00*	0.00*	0.00*
4 vs 6	0.34	1.00	0.07	0.00*	0.01*	0.00*
5 vs 6	1.00	1.00	1.00	1.00	1.00	1.00
1 vs 7	1.00	1.00	1.00	1.00	1.00	1.00
2 vs 7	1.00	1.00	1.00	1.00	1.00	1.00
3 vs 7	0.00*	0.03*	0.00*	0.00*	0.00*	0.00*
4 vs 7	0.05*	1.00	1.00	0.00*	0.01*	0.00*
5 vs 7	1.00	0.50	0.85	1.00	1.00	1.00
6 vs 7	1.00	1.00	0.72	1.00	1.00	1.00

Early prenatal: 20–30 gestational weeks. Late prenatal: 30–40 gestational weeks. Postnatal: birth–7.5 months. Pars basilaris regions of interest: (ROI 1): right anterolateral maxima of the foramen magnum. (ROI 2): left anterolateral maxima of the foramen magnum. (ROI 3): anterior foramen magnum border. (ROI 4): primary ossification site. (ROI 5): right lateral angle. (ROI 6): left lateral angle. (ROI 7): spheno-occipital synchondrosis. *Significant value ($p \leq 0.05$). Values <0.01 are represented as 0.00.

Within the late prenatal pars basilaris, the anterior foramen magnum border (ROI 3) had a significantly higher BV/TV compared to all other ROIs (ROI 1, $p \leq 0.01$; ROI 2, $p \leq 0.01$; ROI 5, $p \leq 0.01$; ROI 6, $p \leq 0.01$; ROI 7, $p \leq 0.03$), except the primary ossification site (ROI 4, $p > 0.05$) (

Table 5, Figure 4a). No significant differences in BV/TV ($p>0.05$) were observed between the anterolateral maxima (ROI 1 and 2), primary ossification site (ROI 4), lateral angles (ROI 5 and 6), and spheno-occipital synchondrosis (ROI 7) within the late prenatal pars basilaris (

Table 5, Figure 4a).

Within the postnatal pars basilaris, the anterior foramen magnum border (ROI 3) had a significantly higher BV/TV compared to all other ROIs (ROI 1, $p \leq 0.01$; ROI 2, $p \leq 0.01$; ROI 4, $p \leq 0.01$; ROI 5, $p \leq 0.01$; ROI 6, $p \leq 0.01$; ROI 7, $p \leq 0.01$) (

Table 5, Figure 4a). The BV/TV of the anterolateral maxima (ROI 1 and 2), primary ossification site (ROI 4), lateral angles (ROI 5 and 6), and spheno-occipital synchondrosis (ROI 7) did not significantly differ ($p>0.05$) from one another within the postnatal pars basilaris (

Table 5, Figure 4a).

Within all three age groups, the anterior foramen magnum border (ROI 3) and the primary ossification site (ROI 4) of the pars basilaris both had a significantly lower BS/BV ($p \leq 0.05$) compared to all other ROIs (

Table 5, Figure 4b). No significant differences in BS/BV ($p>0.05$) were observed between the anterior foramen magnum border (ROI 3) and the primary ossification site (ROI 4) within any of the age groups assessed (

Table 5, Figure 4b). No significant differences in BS/BV ($p>0.05$) were observed between the anterolateral maxima (ROI 1 and 2), lateral angles (ROI 5 and 6), and spheno-occipital synchondrosis (ROI 7) within any of the age groups (

Table 5, Figure 4b).

3.1.2. Pars lateralis

The median BV/TV ranged between 0.24 (0.21-0.29) and 0.56 (0.52-0.66) within the early prenatal pars lateralis, 0.29 (0.21-0.37) and 0.67 (0.57-0.82) within the late prenatal pars lateralis, and 0.31 (0.28-0.36) and 0.69 (0.56-0.77) within the postnatal group (Table 6, Figure 5a). The highest median BV/TV in the pars lateralis was observed in the condylar limb (ROI 2) during the early prenatal stage (Median: 0.56, IQR: 0.52–0.66), in the primary ossification site (ROI 5) during the late prenatal stage (Median: 0.67, IQR: 0.57–0.82), and in the lateral foramen magnum border (ROI 3) during the postnatal stage (Median: 0.69, IQR: 0.56–0.77) (Table 6, Figure 5a). The lowest median BV/TV was observed in the mastoid temporal border (ROI 7) with the early prenatal (Median: 0.24, IQR: 0.21–0.29), late prenatal (Median: 0.29, IQR: 0.21–0.37), and postnatal (Median: 0.31, IQR: 0.28–0.36) pars lateralis (Table 6, Figure 5a).

The median BS/BV ranged between 12.15 (9.28-14.33) and 36.90 (34.60-40.32) within the early prenatal pars lateralis, 8.94 (7.01-12.62) and 29.53 (24.73-34.94) within the late prenatal pars lateral, and6.99 (5.04-8.10) and 27.27 (24.11-32.79) within the postnatal group (Table 6, Figure 5b). The highest median BS/BV was observed in the mastoid temporal border (ROI 7) in the early prenatal (Median: 36.90 mm^2/mm^3, IQR: 34.60–40.32), late prenatal (Median: 29.53 mm^2/mm^3, IQR: 24.73–34.94), and postnatal (Median: 27.27 mm^2/mm^3, IQR: 24.11–32.79) stages (Table 6, Figure 5b). The lowest median BS/BV was observed in the lateral foramen magnum border (ROI 3) in the early prenatal (Median: 12.15 mm^2/mm^3, IQR: 9.28–

14.33), late prenatal (Median: 9.23 mm^2/mm^3, IQR: 5.72–11.41), and postnatal (Median: 6.99 mm^2/mm^3, IQR: 5.04–8.10) stages (Table 6, Figure 5b).

Table 6: Median values and pairwise comparisons of bone volume fraction (BV/TV) and bone surface area fraction (BS/BV) between the early prenatal, late prenatal and postnatal pars lateralis for each region of interest (ROI)

Variable	ROI	Median (Q_1-Q_3)			Group comparisons ($p<0.05$)	
		Early prenatal (n=30)	Late prenatal (n=37)	Postnatal (n=29)	Early prenatal vs. late prenatal	Late prenatal vs. postnatal
BV/TV	1	0.39 (0.32-0.44)	0.47 (0.39-0.70)	0.44 (0.39-0.50)	0.01*	0.51
	2	0.56 (0.52-0.66)	0.63 (0.53-0.69)	0.59 (0.54-0.67)	0.19	0.43
	3	0.52 (0.45-0.60)	0.60 (0.51-0.79)	0.69 (0.56-0.77)	0.01*	0.32
	4	0.38 (0.33-0.41)	0.40 (0.34-0.53)	0.38 (0.32-0.45)	0.22	0.55
	5	0.47 (0.38-0.53)	0.67 (0.57-0.82)	0.66 (0.55-0.68)	0.00*	0.73
	6	0.39 (0.29-0.44)	0.43 (0.33-0.60)	0.40 (0.35-0.47)	0.07	0.77
	7	0.24 (0.21-0.29)	0.29 (0.21-0.37)	0.31 (0.28-0.36)	0.14	0.22
BS/BV (mm^2/mm^3)	1	25.90 (21.04-32.02)	19.62 (15.72-22.84)	20.61 (17.70-23.30)	0.00*	0.98
	2	19.14 (15.38-21.91)	14.62 (10.93-17.05)	14.25 (11.05-16.59)	0.00*	1.00
	3	12.15 (9.28-14.33)	9.23 (5.72-11.41)	6.99 (5.04-8.10)	0.00*	0.03*
	4	28.24 (25.69-33.51)	24.45 (20.55-27.50)	25.78 (23.09-27.53)	0.01*	0.47
	5	17.11 (13.93-19.72)	8.94 (7.01-12.62)	8.71 (7.13-12.82)	0.00*	1.00
	6	26.20 (22.45-30.08)	20.80 (16.49-24.37)	23.35 (19.01-25.59)	0.00*	0.35
	7	36.90 (34.60-40.32)	29.53 (24.73-34.94)	27.27 (24.11-32.79)	0.00*	0.26

Early prenatal: 20–30 gestational weeks. Late prenatal: 30–40 gestational weeks. Postnatal: birth–7.5 months. Pars lateralis regions of interest: (ROI 1): jugular limb. (ROI 2): condylar limb. (ROI 3): lateral foramen magnum border. (ROI 4): posteromedial corner. (ROI 5): primary ossification site. (ROI 6): jugular process. (ROI 7): mastoid temporal border. *Significant value ($p\leq0.05$). Values <0.01 are represented as 0.00.

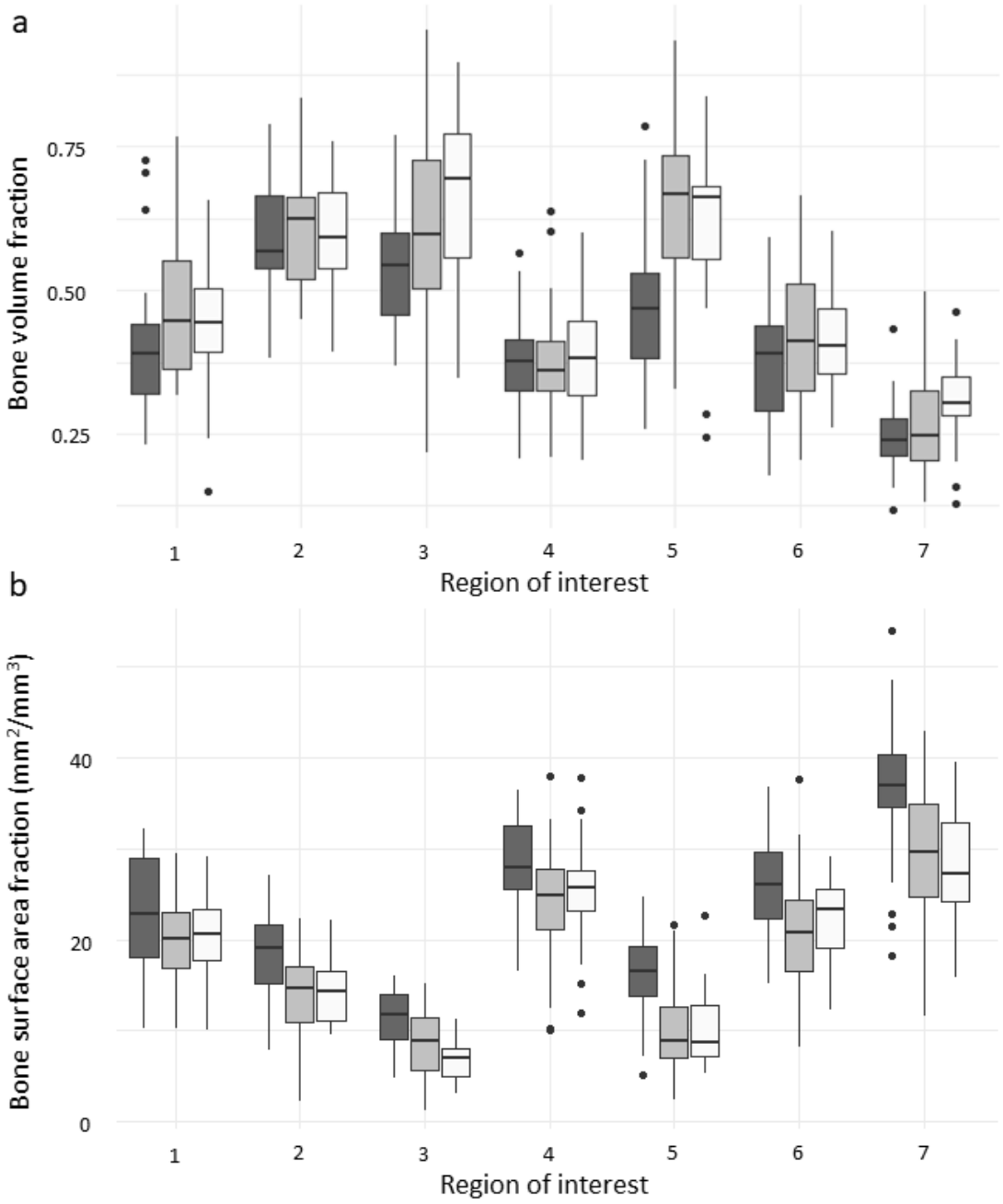


Figure 5: Regional variations of (a) bone volume fraction (BV/TV) and (b) bone surface area fractions (BS/BV) in the pars lateralis. Dark grey: early prenatal (20–30 gestational weeks, n=30). Light grey: late prenatal (30–40 gestational weeks, n=37). White: postnatal (birth–7.5 months, n=29). Dots represent outliers. Pars lateralis regions of interest: (ROI 1): jugular limb. (ROI 2): condylar limb. (ROI 3): lateral foramen magnum border. (ROI 4): posteromedial corner. (ROI 5): primary ossification site. (ROI 6): jugular process. (ROI 7): mastoid temporal border. Graphs were created in RStudio using ggplot2 (Wickham, 2016).

Comparisons between age groups

The BV/TV of the late prenatal pars lateralis was significantly higher compared to the early prenatal age group in the jugular limb (ROI 1, $p \leq 0.01$), lateral foramen magnum border (ROI 3, $p \leq 0.01$), and primary ossification site (ROI 5, $p \leq 0.01$) (Table 6, Figure 5a). The BV/TV of the condylar limb (ROI 2), posteromedial corner (ROI 4), jugular process (ROI 6), and mastoid temporal border (ROI 7) did not significantly differ ($p > 0.05$) between the prenatal age groups (Table 6, Figure 5a). No significant differences in BV/TV ($p > 0.05$) were observed between the late prenatal and postnatal pars lateralis across all seven ROIs (Table 6, Figure 5a).

The late prenatal pars lateralis had a significantly lower BS/BV compared to the early prenatal pars lateralis across all seven regions (ROI 1, $p \leq 0.01$; ROI 2, $p \leq 0.01$; ROI 3, $p \leq 0.01$; ROI 4, $p \leq 0.01$; ROI 5, $p \leq 0.01$; ROI 6, $p \leq 0.01$; ROI 7, $p \leq 0.01$) (Table 6, Figure 5b). The lateral foramen magnum border (ROI 3) had a significantly lower BS/BV ($p \leq 0.03$) in the postnatal pars lateralis compared to the late prenatal pars lateralis (Table 6, Figure 5b). No further statistically significant differences in BS/BV ($p > 0.05$) were observed between the late prenatal and postnatal age groups (Table 6, Figure 5b).

Comparisons within age groups

Within the early prenatal pars lateralis, the condylar limb (ROI 2) and lateral foramen magnum border (ROI 3) both had a significantly higher BV/TV ($p \leq 0.05$) compared to the jugular limb (ROI 1), posteromedial corner (ROI 4), jugular process (ROI 6), and mastoid temporal border (ROI 7) (Table 7, Figure 5a). The mastoid temporal border (ROI 7) had a significantly lower BV/TV compared to all other regions (ROI 1, $p \leq 0.01$; ROI 2, $p \leq 0.01$; ROI 3, $p \leq 0.01$; ROI 4,

p≤0.02; ROI 5, p≤0.01; ROI 6, p≤0.01) within the early prenatal age group (Table 7, Figure 5a). No significant differences in BV/TV (p>0.05) were observed between the condylar limb (ROI 2), lateral foramen magnum border (ROI 3), and primary ossification site (ROI 5) within the early prenatal pars lateralis (Table 7, Figure 5a). In addition, the BV/TV of the jugular limb (ROI 1), posteromedial corner (ROI 4), primary ossification site (ROI 5), and jugular process (ROI 6) did not significantly differ (p>0.05) from one another within the early prenatal pars lateralis (Table 7, Figure 5a).

Within the late prenatal pars lateralis, the condylar limb (ROI 2), lateral foramen magnum border (ROI 3), and primary ossification site (ROI 5) all had a significantly higher BV/TV (p≤0.05) compared to the posteromedial corner (ROI 4), jugular process (ROI 6), and mastoid temporal border (ROI 7) (Table 7, Figure 5a). In addition, the jugular limb (ROI 1) had a significantly higher BV/TV (p≤0.01) compared to the mastoid temporal border (ROI 7) within the late prenatal pars lateralis (Table 7, Figure 5a).

No significant differences in BV/TV (p>0.05) were observed between the jugular limb (ROI 1), condylar limb (ROI 2), lateral foramen magnum border (ROI 3), and the primary ossification site (ROI 5) within the late prenatal pars lateralis (Table 7, Figure 5a). In addition, no significant differences in BV/TV (p>0.05) were observed between the jugular limb (ROI 1), posteromedial corner (ROI 4), and jugular process (ROI 6) within the late prenatal pars lateralis (Table 7, Figure 5a). Furthermore, no significant differences in BV/TV (p>0.05) were observed between the posteromedial corner (ROI 4), jugular process (ROI 6), and mastoid temporal border (ROI 7) within the late prenatal pars lateralis (Table 7, Figure 5a).

Table 7: Pairwise comparisons of bone volume fraction (BV/TV) and bone surface area fraction (BS/BV) between regions of interest (ROI) within the early prenatal, late prenatal and postnatal pars lateralis

ROI comparisons	BV/TV			BS/BV (mm^2/mm^3)		
	Early prenatal (n=30)	Late prenatal (n=37)	Postnatal (n=29)	Early prenatal (n=30)	Late prenatal (n=37)	Postnatal (n=29)
1 vs 2	0.00*	0.20	0.00*	0.05*	0.14	0.11
1 vs 3	0.02*	0.54	0.00*	0.00*	0.00*	0.00*
2 vs 3	1.00	1.00	1.00	0.13	0.11	0.01*
1 vs 4	1.00	1.00	1.00	1.00	0.29	0.10
2 vs 4	0.00*	0.00*	0.00*	0.00*	0.00*	0.00*
3 vs 4	0.00*	0.00*	0.00*	0.00*	0.00*	0.00*
1 vs 5	1.00	0.14	0.00*	0.00*	0.00*	0.00*
2 vs 5	0.16	1.00	1.00	1.00	0.61	0.62
3 vs 5	1.00	1.00	1.00	1.00	1.00	1.00
4 vs 5	0.16	0.00*	0.00*	0.00*	0.00*	0.00*
1 vs 6	1.00	1.00	1.00	1.00	1.00	1.00
2 vs 6	0.00*	0.00*	0.00*	0.01*	0.01*	0.00*
3 vs 6	0.00*	0.01*	0.00*	0.00*	0.00*	0.00*
4 vs 6	1.00	1.00	1.00	1.00	1.00	1.00
5 vs 6	0.25	0.00*	0.00*	0.00*	0.00*	0.00*
1 vs 7	0.00*	0.00*	0.01*	0.00*	0.00*	0.02*
2 vs 7	0.00*	0.00*	0.00*	0.00*	0.00*	0.00*
3 vs 7	0.00*	0.00*	0.00*	0.00*	0.00*	0.00*
4 vs 7	0.02*	0.15	0.98	0.22	0.39	1.00
5 vs 7	0.00*	0.00*	0.00*	0.00*	0.00*	0.00*
6 vs 7	0.01*	0.10	0.27	0.02*	0.01*	0.78

Early prenatal: 20–30 gestational weeks. Late prenatal: 30–40 gestational weeks. Postnatal: birth–7.5 months. Pars lateralis regions of interest: (ROI 1): jugular limb. (ROI 2): condylar limb. (ROI 3): lateral foramen magnum border. (ROI 4): posteromedial corner. (ROI 5): primary ossification site. (ROI 6): jugular process. (ROI 7): mastoid temporal border. *Significant value ($p \leq 0.05$). Values <0.01 are represented as 0.00.

Within the postnatal group, the condylar limb (ROI 2), lateral foramen magnum border (ROI 3), and primary ossification site (ROI 5) of the pars lateralis all had a significantly higher BV/TV ($p \leq 0.05$) compared to the jugular limb (ROI 1), posteromedial corner (ROI 4), jugular process (ROI 6), and mastoid temporal border (ROI 7) (Table 7, Figure 5a). In addition, the jugular limb (ROI 1) had a significantly higher BV/TV ($p \leq 0.01$) compared to the mastoid temporal border (ROI 7) within the postnatal pars lateralis (Table 7, Figure 5a).

No significant differences in BV/TV ($p > 0.05$) were observed between the condylar limb (ROI 2), lateral foramen magnum border (ROI 3), and primary ossification site (ROI 5) within the postnatal pars lateralis (Table 7, Figure 5a). In addition, no significant differences in BV/TV ($p > 0.05$) were observed between the jugular limb (ROI 1), posteromedial corner (ROI 4), and jugular process (ROI 6) within the postnatal pars lateralis (Table 7, Figure 5a). Furthermore, no significant differences in BV/TV ($p > 0.05$) were observed between the posteromedial corner (ROI 4), jugular process (ROI 6), and mastoid temporal border (ROI 7) within the postnatal pars lateralis (Table 7, Figure 5a).

Within the early prenatal pars lateralis, the condylar limb (ROI 2), lateral foramen magnum border (ROI 3) and primary ossification site (ROI 5) all exhibited a significantly lower BS/BV ($p \leq 0.05$) compared to the jugular limb (ROI 1), posteromedial corner (ROI 4), jugular process (ROI 6), and mastoid temporal border (ROI 7) (Table 7, Figure 5b). The mastoid temporal border (ROI 7) had a significantly higher BS/BV compared to the jugular limb (ROI 1, $p \leq 0.01$), condylar limb (ROI 2, $p \leq 0.01$), lateral foramen magnum border (ROI 3, $p \leq 0.01$), primary

ossification site (ROI 5, p≤0.01), and jugular process (ROI 6, p≤0.02) within the early prenatal pars lateralis (Table 7, Figure 5b).

No significant differences in BS/BV (p>0.05) were observed between the condylar limb (ROI 2), lateral foramen magnum border (ROI 3), and primary ossification site (ROI 5) within the early prenatal pars lateralis (Table 7, Figure 5b). In addition, no significant differences in BS/BV (p>0.05) were observed between the jugular limb (ROI 1), posteromedial corner (ROI 4), and jugular process (ROI 6) (Table 7, Figure 5b). Furthermore, the BS/BV of the mastoid temporal border (ROI 7) did not significantly differ (p>0.05) from the posteromedial corner (ROI 4) in the early prenatal pars lateralis (Table 7, Figure 5b).

Within the late prenatal pars lateralis, the condylar limb (ROI 2) exhibited a significantly lower BS/BV compared to the posteromedial corner (ROI 4, p≤0.01), jugular process (ROI 6, p≤0.01), and mastoid temporal border (ROI 7, p≤0.01) (Table 7, Figure 5b). The lateral foramen magnum border (ROI 3) and primary ossification site (ROI 5) both exhibited a significantly lower BS/BV (p≤0.05) relative to the jugular limb (ROI 1), posteromedial corner (ROI 4), jugular process (ROI 6), and mastoid temporal border (ROI 7) (Table 7, Figure 5b). In addition, the jugular limb (ROI 1) and jugular process (ROI 6) both had a significantly lower BS/BV (p≤0.01) than the mastoid temporal border (ROI 7) (Table 7, Figure 5b).

No significant differences in BS/BV (p>0.05) were observed between the condylar limb (ROI 2), lateral foramen magnum border (ROI 3), and primary ossification site (ROI 5) within the

late prenatal pars lateralis (Table 7, Figure 5b). The BS/BV of the jugular (ROI 1) and condylar limbs (ROI 2) did not significantly differ ($p>0.05$) within the late prenatal pars lateralis (Table 7, Figure 5b). No significant differences in BS/BV ($p>0.05$) were observed between the jugular limb (ROI 1), posteromedial corner (ROI 4), and jugular process (ROI 6) within the late prenatal pars lateralis (Table 7, Figure 5b). Furthermore, the BS/BV of the mastoid temporal border (ROI 7) did not significantly differ ($p>0.05$) from the posteromedial corner (ROI 4) in the late prenatal age group (Table 7, Figure 5b).

Within the postnatal pars lateralis, the condylar limb (ROI 2) had a significantly lower BS/BV compared to the posteromedial corner (ROI 4, $p\leq0.01$), the jugular process (ROI 6, $p\leq0.01$), and mastoid temporal border (ROI 7, $p\leq0.01$) (Table 7, Figure 5b). The lateral foramen magnum border (ROI 3) had a significantly lower BS/BV compared to the rest of postnatal pars lateralis (ROI 1, $p\leq0.01$; ROI 2, $p\leq0.01$; ROI 4, $p\leq0.01$; ROI 6, $p\leq0.01$; ROI 7 $p\leq0.01$), except for the primary ossification site (ROI 5, $p>0.05$) (Table 7, Figure 5b). The primary ossification site (ROI 5) had a significantly lower BS/BV compared to the jugular limb (ROI 1, $p\leq0.01$), posteromedial corner (ROI 4, $p\leq0.01$), the jugular process (ROI 6, $p\leq0.01$), and mastoid temporal border (ROI 7, $p\leq0.01$) within the postnatal pars lateralis (Table 7, Figure 5b). In addition, the jugular limb (ROI 1) had a significantly lower BS/BV ($p\leq0.02$) compared to the mastoid temporal border (ROI 7) (Table 7, Figure 5b).

No significant differences in BS/BV ($p>0.05$) were observed between the postnatal jugular limb (ROI 1), posteromedial corner (ROI 4), and jugular process (ROI 6) (Table 7, Figure 5b). In addition, no significant differences in BS/BV ($p>0.05$) were observed between the

posteromedial corner (ROI 4), the jugular process (ROI 6), and mastoid temporal border (ROI 7) within the postnatal group (Table 7, Figure 5b). The BS/BV of the condylar limb (ROI 2) did not significantly differ ($p>0.05$) from that of the jugular limb (ROI 1) or the primary ossification site (ROI 2) within the postnatal pars lateralis (Table 7, Figure 5b). Furthermore, The BS/BV of the primary ossification site (ROI 5) and lateral foramen magnum border (ROI 3) did not significantly differ ($p>0.05$) within the postnatal pars lateralis (Table 7, Figure 5b).

3.2. Trabecular thickness (TbTh), trabecular number (TbN), trabecular separation (TbSp)

3.2.1. Pars basilaris

The median TbTh ranged between 0.07 mm (0.06-0.09) and 0.20 mm (0.14-0.22) within the early prenatal pars basilaris, 0.11 mm (0.09-0.17) and 0.31 mm (0.22-0.41) within the late prenatal pars basilaris, and 0.10 mm (0.08-0.11) and 0.34 mm (0.27-0.45) within the postnatal group (Table 8, Figure 6a). The anterior foramen magnum border (ROI 3) had the highest median TbTh with a value of 0.20 mm (0.14-0.22) in the early prenatal group, 0.31 mm (0.22-0.41) in the late prenatal group, and 0.34 mm (0.27-0.45) in the postnatal group (Table 8, Figure 6a). The next highest TbTh was found in the primary ossification site (ROI 4) with a value of 0.15 mm (0.11-0.19) in the early prenatal group, 0.21 mm (0.16-0.28) in the late prenatal group, and 0.18 mm (0.15-0.22) in the postnatal group (Table 8, Figure 6a). The TbTh of remaining ROIs ranged between 0.07 mm (0.06-0.09) and 0.08 mm (0.08-0.10) in the early prenatal group, 0.11 mm (0.09-0.17) and 0.13 mm (0.10-0.18) in the late prenatal group, and 0.10 mm (0.08-0.11) and 0.11 mm (0.10-0.13) in the postnatal group (Table 8, Figure 6a).

Table 8: Median values and pairwise comparisons of trabecular thickness (TbTh), trabecular number (TbN) and trabecular separation (TbSp) between the early prenatal, late prenatal and postnatal pars basilaris for each region of interest (ROI)

Variable	ROI	Median (Q_1-Q_3)			Group comparisons (p<0.05)	
		Early prenatal (n=28)	Late prenatal (n=31)	Postnatal (n=25)	Early prenatal vs. late prenatal	Late prenatal vs. postnatal
TbTh (mm)	1	0.08 (0.08-0.10)	0.11 (0.09-0.17)	0.11 (0.10-0.13)	0.00*	1.00
	2	0.08 (0.07-0.10)	0.13 (0.10-0.18)	0.11 (0.10-0.13)	0.00*	1.00
	3	0.20 (0.14-0.22)	0.31 (0.22-0.41)	0.34 (0.27-0.45)	0.00*	0.24
	4	0.15 (0.11-0.19)	0.21 (0.16-0.28)	0.18 (0.15-0.22)	0.00*	1.00
	5	0.08 (0.07-0.10)	0.12 (0.09-0.17)	0.11 (0.10-0.14)	0.00*	1.00
	6	0.08 (0.07-0.10)	0.12 (0.10-0.16)	0.11 (0.10-0.14)	0.00*	0.95
	7	0.07 (0.06-0.09)	0.11 (0.09-0.23)	0.10 (0.08-0.11)	0.00*	0.65
TbN (mm^{-1})	1	4.82 (4.19-5.08)	4.41 (3.73-4.70)	4.42 (4.07-4.64)	0.05*	1.00
	2	4.74 (4.40-5.31)	4.32 (3.76-4.74)	4.31 (3.97-4.70)	0.03*	1.00
	3	3.05 (2.81-3.53)	2.23 (1.85-2.87)	2.11 (1.80-2.42)	0.00*	0.17
	4	3.35 (3.01-3.77)	2.79 (2.48-3.29)	2.80 (2.25-2.93)	0.01*	0.25
	5	4.75 (4.46-5.14)	3.91 (3.27-4.42)	3.58 (3.02-4.00)	0.00*	0.59
	6	4.75 (4.48-5.26)	4.02 (3.36-4.61)	3.75 (3.20-4.35)	0.00*	0.60
	7	4.59 (4.04-5.21)	4.25 (3.38-4.97)	4.64 (4.22-5.36)	0.32	0.27
TbSp (mm)	1	0.12 (0.11-0.13)	0.10 (0.08-0.12)	0.11 (0.09-0.12)	0.08	1.00
	2	0.11 (0.10-0.13)	0.10 (0.08-0.12)	0.10 (0.09-0.12)	0.07	1.00
	3	0.13 (0.12-0.16)	0.12 (0.10-0.14)	0.11 (0.10-0.13)	0.19	0.83
	4	0.15 (0.11-0.17)	0.14 (0.11-0.16)	0.17 (0.13-0.21)	0.97	0.13
	5	0.12 (0.10-0.14)	0.13 (0.09-0.16)	0.16 (0.11-0.22)	1.00	0.11
	6	0.12 (0.10-0.13)	0.12 (0.09-0.14)	0.15 (0.11-0.20)	1.00	0.02*
	7	0.12 (0.10-0.15)	0.09 (0.07-0.11)	0.10 (0.09-0.13)	0.01*	0.68

Early prenatal: 20–30 gestational weeks. Late prenatal: 30–40 gestational weeks. Postnatal: birth–7.5 months. Pars basilaris regions of interest: (ROI 1): right anterolateral maxima of the foramen magnum. (ROI 2): left anterolateral maxima of the foramen magnum. (ROI 3): anterior foramen magnum border. (ROI 4): primary ossification site. (ROI 5): right lateral angle. (ROI 6): left lateral angle. (ROI 7): spheno-occipital synchondrosis. *Significant value (p≤0.05). Values <0.01 are represented as 0.00.

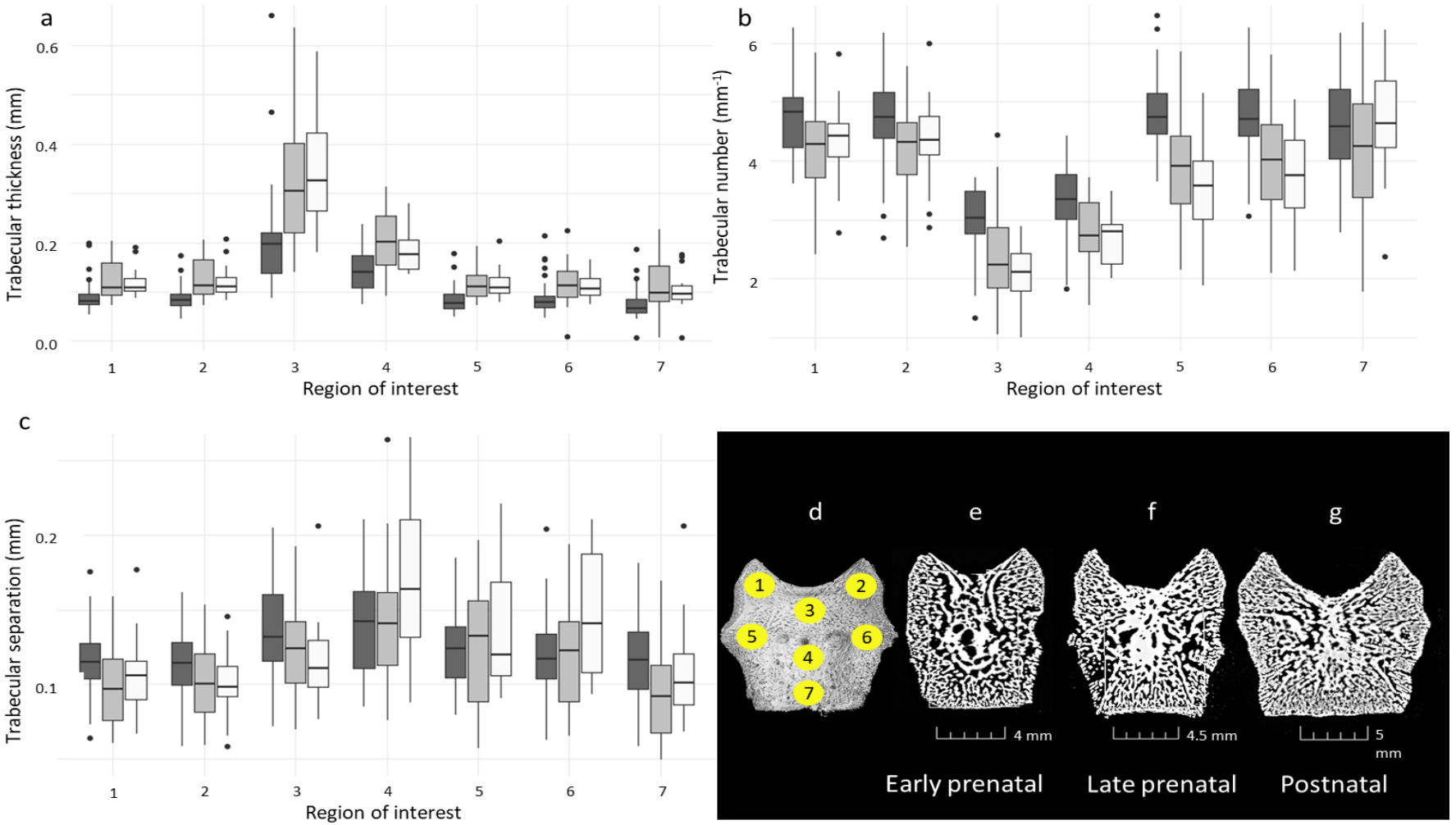


Figure 6: Regional variations of (a) trabecular thickness (TbTh), (b) trabecular number (TbN) and (c) trabecular separation (TbSp) in the pars basilaris. Dark grey: early prenatal (20–30 gestational weeks, n=28). Light grey: late prenatal (30–40 gestational weeks, n=31). White: postnatal (birth–7.5 months, n=25). Dots represent outliers. Regions of interest (ROI) are illustrated on (d) 3D reconstruction of the intracranial late prenatal pars basilaris. Yellow circles represent ROIs: (ROI 1): right anterolateral maxima of the foramen magnum. (ROI 2): left anterolateral maxima of the foramen magnum. (ROI 3): anterior foramen magnum border. (ROI 4): primary ossification site. (ROI 5): right lateral angle. (ROI 6): left lateral angle. (ROI 7): spheno-occipital synchondrosis. Differences in TbTh, TbN, TbSp are illustrated on the (e) early prenatal, (f) late prenatal, and (g) postnatal pars basilaris. Contrast and brightness have been adjusted to highlight trabeculae; therefore, the colour intensity is not representative of density. Graphs were created in RStudio using ggplot2 (Wickham, 2016). Images were generated using VGStudio Max V2.2 software (Volume Graphics GmbH, Heidelberg, Germany).

The median TbN ranged between 3.05 mm^{-1} (2.81-3.53) and 4.82 mm^{-1} (4.19-5.08) within the early prenatal pars basilaris, 2.23 mm^{-1} (1.85-2.87) and 4.41 mm^{-1} (3.73-4.70) within the late prenatal pars basilaris, and 2.11 mm^{-1} (1.80-2.42) and 4.64 mm^{-1} (4.22-5.36) within the postnatal group (Table 8, Figure 6b). The anterior foramen magnum border (ROI 3) had the lowest median TbN with a value of 3.05 mm^{-1} (2.81-3.53) in the early prenatal group, 2.23 mm^{-1} (1.85-2.87) in the late prenatal group, and 2.11 mm^{-1} (1.80-2.42) in the postnatal group (Table 8, Figure 6b). The next lowest median TbN was found in the primary ossification site (ROI 4) with a value of 3.35 mm^{-1} (3.01-3.77) in the early prenatal group, 2.79 mm^{-1} (2.48-3.29) in the late prenatal group, and 2.80 mm^{-1} (2.25-2.93) in the postnatal group (Table 8, Figure 6b). The TbN of remaining ROIs ranged between 4.59 mm^{-1} (4.04-5.21) and 4.82 mm^{-1} (4.19-5.08) in the early prenatal group, 3.91 mm^{-1} (3.27-4.42) 3.91 mm^{-1} (3.27-4.42) in the late prenatal group, and 3.58 mm^{-1} (3.02-4.00) and 4.64 mm^{-1} (4.22-5.36) in the postnatal group (Table 8, Figure 6b).

The median TbSp ranged between 0.11 mm (0.10-0.13) and 0.15 mm (0.11-0.17) within the early prenatal pars basilaris, 0.09 mm (0.07-0.11) and 0.14 mm (0.11-0.16) within the late prenatal pars basilaris, and 0.10 mm (0.09-0.12) and 0.17 mm (0.13-0.21) within the postnatal group (Table 8, Figure 6c). The primary ossification site (ROI 4) had the highest median TbSp with a value of 0.15 mm (0.11-0.17) in the early prenatal group, 0.14 mm (0.11-0.16) in the late prenatal group, and 0.17 mm (0.13-0.21) in the postnatal group (Table 8, Figure 6c).

Comparisons between age groups

The trabeculae were significantly thicker (higher TbTh) in the late prenatal group compared to the early prenatal group in all the regions of the pars basilaris (ROI 1, $p \leq 0.01$, ROI 2, $p \leq 0.01$, ROI 3, $p \leq 0.01$, ROI 4, $p \leq 0.01$, ROI 5, $p \leq 0.01$, ROI 6, $p \leq 0.01$, ROI 7, $p \leq 0.01$) (Table 8, Figure 6a). No significant differences in TbTh ($p > 0.05$) were observed between the late prenatal and postnatal pars basilaris (Table 8, Figure 6a).

The late prenatal pars basilaris had significantly less trabeculae (lower TbN) compared to the early prenatal pars basilaris in the anterolateral maxima (ROI 1, $p \leq 0.05$ and ROI 2, $p \leq 0.03$), anterior foramen magnum border (ROI 3, $p \leq 0.01$), primary ossification site (ROI 4, $p \leq 0.01$), and lateral angles (ROI 5, $p \leq 0.01$ and ROI 6, $p \leq 0.01$) (Table 8, Figure 6b). The TbN of the spheno-occipital synchondrosis (ROI 7) did not significantly differ ($p > 0.05$) between the prenatal age groups (Table 8, Figure 6b). No significant differences in TbN ($p > 0.05$) were observed between the late prenatal and postnatal pars basilaris (Table 8, Figure 6b).

The late prenatal spheno-occipital synchondrosis (ROI 7) had significantly less TbSp ($p \leq 0.01$) compared to the early prenatal group (Table 8, Figure 6c). No further significant differences in TbSp ($p > 0.05$) were observed between the early and late prenatal age pars basilaris (Table 8, Figure 6c). The left lateral angle (ROI 6) of the pars basilaris had significantly greater TbSp ($p \leq 0.02$) in the postnatal group compared to the late prenatal group (Table 8, Figure 6c). None of the other ROIs significantly differed in TbSp ($p > 0.05$) between the late prenatal and postnatal pars basilaris (Table 8, Figure 6c).

Comparisons within age groups

Within all three age groups, the anterior foramen magnum border (ROI 3) and the primary ossification site (ROI 4) of the pars basilaris had significantly thicker ($p \leq 0.05$) and significantly fewer trabeculae ($p \leq 0.05$) compared to the anterolateral maxima (ROI 1 and ROI 2), lateral angles (ROI 5 and ROI 6), and spheno-occipital synchondrosis (ROI 7) (Table 9, Figure 6a-b). No significant differences in TbN or TbTh ($p > 0.05$) were observed between the anterior foramen magnum border (ROI 3) and the primary ossification site (ROI 4) within any of the assessed age categories (Table 9, Figure 6a-b). Additionally, no significant differences in TbN or TbTh ($p > 0.05$) were observed between anterolateral maxima (ROI 1 and ROI 2), lateral angles (ROI 5 and ROI 6), and spheno-occipital synchondrosis (ROI 7) within the early prenatal, late prenatal or postnatal pars basilaris (Table 9, Figure 6a-b).

No significant differences in TbSp ($p > 0.05$) were observed between any of the ROIs within the early prenatal pars basilaris (Table 9, Figure 6c). Within the late prenatal pars basilaris, the primary ossification site (ROI 4) had significantly less TbSp compared to the anterolateral maxima (ROI 1, $p \leq 0.01$ and ROI 2, $p \leq 0.01$) (Table 9, Figure 6c). In addition, the left anterolateral maxima (ROI 2) had significantly less TbSp ($p \leq 0.05$) than the right lateral angle (ROI 5) (Table 9, Figure 6c). However, no significant differences in TbSp ($p > 0.05$) were observed between the right anterolateral maxima (ROI 1) and right lateral angle (ROI 5) (Table 9, Figure 6c). Moreover, the TbSp of the left lateral angle (ROI 6) did not significantly differ ($p > 0.05$) from either of the anterolateral maxima (ROI 1 and ROI 2) within the late prenatal pars basilaris (Table 9, Figure 6c).

Table 9: Pairwise comparisons of trabecular thickness (TbTh), trabecular number (TbN) and trabecular separation (TbSp) between regions of interest (ROI) within the early prenatal, late prenatal and postnatal pars basilaris

ROI comparisons	TbTh (mm)			TbN (mm^{-1})			TbSp (mm)		
	Early prenatal (n=28)	Late prenatal (n=31)	Postnatal (n=25)	Early prenatal (n=28)	Late prenatal (n=31)	Postnatal (n=25)	Early prenatal (n=28)	Late prenatal (n=31)	Postnatal (n=25)
1 vs 2	1.00	1.00	1.00	1.00	1.00	1.00	1.00	1.00	1.00
1 vs 3	0.00*	0.00*	0.00*	0.00*	0.00*	0.00*	0.37	0.26	1.00
2 vs 3	0.00*	0.00*	0.00*	0.00*	0.00*	0.00*	0.16	0.09	1.00
1 vs 4	0.00*	0.01*	0.00*	0.00*	0.00*	0.00*	0.17	0.00*	0.00*
2 vs 4	0.00*	0.02*	0.00*	0.00*	0.00*	0.00*	0.07	0.00*	0.00*
3 vs 4	1.00	0.23	0.82	1.00	0.95	1.00	1.00	1.00	0.11
1 vs 5	1.00	1.00	1.00	1.00	1.00	0.75	1.00	0.18	0.01*
2 vs 5	1.00	1.00	1.00	1.00	1.00	0.93	1.00	0.05*	0.01*
3 vs 5	0.00*	0.00*	0.00*	0.00*	0.00*	0.00*	1.00	1.00	0.36
4 vs 5	0.00*	0.00*	0.00*	0.00*	0.00*	0.02*	1.00	1.00	1.00
1 vs 6	1.00	1.00	1.00	1.00	1.00	1.00	1.00	1.00	0.03*
2 vs 6	1.00	1.00	1.00	1.00	1.00	1.00	1.00	0.56	0.01*
3 vs 6	0.00*	0.00*	0.00*	0.00*	0.00*	0.00*	0.29	1.00	0.60
4 vs 6	0.00*	0.01*	0.00*	0.00*	0.00*	0.01*	0.13	0.39	1.00
5 vs 6	1.00	1.00	1.00	1.00	1.00	1.00	1.00	1.00	1.00
1 vs 7	1.00	1.00	1.00	1.00	1.00	1.00	1.00	1.00	1.00
2 vs 7	1.00	1.00	1.00	1.00	1.00	1.00	1.00	1.00	1.00
3 vs 7	0.00*	0.00*	0.00*	0.00*	0.00*	0.00*	1.00	0.02*	1.00
4 vs 7	0.00*	0.02*	0.00*	0.00*	0.00*	0.00*	0.62	0.00*	0.00*
5 vs 7	1.00	1.00	1.00	1.00	1.00	0.08	1.00	0.01*	0.00*
6 vs 7	1.00	1.00	1.00	1.00	1.00	0.21	1.00	0.17	0.01*

Early prenatal: 20–30 gestational weeks. Late prenatal: 30–40 gestational weeks. Postnatal: birth–7.5 months. Pars basilaris regions of interest: (ROI 1): right anterolateral maxima of the foramen magnum. (ROI 2): left anterolateral maxima of the foramen magnum. (ROI 3): anterior foramen magnum border. (ROI 4): primary ossification site. (ROI 5): right lateral angle. (ROI 6): left lateral angle. (ROI 7): spheno-occipital synchondrosis. *Significant value ($p \leq 0.05$). Values <0.01 are represented as 0.00.

In addition, the spheno-occipital synchondrosis (ROI 7) had significantly less TbSp compared to the anterior foramen magnum border (ROI 3, $p \leq 0.02$), primary ossification site (ROI 4, $p \leq 0.01$) and right lateral angle (ROI 5, $p \leq 0.01$), but did not significantly differ from the left lateral angle (ROI 6, $p > 0.05$) within the late prenatal pars basilaris (Table 9, Figure 6c).

The TbSp of the anterior foramen magnum border (ROI 3), the primary ossification site (ROI 4), and the lateral angles (ROI 5 and ROI 6) did not significantly differ ($p > 0.05$) from one another within the late prenatal age group (Table 9, Figure 6c). In addition, the TbSp of the anterolateral maxima (ROI 1 and 2) did not significantly differ ($p > 0.05$) from the anterior foramen magnum border (ROI 3) or the spheno-occipital synchondrosis (ROI 7) within the late prenatal age group (Table 9, Figure 6c).

Within the postnatal pars basilaris, the anterolateral maxima (ROI 1 and ROI 2) had significantly less TbSp ($p \leq 0.05$) compared to the primary ossification site (ROI 4) and the lateral angles (ROI 5 and ROI 6) (Table 9, Figure 6c). In addition, the spheno-occipital synchondrosis has significantly less TbSp compared to the primary ossification site (ROI 4, $p \leq 0.01$) and the lateral angles (ROI 5, $p \leq 0.01$ and ROI 6, $p \leq 0.01$) (Table 9, Figure 6c). The TbSp of the anterior foramen magnum border (ROI 3) did not significantly differ ($p > 0.05$) from any of the other regions within the postnatal pars basilaris (Table 9, Figure 6c). No significant differences in TbSp ($p > 0.05$) were observed between the anterolateral maxima (ROI 1 and ROI 2) and the spheno-occipital synchondrosis (ROI 7) (Table 9, Figure 6c). Furthermore, TbSp did not significantly differ ($p > 0.05$) between the primary ossification site (ROI 4) and the lateral angles (ROI 5 and ROI 6) within the postnatal age group (Table 9, Figure 6c).

3.2.2. Pars lateralis

The median TbTh ranged between 0.05mm (0.05-0.06) and 0.16 mm (0.14-0.22) within the early prenatal pars lateralis, 0.07mm (0.06-0.09) and 0.22 mm (0.18-0.35) within the late prenatal pars lateralis, and 0.07 mm (0.06-0.08) and 0.29 mm (0.25-0.40) within the postnatal group (Table 10, Figure 7a). The lateral foramen magnum border (ROI 3) had the highest median TbTh with a value of 0.16 mm (0.14-0.22) in the early prenatal group, 0.22 mm (0.18-0.35) in the late prenatal group, and 0.29 mm (0.25-0.40) in the postnatal group (Table 10, Figure 7a). The next highest TbTh was found in the primary ossification site (ROI 5) with a value of 0.12 mm (0.10-0.14) in the early prenatal group, 0.22 mm (0.16-0.29) in the late prenatal group, and 0.23 mm (0.16-0.28) in the postnatal group (Table 10, Figure 7a). The temporal mastoid border had the lowest median TbTh, with a value of 0.05 mm (0.05-0.06) in the early prenatal group, 0.07 mm (0.06-0.09) in the late prenatal group, and 0.07 mm (0.06-0.08) in the postnatal group (Table 10, Figure 7a).

The median TbN ranged between 3.03 mm^{-1} (2.49–3.39) and 5.29 mm^{-1} (4.41–5.54) within the early prenatal pars lateralis, 2.39 mm^{-1} (2.11–2.78) and 4.58 mm^{-1} (4.03–5.03) within the late prenatal pars lateralis, and 2.16 mm^{-1} (1.85–2.43) and 4.81 mm^{-1} (4.32–5.25) within the postnatal group (Table 10, Figure 7b). The posteromedial corner (ROI 4) had the highest median TbN in all age groups, with values of 5.29 mm^{-1} (4.41–5.54) in the early prenatal group, 4.58 mm^{-1} (4.03–5.03) in the late prenatal group, and 4.81 mm^{-1} (I4.32–5.25) in the postnatal group (Table 10, Figure 7b). The lateral foramen magnum border (ROI 3) had the lowest median TbN across all age groups, with values of 3.03 mm^{-1} (2.49–3.39) in the early prenatal group, 2.39 mm^{-1} (2.11–2.78) in the late prenatal group, and 2.16 mm^{-1} (1.85–2.43) in the postnatal group (Table 10, Figure 7b).

Table 10: Median values and pairwise comparisons of trabecular thickness (TbTh), trabecular number (TbN) and trabecular separation (TbSp) between the early prenatal, late prenatal and postnatal pars lateralis for each region of interest (ROI)

Variable	ROI	Median (Q_1-Q_3)			Group comparisons (p<0.05)	
		Early prenatal (n=30)	Late prenatal (n=37)	Postnatal (n=29)	Early prenatal vs. late prenatal	Late prenatal vs. postnatal
TbTh (mm)	1	0.08 (0.06-0.10)	0.11 (0.09-0.15)	0.10 (0.09-0.12)	0.00*	1.00
	2	0.10 (0.09-0.13)	0.14 (0.12-0.18)	0.14 (0.12-0.18)	0.00*	1.00
	3	0.16 (0.14-0.22)	0.22 (0.18-0.35)	0.29 (0.25-0.40)	0.00*	0.02*
	4	0.07 (0.06-0.08)	0.08 (0.07-0.10)	0.08 (0.07-0.09)	0.00*	0.33
	5	0.12 (0.10-0.14)	0.22 (0.16-0.29)	0.23 (0.16-0.28)	0.00*	1.00
	6	0.08 (0.07-0.09)	0.10 (0.08-0.13)	0.09 (0.08-0.11)	0.00*	0.33
	7	0.05 (0.05-0.06)	0.07 (0.06-0.09)	0.07 (0.06-0.08)	0.00*	0.64
TbN (mm^{-1})	1	4.77 (4.18-5.36)	4.35 (3.92-4.63)	4.26 (3.79-4.45)	0.05*	0.92
	2	5.13 (4.82-5.70)	4.29 (3.84-4.61)	3.94 (3.65-4.63)	0.00*	0.83
	3	3.03 (2.49-3.39)	2.39 (2.11-2.78)	2.16 (1.85-2.43)	0.00*	0.10
	4	5.29 (4.41-5.54)	4.58 (4.03-5.03)	4.81 (4.32-5.25)	0.01*	0.49
	5	3.76 (2.92-4.20)	2.87 (2.28-3.57)	2.77 (2.41-3.33)	0.01*	1.00
	6	4.77 (4.15-5.06)	4.30 (3.81-4.59)	4.65 (4.10-5.00)	0.00*	0.02*
	7	4.42 (3.85-4.68)	4.09 (3.59-4.48)	3.98 (3.50-4.76)	0.22	1.00
TbSp (mm)	1	0.12 (0.11-0.14)	0.12 (0.10-0.14)	0.13 (0.11-0.15)	0.79	0.33
	2	0.08 (0.07-0.09)	0.09 (0.08-0.10)	0.10 (0.08-0.10)	0.23	0.28
	3	0.16 (0.14-0.17)	0.16 (0.12-0.18)	0.13 (0.10-0.18)	1.00	0.12
	4	0.12 (0.11-0.14)	0.13 (0.10-0.15)	0.13 (0.11-0.15)	0.78	1.00
	5	0.13 (0.12-0.17)	0.12 (0.08-0.15)	0.13 (0.08-0.16)	0.11	1.00
	6	0.13 (0.11-0.16)	0.13 (0.11-0.17)	0.13 (0.11-0.15)	1.00	0.82
	7	0.17 (0.16-0.20)	0.17 (0.14-0.22)	0.17 (0.14-0.19)	1.00	0.72

Early prenatal: 20–30 gestational weeks. Late prenatal: 30–40 gestational weeks. Postnatal: birth–7.5 months. Pars lateralis regions of interest: (ROI 1): jugular limb. (ROI 2): condylar limb. (ROI 3): lateral foramen magnum border. (ROI 4): posteromedial corner. (ROI 5): primary ossification site. (ROI 6): jugular process. (ROI 7): mastoid temporal border. *Significant value (p≤0.05). Values <0.01 are represented as 0.00.

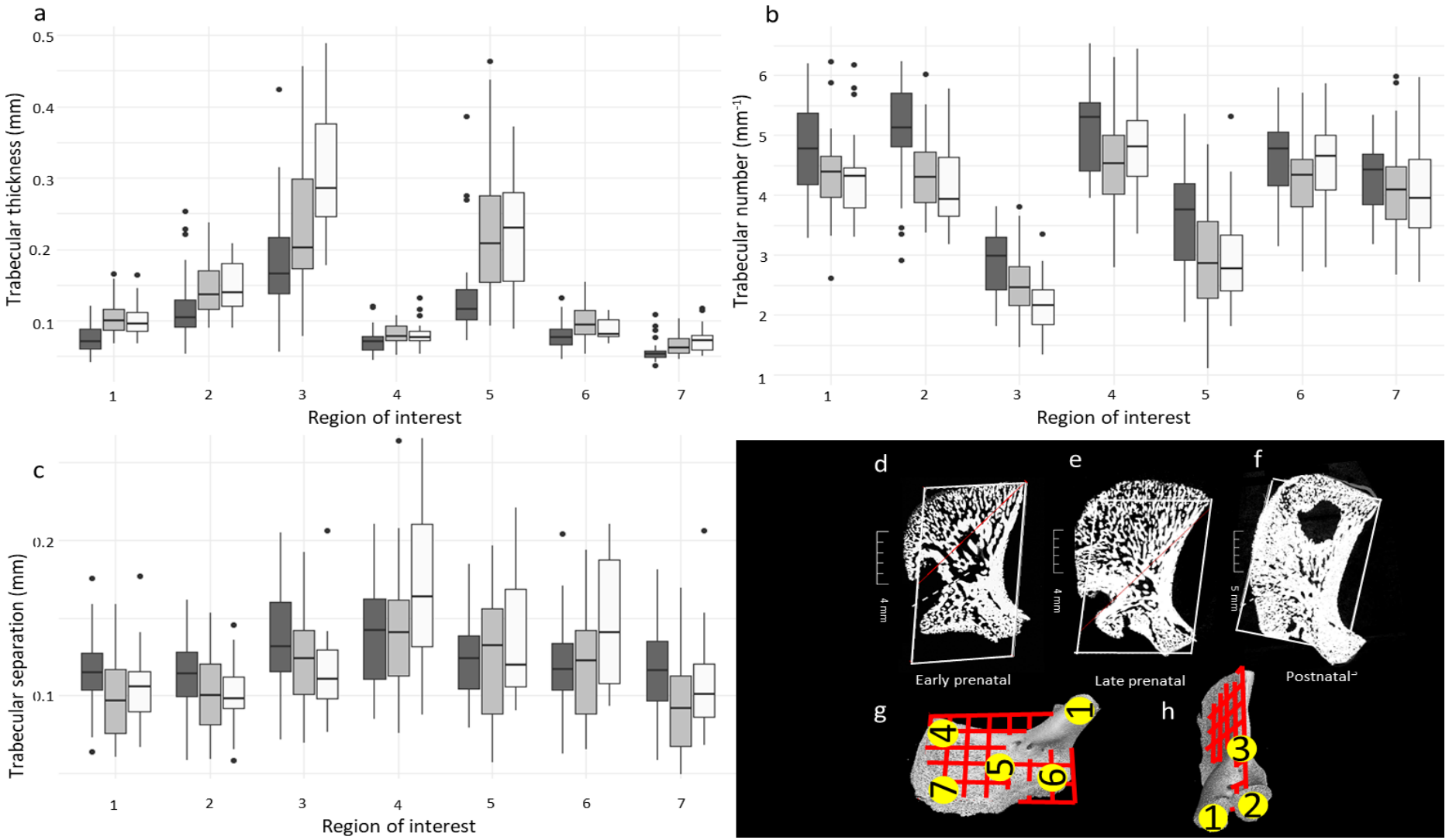


Figure 7: Regional variations of (a) trabecular thickness (TbTh), (b) trabecular number (TbN) and (c) trabecular separation (TbSp) in the pars lateralis. Dark grey: early prenatal (20–30 gestational weeks, n=30). Light grey: late prenatal (30–40 gestational weeks, n=37). White: postnatal (birth–7.5 months, n=29). Dots represent outliers. Differences in TbTh, TbN, TbSp are illustrated on the (d) early prenatal, (e) late prenatal and (f) postnatal pars lateralis. Contrast and brightness have been adjusted to highlight trabeculae; therefore, the colour intensity is not representative of density. Regions of interest (ROI) are illustrated on (g) 3D reconstruction of the intracranial late prenatal pars lateralis and (h) 3D reconstruction of the hypoglossal region of the late prenatal pars lateralis. Yellow circles represent ROIs: (ROI 1): jugular limb. (ROI 2): condylar limb. (ROI 3): lateral foramen magnum border. (ROI 4): posteromedial corner. (ROI 5): primary ossification site. (ROI 6): jugular process. (ROI 7): mastoid temporal border. Graphs were created in RStudio using ggplot2 (Wickham, 2016). Images were generated using VGStudio Max V2.2 software (Volume Graphics GmbH, Heidelberg, Germany).

Within the early prenatal age group, the condylar limb (ROI 2) had the lowest median TbSp (0.08 mm, IQR: 0.07–0.09), and the mastoid temporal border (ROI 7) had the highest median TbSp (0.17 mm, IQR: 0.16–0.20) (Table 10, Figure 7c). The median TbSp of the remaining ROIs ranged between 0.12 mm and 0.16 mm within the early prenatal age group (Table 10, Figure 7c). Within the late prenatal age group, the condylar limb (ROI 2) had the lowest median TbSp (0.09 mm, IQR: 0.08–0.10), and the mastoid temporal border (ROI 7) had the highest median TbSp (0.17 mm, IQR: 0.14–0.22) (Table 10, Figure 7c). The median TbSp of the remaining ROIs ranged between 0.12 mm and 0.16 mm within the late prenatal age group (Table 10, Figure 7c). Within the postnatal age group, the condylar limb (ROI 2) had the lowest median TbSp (0.10 mm, IQR: 0.08–0.10), and the mastoid temporal border (ROI 7) had the highest median TbSp (0.17 mm, IQR: 0.14–0.19) (Table 10, Figure 7c). The median TbSp of the remaining ROIs ranged between 0.13 mm and 0.13 mm within the postnatal age group (Table 10, Figure 7c).

Comparisons between age groups

The late prenatal pars lateralis had significantly thicker trabeculae compared to the early prenatal pars lateralis across all seven regions of interest (ROI 1, $p \leq 0.01$; ROI 2, $p \leq 0.01$; ROI 3, $p \leq 0.01$; ROI 4, $p \leq 0.01$; ROI 5, $p \leq 0.01$; ROI 6, $p \leq 0.01$; ROI 7, $p \leq 0.01$) (Table 10, Figure 7a). The lateral foramen magnum border (ROI 3) had significantly thicker trabeculae ($p \leq 0.02$) in the postnatal pars lateralis compared to the late prenatal pars lateralis (Table 10, Figure 7a). No further significant differences in TbTh ($p > 0.05$) were observed between the late prenatal and postnatal age groups (Table 10, Figure 7a).

The early prenatal pars lateralis had significantly more trabeculae compared to the late prenatal pars lateralis in all ROIs (ROI 1, p≤0.05; ROI 2, p≤0.01; ROI 3, p≤0.01; ROI 4, p≤0.01; ROI 5, p≤0.01; ROI 6, p≤0.01) except the mastoid temporal border (ROI 7) which did not differ significantly (p>0.05) between the prenatal age groups (Table 10, Figure 7b). The postnatal jugular process (ROI 6) had significantly more trabeculae (p≤0.02) compared to the late prenatal group (Table 10, Figure 7b). No further significant differences in TbTh (p>0.05) were observed between the late prenatal and postnatal pars lateralis (Table 10, Figure 7b).

No significant differences in TbSp (p>0.05) were observed between the early and late prenatal, or the late prenatal and postnatal age groups for any of the ROIs of the pars lateralis (Table 10, Figure 7c).

Comparisons within age groups

Within the early prenatal pars lateralis, the condylar limb (ROI 2), lateral foramen magnum border (ROI 3), and primary ossification site (ROI 5) all exhibited significantly thicker trabeculae (p≤0.05) than the jugular limb (ROI 1), posteromedial corner (ROI 4), jugular process (ROI 6), and mastoid temporal border (ROI 7) (Table 11, Figure 7a). The mastoid temporal border (ROI 7) had significantly thinner trabeculae compared to the jugular limb (ROI 1, p≤0.01), condylar limb (ROI 2, p≤0.01), lateral foramen magnum border (ROI 3, p≤0.01), primary ossification site (ROI 5, p≤0.01), and jugular process (ROI 6, p≤0.02) within the early prenatal pars lateralis (Table 11, Figure 7a).

Table 11: Pairwise comparisons of trabecular thickness (TbTh), trabecular number (TbN) and trabecular separation (TbSp) between regions of interest (ROI) within the early prenatal, late prenatal and postnatal pars lateralis

ROI comparisons	TbTh (mm)			TbN (mm^{-1})			TbSp (mm)		
	Early prenatal (n=30)	Late prenatal (n=37)	Postnatal (n=29)	Early prenatal (n=30)	Late prenatal (n=37)	Postnatal (n=29)	Early prenatal (n=30)	Late prenatal (n=37)	Postnatal (n=29)
1 vs 2	0.05*	0.24	0.18	1.00	1.00	1.00	0.00*	0.01*	0.01*
1 vs 3	0.00*	0.00*	0.00*	0.00*	0.00*	0.00*	0.04*	0.01*	1.00
2 vs 3	0.13	0.11	0.01*	0.00*	0.00*	0.00*	0.00*	0.00*	0.00*
1 vs 4	1.00	0.57	0.07	1.00	1.00	0.44	1.00	1.00	1.00
2 vs 4	0.00*	0.00*	0.00*	1.00	0.69	0.12	0.00*	0.00*	0.01*
3 vs 4	0.00*	0.00*	0.00*	0.00*	0.00*	0.00*	0.04*	0.15	1.00
1 vs 5	0.00*	0.00*	0.00*	0.00*	0.00*	0.00*	1.00	1.00	1.00
2 vs 5	1.00	0.59	0.58	0.00*	0.00*	0.00*	0.00*	0.02*	0.03*
3 vs 5	1.00	1.00	1.00	0.33	0.83	0.48	1.00	0.03*	1.00
4 vs 5	0.00*	0.00*	0.00*	0.00*	0.00*	0.00*	1.00	1.00	1.00
1 vs 6	1.00	1.00	1.00	1.00	1.00	1.00	1.00	1.00	1.00
2 vs 6	0.01*	0.01*	0.00*	1.00	1.00	0.88	0.00*	0.00*	0.00*
3 vs 6	0.00*	0.00*	0.00*	0.00*	0.00*	0.00*	0.59	0.97	1.00
4 vs 6	1.00	1.00	1.00	0.83	0.73	1.00	1.00	1.00	1.00
5 vs 6	0.00*	0.00*	0.00*	0.00*	0.00*	0.00*	1.00	1.00	1.00
1 vs 7	0.00*	0.02*	0.01*	0.94	1.00	1.00	0.00*	0.00*	0.06
2 vs 7	0.00*	0.00*	0.00*	0.10	1.00	1.00	0.00*	0.00*	0.00*
3 vs 7	0.00*	0.00*	0.00*	0.00*	0.00*	0.00*	1.00	1.00	0.15
4 vs 7	0.22	1.00	1.00	0.02*	0.24	0.20	0.00*	0.01*	0.05*
5 vs 7	0.00*	0.00*	0.00*	0.23	0.00*	0.00*	0.26	0.00*	0.02*
6 vs 7	0.02*	0.35	0.78	1.00	1.00	1.00	0.03*	0.08	0.10

Early prenatal: 20–30 gestational weeks. Late prenatal: 30–40 gestational weeks. Postnatal: birth–7.5 months. Pars lateralis regions of interest: (ROI 1): jugular limb. (ROI 2): condylar limb. (ROI 3): lateral foramen magnum border. (ROI 4): posteromedial corner. (ROI 5): primary ossification site. (ROI 6): jugular process. (ROI 7): mastoid temporal border. *Significant value ($p \leq 0.05$). Values <0.01 are represented as 0.00.

No significant differences in TbTh ($p>0.05$) were observed between the condylar limb (ROI 2), lateral foramen magnum border (ROI 3), and primary ossification site (ROI 5) within the early prenatal pars lateralis (Table 11, Figure 7a). In addition, no significant differences in TbTh ($p>0.05$) were observed between the jugular limb (ROI 1), posteromedial corner (ROI 4), and jugular process (ROI 6) within the early prenatal pars lateralis (Table 11, Figure 7a). Furthermore, the TbTh of the mastoid temporal border (ROI 7) did not significantly differ ($p>0.05$) from the posteromedial corner (ROI 4) in the early prenatal pars lateralis (Table 11, Figure 7a).

Within the late prenatal pars lateralis, the condylar limb (ROI 2) exhibited significantly thicker trabeculae compared to the posteromedial corner (ROI 4, $p\leq0.01$), jugular process (ROI 6, $p\leq0.01$), and mastoid temporal border (ROI 7, $p\leq0.01$) (Table 11, Figure 7a). The lateral foramen magnum border (ROI 3) and primary ossification site (ROI 5) both exhibited significantly thicker trabeculae ($p\leq0.05$) relative to the jugular limb (ROI 1), posteromedial corner (ROI 4), jugular process (ROI 6), and mastoid temporal border (ROI 7) (Table 11, Figure 7a). In addition, the jugular limb (ROI 1) had significantly thicker trabeculae ($p\leq0.02$) than the mastoid temporal border (ROI 7) within the late prenatal pars lateralis (Table 11, Figure 7a).

Within the late prenatal pars lateralis, TbTh did not significantly differ ($p>0.05$) between the condylar limb (ROI 2), lateral foramen magnum border (ROI 3), and primary ossification site (ROI 5) (Table 11, Figure 7a). Additionally, no significant differences in TbTh ($p>0.05$) were observed between the jugular limb (ROI 1) and condylar limb (ROI 2) (Table 11, Figure 7a). No significant differences in TbTh ($p>0.05$) were exhibited between the jugular limb (ROI 1),

posteromedial corner (ROI 4), and jugular process (ROI 6) within the late prenatal pars lateralis (Table 11, Figure 7a). Moreover, TbTh did not significantly differ ($p>0.05$) between the posteromedial corner (ROI 4), jugular process (ROI 6), and mastoid temporal border (ROI 7) within the late prenatal pars lateralis (Table 11, Figure 7a).

Within the postnatal pars lateralis, the lateral foramen magnum border (ROI 3) had significantly thicker trabeculae compared to the rest of postnatal pars lateralis (ROI 1, $p\leq0.01$; ROI 2, $p\leq0.01$; ROI 4, $p\leq0.01$; ROI 6, $p\leq0.01$; ROI 7 $p\leq0.01$), except for the primary ossification site (ROI 5, $p>0.05$) (Table 11, Figure 7a). The primary ossification site (ROI 5) had significantly thicker trabeculae compared to the jugular limb (ROI 1, $p\leq0.01$), posteromedial corner (ROI 4, $p\leq0.01$), jugular process (ROI 6, $p\leq0.01$), and mastoid temporal border (ROI 7, $p\leq0.01$) within the postnatal pars lateralis (Table 11, Figure 7a). The condylar limb (ROI 2) had significantly thicker trabeculae compared to the posteromedial corner (ROI 4, $p\leq0.01$), jugular process (ROI 6, $p\leq0.01$), and mastoid temporal border (ROI 7, $p\leq0.01$) (Table 11, Figure 7a). In addition, the jugular limb (ROI 1) had significantly thicker trabeculae ($p\leq0.01$) than the mastoid temporal border (ROI 7) within the postnatal pars lateralis (Table 11, Figure 7a).

The TbTh of the lateral foramen magnum border (ROI 3) and primary ossification site (ROI 5) did not significantly differ ($p>0.05$) within the postnatal pars lateralis (Table 11, Figure 7a). No significant differences in TbTh ($p>0.05$) were observed between the postnatal jugular limb (ROI 1), posteromedial corner (ROI 4), and jugular process (ROI 6) (Table 11, Figure 7a). In addition, no significant differences in TbTh ($p>0.05$) were observed between the posteromedial corner (ROI 4), jugular process (ROI 6), and mastoid temporal border (ROI 7)

within the postnatal group (Table 11, Figure 7a). The TbTh of the condylar limb (ROI 2) did not significantly differ ($p>0.05$) from that of the jugular limb (ROI 1) or the primary ossification site (ROI 2) within the postnatal pars lateralis (Table 11, Figure 7a).

Within the early prenatal pars lateralis, the lateral foramen magnum border (ROI 3) exhibited significantly fewer trabeculae compared to the jugular limb (ROI 1, $p\leq0.01$), condylar limb (ROI 2, $p\leq0.01$), posteromedial corner (ROI 4, $p\leq0.01$), jugular process (ROI 6, $p\leq0.01$), and mastoid temporal border (ROI 7, $p\leq0.01$) (Table 11, Figure 7b). In addition the primary ossification site had significantly fewer trabeculae compared to the jugular limb (ROI 1, $p\leq0.01$), condylar limb (ROI 2, $p\leq0.01$), posteromedial corner (ROI 4, $p\leq0.01$), and jugular process (ROI 6, $p\leq0.01$) (Table 11, Figure 7b). The jugular process (ROI 4) had significantly more trabeculae ($p\leq0.02$) compared to the mastoid temporal border within the early prenatal pars lateralis (Table 11, Figure 7b).

The TbN of the primary ossification site (ROI 5) did not significantly differ ($p>0.05$) from the lateral foramen magnum border (ROI 3) within the early prenatal pars lateralis (Table 11, Figure 7b). No significant differences in TbN ($p>0.05$) were observed between the jugular limb (ROI 1), condylar limb (ROI 2), posteromedial corner (ROI 4), and jugular process (ROI 6) within the early prenatal pars lateralis (Table 11, Figure 7b). The TbN of the mastoid temporal border (ROI 7) did not significantly differ ($p>0.05$) from the jugular limb (ROI 1), condylar limb (ROI 2), primary ossification site (ROI 5) or jugular process (ROI 6) within the early prenatal group (Table 11, Figure 7b).

Within the late prenatal and postnatal pars lateralis, the lateral foramen magnum border (ROI 3) and primary ossification site (ROI 5) both had significantly fewer trabeculae ($p \leq 0.05$) compared to the rest of the pars lateralis (Table 11, Figure 7b). No significant differences in TbN ($p > 0.05$) were observed between the lateral foramen magnum border (ROI 3) and primary ossification site (ROI 5) within the late prenatal and postnatal pars lateralis (Table 11, Figure 7b). In addition, no significant differences in TbN ($p > 0.05$) were observed between the jugular limb (ROI 1), condylar limb (ROI 2), posteromedial corner (ROI 4), jugular process (ROI 6), and mastoid temporal border (ROI 7) within the late prenatal and postnatal pars lateralis (Table 11, Figure 7b).

Within the early prenatal pars lateralis, the condylar limb (ROI 2) exhibited significantly less TbSp compared to all other ROIs (ROI 1, $p \leq 0.01$; ROI 3, $p \leq 0.01$; ROI 4, $p \leq 0.01$; ROI 5, $p \leq 0.01$; ROI 6, $p \leq 0.01$; ROI 7 $p \leq 0.01$) (Table 11, Figure 7c). The mastoid temporal border (ROI 7) exhibited significantly greater TbSp compared to the jugular limb (ROI 1, $p \leq 0.01$), condylar limb (ROI 2, $p \leq 0.01$), posteromedial corner (ROI 4, $p \leq 0.01$), and jugular process (ROI 6, $p \leq 0.03$) (Table 11, Figure 7c). The lateral foramen magnum border (ROI 3) exhibited significantly greater TbSp compared to the jugular limb (ROI 1, $p \leq 0.04$), condylar limb (ROI 2, $p \leq 0.01$), and posteromedial border (ROI 4, $p \leq 0.04$) (Table 11, Figure 7c).

No significant differences in TbSp ($p > 0.05$) were observed between the jugular limb (ROI 1), posteromedial corner (ROI 4), primary ossification site (ROI 5), and jugular process (ROI 6) within the early prenatal pars lateralis (Table 11, Figure 7c). In addition, no significant differences in TbSp ($p > 0.05$) were observed between the lateral foramen magnum border (ROI

3), primary ossification site (ROI 5), and jugular process (ROI 6) within the early prenatal pars lateralis (Table 11, Figure 7c). Furthermore, no significant differences in TbSp ($p>0.05$) were observed between the lateral foramen magnum border (ROI 3), primary ossification site (ROI 5), and mastoid temporal border within the early prenatal pars lateralis (Table 11, Figure 7c).

Within the late prenatal pars lateralis, the condylar limb (ROI 2) had a significantly less TbSp compared to the rest of the pars lateralis (ROI 1, $p\leq0.01$; ROI 3, $p\leq0.01$; ROI 4, $p\leq0.01$; ROI 5, $p\leq0.02$; ROI 6, $p\leq0.01$; ROI 7, $p\leq0.01$) (Table 11, Figure 7c). The late prenatal lateral foramen magnum border (ROI 3) exhibited significantly greater TbSp compared to the jugular limb (ROI 1, $p\leq0.01$), condylar limb (ROI 2, $p\leq0.01$), and primary ossification site (ROI 5, $p\leq0.03$) (Table 11, Figure 7c). The mastoid temporal border (ROI 7) exhibited significantly more TbSp compared to the jugular limb (ROI 1, $p\leq0.01$), condylar limb (ROI 2, $p\leq0.01$), posteromedial border (ROI 4, $p\leq0.01$), and primary ossification site (ROI 5, $p\leq0.01$) (Table 11, Figure 7c).

No significant differences in TbSp ($p>0.05$) were observed between the jugular limb (ROI 1), posteromedial corner (ROI 4), primary ossification site (ROI 5), and jugular process (ROI 6) within the late prenatal pars lateralis (Table 11, Figure 7c). In addition, no significant differences in TbSp ($p>0.05$) were observed between the lateral foramen magnum border (ROI 3), jugular process (ROI 6), and mastoid temporal border (ROI 7) of the early prenatal pars lateralis (Table 11, Figure 7c). No significant differences in TbSp ($p>0.05$) were observed between the lateral foramen magnum border (ROI 3) and posteromedial corner (ROI 4) within the late prenatal pars lateralis (Table 11, Figure 7c).

Within the postnatal pars lateralis, the condylar limb (ROI 2) had significantly less TbSp compared to all other ROIs (ROI 1, p≤0.01; ROI 3, p≤0.01; ROI 4, p≤0.01; ROI 5, p≤0.03; ROI 6, p≤0.01; ROI 7, p≤0.01) (Table 11, Figure 7c). In addition, the mastoid temporal border (ROI 7) had significantly more TbSp compared to the condylar limb (ROI 2, p≤0.01), posteromedial border (ROI 4, p≤0.05), and primary ossification site (ROI 5, p≤0.02) (Table 11, Figure 7c).

No significant differences in TbSp (p>0.05) were observed between the jugular limb (ROI 1), lateral foramen magnum border (ROI 3), posteromedial corner (ROI 4), primary ossification site (ROI 5), and jugular process (ROI 6) within the postnatal pars lateralis (Table 11, Figure 7c). In addition, no significant differences in TbSp (p>0.05) were observed between the jugular limb (ROI 1), lateral foramen magnum border (ROI 3), and jugular process (ROI 6), and mastoid temporal border (ROI 7) of the postnatal pars lateralis (Table 11, Figure 7c).

3.3. Degree of anisotropy (DA)

3.3.1. Pars basilaris

The median DA values ranged between 0.22 (0.18–0.24) and 0.33 (0.28–0.37) in the early prenatal group, 0.21 (0.18–0.28) and 0.35 (0.29–0.40) in the late prenatal group and 0.20 (0.15–0.23) and 0.31 (0.28–0.36) in the postnatal group (Table 12, Figure 8). The median DA of the anterolateral maxima (ROI 1 and ROI 2) and the lateral angles (ROI 5 and ROI 6) ranged between 0.27 (0.23-0.33) and 0.35 (0.29-0.40) across all three age groups (Table 12, Figure 8). The median DA for the rest of the ROIs ranged between 0.20 (0.15–0.23) and 0.25 (0.19-0.28) across all three age groups (Table 12, Figure 8).

Table 12: Median values and pairwise comparisons of degree of anisotropy (DA*J*) between the early prenatal, late prenatal and postnatal pars basilaris for each region of interest (ROI)

Variable	ROI	Median (Q_1-Q_3)			Group comparisons (p<0.05)	
		Early prenatal (n=28)	Late prenatal (n=31)	Postnatal (n=25)	Early prenatal vs. late prenatal	Late prenatal vs. postnatal
DA	1	0.31 (0.25-0.37)	0.34 (0.30-0.37)	0.31 (0.29-0.35)	0.21	0.25
	2	0.33 (0.28-0.37)	0.35 (0.29-0.40)	0.31 (0.28-0.36)	0.72	0.45
	3	0.22 (0.18-0.24)	0.24 (0.20-0.27)	0.23 (0.19-0.26)	0.16	0.97
	4	0.25 (0.19-0.28)	0.24 (0.19-0.28)	0.20 (0.15-0.23)	1.00	0.04*
	5	0.31 (0.26-0.37)	0.32 (0.27-0.35)	0.30 (0.26-0.33)	1.00	0.42
	6	0.27 (0.23-0.33)	0.32 (0.26-0.33)	0.30 (0.25-0.33)	0.19	0.38
	7	0.24 (0.18-0.29)	0.21 (0.18-0.28)	0.21 (0.20-0.24)	0.87	0.98

Early prenatal: 20–30 gestational weeks. Late prenatal: 30–40 gestational weeks. Postnatal: birth–7.5 months. Pars basilaris regions of interest: (ROI 1): right anterolateral maxima of the foramen magnum. (ROI 2): left anterolateral maxima of the foramen magnum. (ROI 3): anterior foramen magnum border. (ROI 4): primary ossification site. (ROI 5): right lateral angle. (ROI 6): left lateral angle. (ROI 7): spheno-occipital synchondrosis. *Significant value (p≤0.05). Values <0.01 are represented as 0.00.

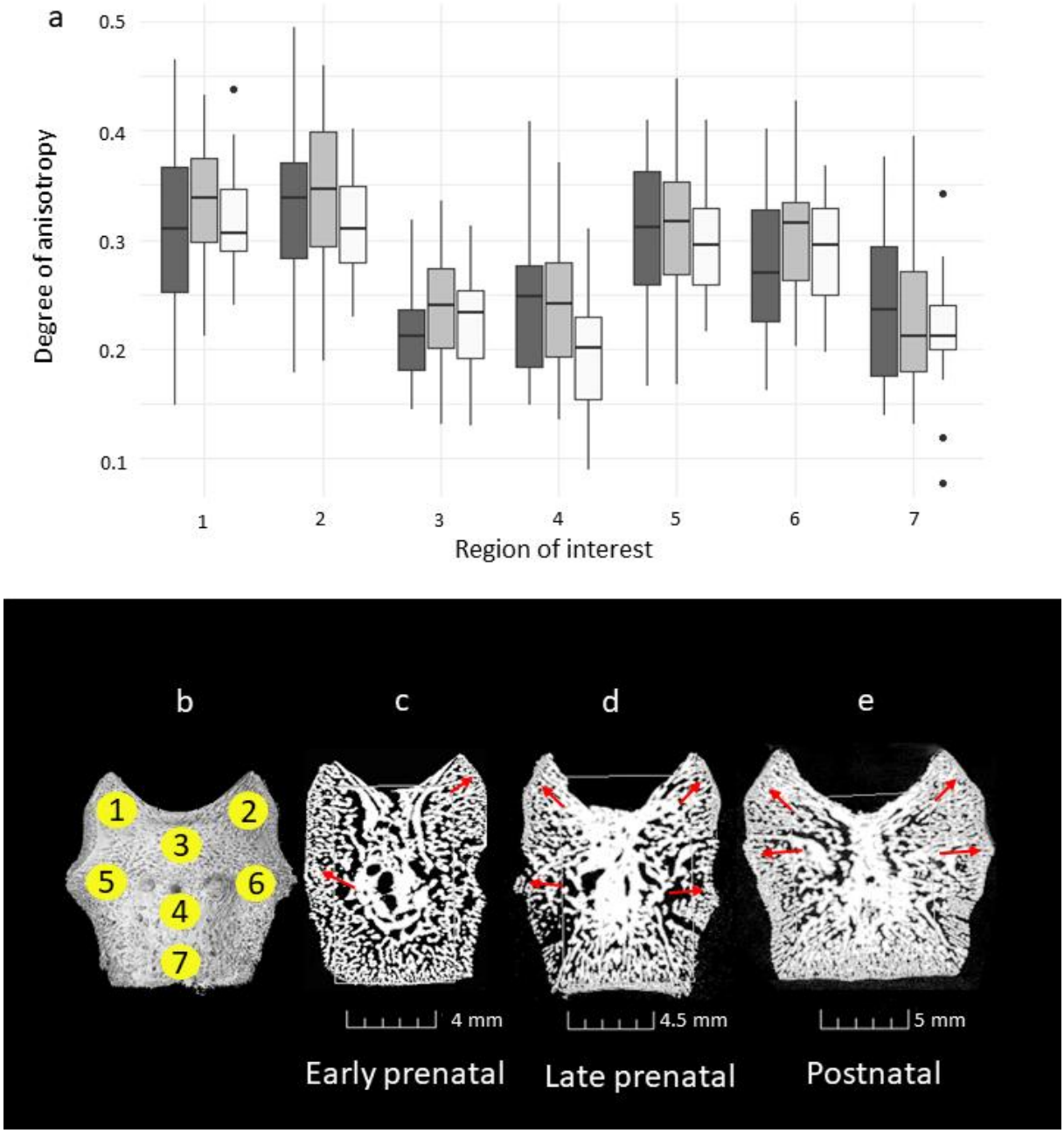


Figure 8: Regional variations of the degree of anisotropy (DA) in the pars basilaris. (a) Dark grey: early prenatal (20–30 gestational weeks, n=28). Light grey: late prenatal (30–40 gestational weeks, n=31). White: postnatal (birth–7.5 months, n=25). Dots represent outliers. Regions of interest (ROI) are illustrated (b) 3D reconstruction of the intracranial late prenatal pars basilaris. Yellow circles represent regions of interest (ROI): (ROI 1): right anterolateral maxima of the foramen magnum. (ROI 2): left anterolateral maxima of the foramen magnum. (ROI 3): anterior foramen magnum border. (ROI 4): primary ossification site. (ROI 5): right lateral angle. (ROI 6): left lateral angle. (ROI 7): spheno-occipital synchondrosis. Differences in DA are illustrated on the (c) early prenatal, (d) late prenatal and (e) postnatal pars basilaris. Red arrows represent the direction of the trabeculae in the anterolateral maxima (ROI 1 and ROI 2) and lateral angles (ROI 5 and ROI 6). Contrast and brightness have been adjusted to highlight trabeculae; therefore, the colour intensity is not representative of density. Graphs were created in RStudio using ggplot2 (Wickham, 2016). Images were generated using VGStudio Max V2.2 software (Volume Graphics GmbH, Heidelberg, Germany).

Comparisons between age groups

No significant differences in DA ($p>0.05$) were observed between the early and late prenatal age groups for any of the ROIs of the pars basilaris (Table 12, Figure 8). The postnatal primary ossification site (ROI 4) was significantly more isotropic (lower DA) ($p\leq0.04$) compared to the late prenatal group (Table 12, Figure 8). No further significant differences in DA ($p>0.05$) were observed between late prenatal and postnatal pars basilaris (Table 12, Figure 8).

Comparisons within age groups

Within the early prenatal pars basilaris, the anterior foramen magnum border (ROI 3) was significantly more isotropic (lower DA) compared to the anterolateral maxima (ROI 1, $p\leq0.01$ and ROI 2, $p\leq0.01$) and the lateral angles (ROI 5, $p\leq0.01$ and ROI 6, $p\leq0.05$) (Table 13, Figure 8). The primary ossification site (ROI 4) of the early prenatal pars basilaris was significantly more isotropic compared to the left anterolateral maxima (ROI 2, $p\leq0.04$) and the right lateral angle (ROI 5, $p\leq0.03$) (Table 13, Figure 8). However, the primary ossification site (ROI 4) did not significantly differ from the right anterolateral maxima (ROI 1, $p>0.05$) and the left lateral angle (ROI 6, $p>0.05$) (Table 13, Figure 8). The early prenatal spheno-occipital synchondrosis (ROI 7) was significantly more isotropic compared to both of the anterolateral maxima (ROI 1, $p\leq0.04$ and ROI 2, $p\leq0.01$) and the right lateral angle (ROI 5, $p\leq0.01$), but did not significantly differ from the left lateral angle (ROI 6, $p>0.05$) (Table 13, Figure 8).

Table 13: Pairwise comparisons of degree of anisotropy (DA) between regions of interest (ROI) within the early prenatal, late prenatal and postnatal pars basilaris

ROI comparisons	DA		
	Early prenatal (n=28)	Late prenatal (n=31)	Postnatal (n=25)
1 vs 2	1.00	1.00	1.00
1 vs 3	0.00*	0.00*	0.00*
2 vs 3	0.00*	0.00*	0.00*
1 vs 4	0.14	0.00*	0.00*
2 vs 4	0.04*	0.00*	0.00*
3 vs 4	1.00	1.00	1.00
1 vs 5	1.00	1.00	1.00
2 vs 5	1.00	1.00	1.00
3 vs 5	0.00*	0.00*	0.01*
4 vs 5	0.03*	0.00*	0.00*
1 vs 6	1.00	1.00	1.00
2 vs 6	1.00	1.00	1.00
3 vs 6	0.05*	0.00*	0.04*
4 vs 6	1.00	0.00*	0.00*
5 vs 6	1.00	1.00	1.00
1 vs 7	0.04*	0.00*	0.00*
2 vs 7	0.01*	0.00*	0.00*
3 vs 7	1.00	1.00	1.00
4 vs 7	1.00	1.00	1.00
5 vs 7	0.01*	0.00*	0.00*
6 vs 7	0.71	0.00*	0.00*

Early prenatal: 20–30 gestational weeks. Late prenatal: 30–40 gestational weeks. Postnatal: birth–7.5 months. Pars basilaris regions of interest: (ROI 1): right anterolateral maxima of the foramen magnum. (ROI 2): left anterolateral maxima of the foramen magnum. (ROI 3): anterior foramen magnum border. (ROI 4): primary ossification site. (ROI 5): right lateral angle. (ROI 6): left lateral angle. (ROI 7): spheno-occipital synchondrosis. *Significant value ($p \leq 0.05$). Values <0.01 are represented as 0.00.

Within the late prenatal and postnatal pars basilaris, the anterolateral maxima (ROI 1 and ROI 2) and the lateral angles (ROI 5 and ROI 6) were significantly less isotropic ($p \leq 0.05$) compared to the anterior foramen magnum border (ROI 3), the primary ossification site (ROI 4), and the spheno-occipital synchondrosis (ROI 7) (Table 13, Figure 8). Across all three age groups, no significant differences in DA ($p > 0.05$) were observed between the anterolateral maxima (ROI 1 and ROI 2) and the lateral angles (ROI 5 and ROI 6) (Table 13, Figure 8). Additionally, no significant differences in DA ($p > 0.05$) were observed between the anterior foramen magnum border (ROI 3), the primary ossification site (ROI 4), and the spheno-occipital synchondrosis (ROI 7) within any of the assessed age groups (Table 13, Figure 8).

3.3.2. Pars lateralis

Throughout all three age groups the posteromedial corner (ROI 4) had the highest median DA with a value of 0.29 (0.25-0.37) in the early prenatal age group, 0.35 (0.26-0.38) in the late prenatal age group and 0.37 (0.30-0.39) in the postnatal age group (Table 14, Figure 9). The remaining ROIs exhibited median DA values ranging between 0.24(0.19-0.28) and 0.29(0.25-0.34) across all three age groups (Table 14, Figure 9).

Comparisons between age groups

No significant differences in DA ($p > 0.05$) were observed between the early and late prenatal groups or between the late prenatal and postnatal age groups across all seven ROIs of the pars lateralis (Table 14, Figure 9).

Table 14: Median values and pairwise comparisons of degree of anisotropy (DA) between the early prenatal, late prenatal and postnatal pars lateralis for each region of interest (ROI)

Variable	ROI	Median (Q_1-Q_3)			Group comparisons (p<0.05)	
		Early prenatal (n=30)	Late prenatal (n=37)	Postnatal (n=29)	Early prenatal vs. late prenatal	Late prenatal vs. postnatal
DA	1	0.27 (0.19-0.34)	0.25 (0.18-0.32)	0.25 (0.22-0.30)	0.74	1.00
	2	0.29 (0.25-0.34)	0.29 (0.23-0.32)	0.25 (0.22-0.29)	0.91	0.24
	3	0.25 (0.19-0.28)	0.25 (0.22-0.27)	0.26 (0.22-0.28)	0.68	1.00
	4	0.29 (0.25-0.37)	0.35 (0.26-0.38)	0.37 (0.30-0.39)	0.26	0.65
	5	0.24 (0.19-0.28)	0.24 (0.20-0.30)	0.24 (0.20-0.28)	0.88	1.00
	6	0.27 (0.24-0.31)	0.29 (0.25-0.34)	0.28 (0.22-0.33)	0.33	0.47
	7	0.26 (0.20-0.34)	0.28 (0.23-0.33)	0.27 (0.19-0.32)	0.95	0.70

Early prenatal: 20–30 gestational weeks. Late prenatal: 30–40 gestational weeks. Postnatal: birth–7.5 months. Pars lateralis regions of interest: (ROI 1): jugular limb. (ROI 2): condylar limb. (ROI 3): lateral foramen magnum border. (ROI 4): posteromedial corner. (ROI 5): primary ossification site. (ROI 6): jugular process. (ROI 7): mastoid temporal border. *Significant value (p≤0.05). Values <0.01 are represented as 0.00.

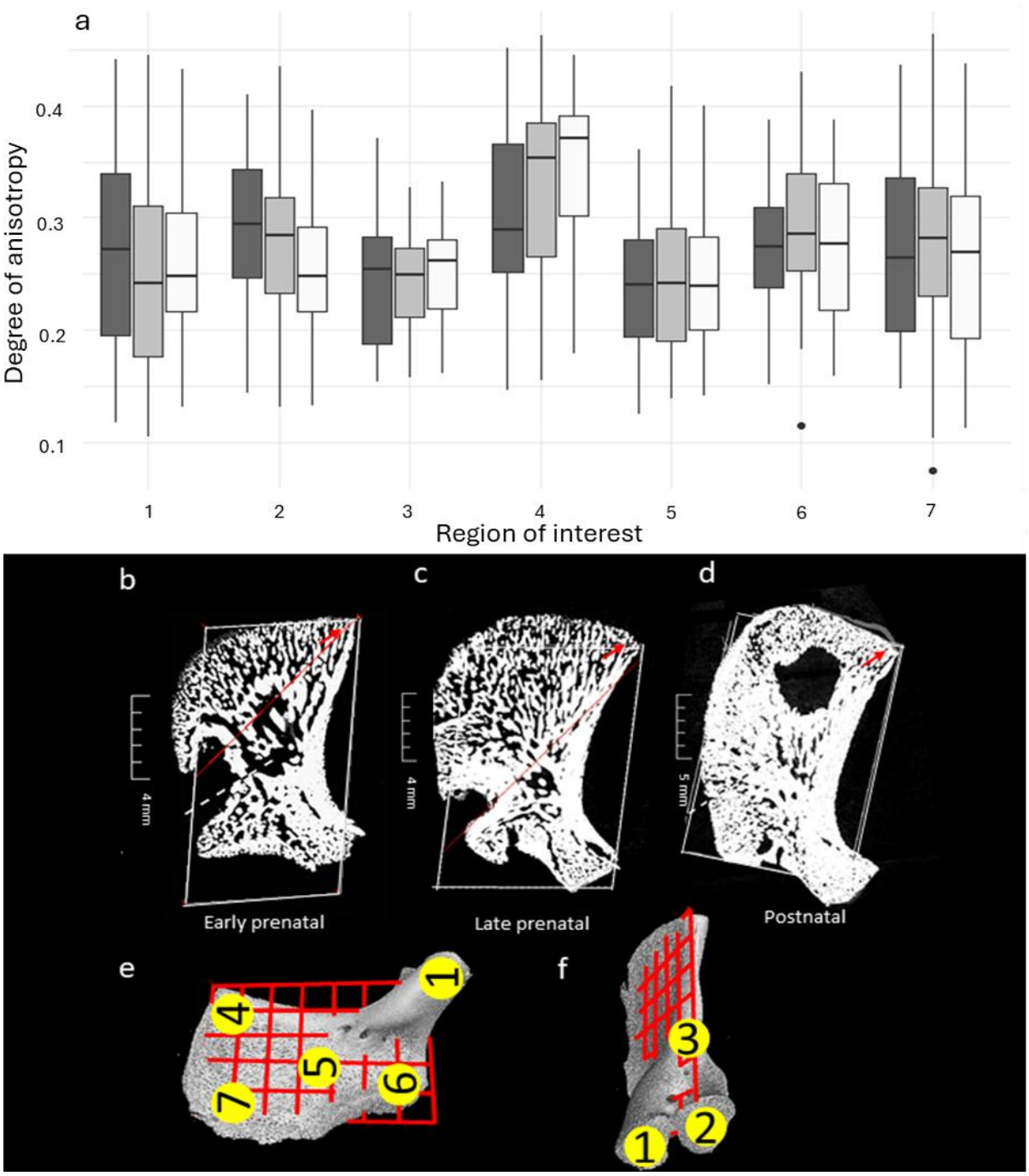


Figure 9: Regional variations of the degree of anisotropy (DA) in the pars lateralis. (a) Dark grey: early prenatal (20–30 gestational weeks, n=30). Light grey: late prenatal (30–40 gestational weeks, n=37). White: postnatal (birth–7.5 months, n=29). Dots represent outliers. Differences in DA are illustrated on the (b) early prenatal, (c) late prenatal and (d) postnatal pars lateralis. Red arrows represent the direction of the trabeculae in the posteromedial corner (ROI 4). Contrast and brightness have been adjusted to highlight trabeculae; therefore, the colour intensity is not representative of density. Regions of interest (ROI) are illustrated on (e) 3D reconstruction of the intracranial late prenatal pars lateralis and (f) 3D reconstruction of the hypoglossal region of the late prenatal pars lateralis. Yellow circles represent regions of interest (ROI): (ROI 1): jugular limb. (ROI 2): condylar limb. (ROI 3): lateral foramen magnum border. (ROI 4): posteromedial corner. (ROI 5): primary ossification site. (ROI 6): jugular process. (ROI 7): mastoid temporal border. Graphs were created in RStudio using ggplot2 (Wickham, 2016). Images were generated using VGStudio Max V2.2 software (Volume Graphics GmbH, Heidelberg, Germany).

Comparisons within age groups

Within the early prenatal pars lateralis, the posteromedial corner (ROI 4) was significantly less isotropic (higher DA) compared to the lateral foramen magnum border (ROI 3, p≤0.03) and the primary ossification site (ROI 5, p≤0.05) (Table 15, Figure 9). The posteromedial corner (ROI 4) did not significantly differ (p>0.05) from any of the other ROIs within the early prenatal pars lateralis (Table 15, Figure 9).

Within the late prenatal pars lateralis, the posteromedial corner (ROI 4) exhibited a significantly higher DA compared to the jugular limb (ROI 1, p≤0.01), lateral foramen magnum border (ROI 3, p≤0.01), and primary ossification site (ROI 5, p≤0.01), (**Error! Not a valid bookmark self-reference.**, Figure 9). The DA of the late prenatal posteromedial corner (ROI 4) did not significantly differ (p>0.05) from the condylar limb (ROI 2), jugular process (ROI 6), and mastoid temporal border (ROI 7) within the late prenatal pars lateralis (Table 15, Figure 9).

Within the postnatal pars lateralis, the posteromedial corner (ROI 4) was significantly less isotropic (higher DA) compared to all other ROIs (ROI 1, p≤0.01; ROI 2, p≤0.01; ROI 3, p≤0.01; ROI 5, p≤0.01; ROI 6, p≤0.01; ROI 7, p≤0.01) (**Error! Not a valid bookmark self-reference.**, Figure 9). Throughout all three developmental stages, no significant differences in DA (p>0.05) were observed between the jugular limb (ROI 1), condylar limb (ROI 2), lateral foramen magnum border (ROI 3), primary ossification site (ROI 5), jugular process (ROI 6), and mastoid temporal border (ROI 7) (**Error! Not a valid bookmark self-reference.**, Figure 9).

Table 15: Pairwise comparisons of degree of anisotropy (DA) between regions of interest (ROI) within the early prenatal, late prenatal and postnatal pars lateralis

ROI comparisons	DA		
	Early prenatal (n=30)	Late prenatal (n=37)	Postnatal (n=29)
1 vs 2	1.00	1.00	1.00
1 vs 3	1.00	1.00	1.00
2 vs 3	0.22	1.00	1.00
1 vs 4	1.00	0.01*	0.00*
2 vs 4	1.00	0.29	0.00*
3 vs 4	0.03*	0.00*	0.00*
1 vs 5	1.00	1.00	1.00
2 vs 5	0.28	1.00	1.00
3 vs 5	1.00	1.00	1.00
4 vs 5	0.05*	0.01*	0.00*
1 vs 6	1.00	0.60	1.00
2 vs 6	1.00	1.00	1.00
3 vs 6	1.00	0.36	1.00
4 vs 6	1.00	1.00	0.01*
5 vs 6	1.00	0.68	1.00
1 vs 7	1.00	1.00	1.00
2 vs 7	1.00	1.00	1.00
3 vs 7	1.00	1.00	1.00
4 vs 7	1.00	0.19	0.00*
5 vs 7	1.00	1.00	1.00
6 vs 7	1.00	1.00	1.00

Early prenatal: 20–30 gestational weeks. Late prenatal: 30–40 gestational weeks. Postnatal: birth–7.5 months. Pars lateralis regions of interest: (ROI 1): jugular limb. (ROI 2): condylar limb. (ROI 3): lateral foramen magnum border. (ROI 4): posteromedial corner. (ROI 5): primary ossification site. (ROI 6): jugular process. (ROI 7): mastoid temporal border. *Significant value ($p \leq 0.05$). Values <0.01 are represented as 0.00.

3.4. Mean grey value (MGV)

3.4.1. Pars basilaris

Median MGV values were higher in the early prenatal age group (ranging between 33059.12 and 35136.98) compared to the late prenatal stage (ranging between 21402.07 and 27539.86) across all ROIs of the pars basilaris, (Table 16, Figure 10). In the postnatal group, MGV values were similar to or slightly lower than those of the late prenatal pars basilaris across all ROIs, with median MGV ranging between 19866.53 and 26282.71 in the postnatal group (Table 16, Figure 10).

Within the early prenatal pars basilaris, the median MGV ranged between 33059.12 (IQR: 17954.41–35654.89) in the spheno-occipital synchondrosis (ROI 7) and 35136.98 (IQR: 21648.12–37707.30) in the anterior foramen magnum border (ROI 3) (Table 16, Figure 10). Within the late prenatal age group, the highest median MGV was observed in the anterior foramen magnum border (ROI 3: Median: 27539.86, IQR: 20333.64–34089.83) (Table 16, Figure 10). The median MGV for the remaining ROIs in the late prenatal group ranged between 21402.07 and 24757.80 (Table 16, Figure 10). Within the postnatal pars basilaris, the highest median MGV was observed in the anterior foramen magnum border (ROI 3: Median: 26282.71, IQR: 22209.71–35577.99) (Table 16, Figure 10). The lowest median MGV was found in the left lateral angle (ROI 6: Median 19866.53, IQR: 16997.45–27551.93), with the remaining ROIs ranging between 21682.06 and 23692.49 (Table 16, Figure 10).

Table 16: Median values and pairwise comparisons of mean grey value (MGV) between the early prenatal, late prenatal and postnatal pars basilaris for each region of interest (ROI)

Variable	ROI	Median (Q_1-Q_3)			Group comparisons (p<0.05)	
		Early prenatal (n=28)	Late prenatal (n=31)	Postnatal (n=25)	Early prenatal vs. late prenatal	Late prenatal vs. postnatal
MGV	1	34245.88 (18665.11-36157.70)	24185.88 (18001.22-29244.38)	22039.97 (17770.08-29456.23)	0.04*	1.00
	2	34368.64 (18973.63-36307.08)	23942.13 (17042.38-30152.28)	22374.95 (18661.58-30028.05)	0.03*	1.00
	3	35136.98 (21648.12-37707.30)	27539.86 (20333.64-34089.83)	26282.71 (22209.71-35577.99)	0.14	0.84
	4	33124.16 (20678.09-37244.42)	24757.80 (17932.23-30076.63)	23692.49 (17779.66-28815.88)	0.04*	1.00
	5	33799.05 (21412.22-36200.48)	21402.07 (17459.76-28067.68)	21764.19 (16916.56-27129.49)	0.03*	1.00
	6	33306.95 (18382.19-36062.97)	21634.73 (15719.84-29089.81)	19866.53 (16997.45-27551.93)	0.02*	1.00
	7	33059.12 (17954.41-35654.89)	23803.30 (16577.55-29970.14)	21682.06 (17179.44-27851.64)	0.04*	1.00

Early prenatal: 20–30 gestational weeks. Late prenatal: 30–40 gestational weeks. Postnatal: birth–7.5 months. Pars basilaris regions of interest: (ROI 1): right anterolateral maxima of the foramen magnum. (ROI 2): left anterolateral maxima of the foramen magnum. (ROI 3): anterior foramen magnum border. (ROI 4): primary ossification site. (ROI 5): right lateral angle. (ROI 6): left lateral angle. (ROI 7): spheno-occipital synchondrosis. *Significant value (p≤0.05). Values <0.01 are represented as 0.00.

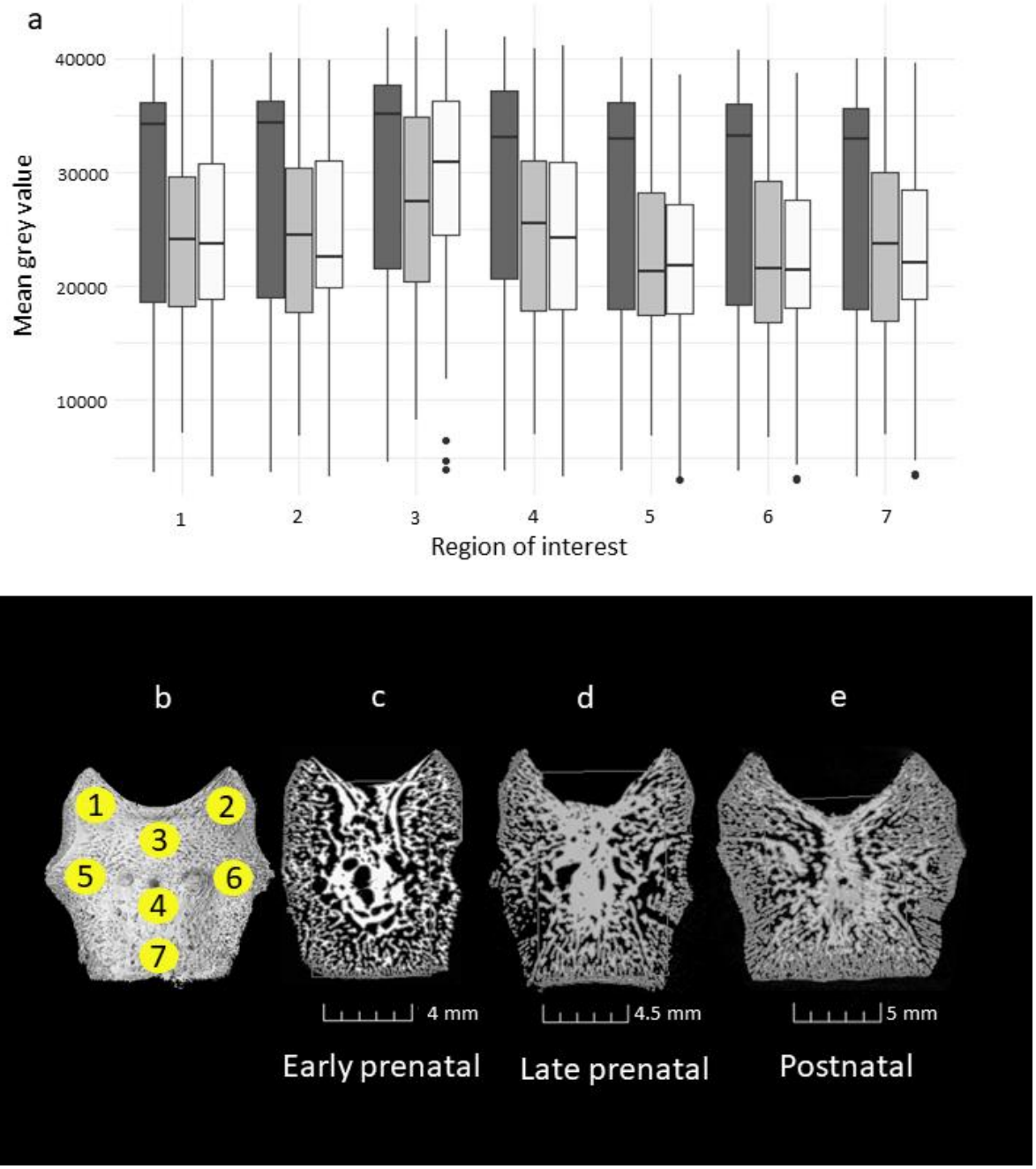


Figure 10: Regional variations of the mean grey value (MGV) in the pars basilaris. (a) Dark grey: early prenatal (20–30 gestational weeks, n=28). Light grey: late prenatal (30–40 gestational weeks, n=31). White: postnatal (birth–7.5 months, n=25). Dots represent outliers. Regions of interest (ROI) are illustrated (b) 3D reconstruction of the intracranial late prenatal pars basilaris. Yellow circles represent regions of interest (ROI): (ROI 1): right anterolateral maxima of the foramen magnum. (ROI 2): left anterolateral maxima of the foramen magnum. (ROI 3): anterior foramen magnum border. (ROI 4): primary ossification site. (ROI 5): right lateral angle. (ROI 6): left lateral angle. (ROI 7): spheno-occipital synchondrosis. Differences in MGV are illustrated on the (c) early prenatal, (d) late prenatal and (e) postnatal pars basilaris. Brighter areas represent regions of higher MGV. Graphs were created in RStudio using ggplot2 (Wickham, 2016). Images were generated using VGStudio Max V2.2 software (Volume Graphics GmbH, Heidelberg, Germany).

Comparisons between age groups

The late prenatal pars basilaris had a significantly lower mean grey value (MGV) compared to the early prenatal pars basilaris across all ROIs (ROI 1, $p \leq 0.04$; ROI 2, $p \leq 0.03$; ROI 4, $p \leq 0.04$; ROI 5, $p \leq 0.03$; ROI 6, $p \leq 0.02$; ROI 7, $p \leq 0.04$) except for the anterior foramen magnum border (ROI 3, $p > 0.05$) (Table 16, Figure 10). Comparisons of MGV between the late prenatal and postnatal pars basilaris yielded no significant results ($p > 0.05$) for any of the ROIs (Table 16, Figure 10)

Comparisons within age groups

The MGV did not significantly differ ($p > 0.05$) among any of the ROIs of the pars basilaris within any of the assessed age groups (Table 17, Figure 10).

Table 17: Pairwise comparisons of mean grey value (MGV) between regions of interest (ROI) within the early prenatal, late prenatal and postnatal pars basilaris

ROI comparisons	MGV		
	Early prenatal (n=28)	Late prenatal (n=31)	Postnatal (n=25)
1 vs 2	1.00	1.00	1.00
1 vs 3	1.00	1.00	0.96
2 vs 3	1.00	1.00	1.00
1 vs 4	1.00	1.00	1.00
2 vs 4	1.00	1.00	1.00
3 vs 4	1.00	1.00	1.00
1 vs 5	1.00	1.00	1.00
2 vs 5	1.00	1.00	1.00
3 vs 5	1.00	0.49	0.08
4 vs 5	1.00	1.00	1.00
1 vs 6	1.00	1.00	1.00
2 vs 6	1.00	1.00	1.00
3 vs 6	1.00	0.52	0.06
4 vs 6	1.00	1.00	1.00
5 vs 6	1.00	1.00	1.00
1 vs 7	1.00	1.00	1.00
2 vs 7	1.00	1.00	1.00
3 vs 7	1.00	1.00	0.47
4 vs 7	1.00	1.00	1.00
5 vs 7	1.00	1.00	1.00
6 vs 7	1.00	1.00	1.00

Early prenatal: 20–30 gestational weeks. Late prenatal: 30–40 gestational weeks. Postnatal: birth–7.5 months. Pars basilaris regions of interest: (ROI 1): right anterolateral maxima of the foramen magnum. (ROI 2): left anterolateral maxima of the foramen magnum. (ROI 3): anterior foramen magnum border. (ROI 4): primary ossification site. (ROI 5): right lateral angle. (ROI 6): left lateral angle. (ROI 7): spheno-occipital synchondrosis. *Significant value ($p \leq 0.05$). Values <0.01 are represented as 0.00.

3.4.2. Pars lateralis

MGV values were higher in the early prenatal age group (ranging between 32888.22 and 35448.38) compared to the late prenatal stage (ranging between 19039.85 and 26437.41) across all ROIs of the pars lateralis (Table 18, Figure 11). In the postnatal group, MGV values were similar to or slightly lower than those of the late prenatal pars lateralis across all ROIs, ranging between 18080.65 and 27358.45 in the postnatal group (Table 18, Figure 11).

Within the early prenatal pars lateralis, the median MGV ranged between 32888.22 (IQR: 18045.37–34,504.88) in the mastoid temporal border (ROI 7) and 35448.38 (IQR: 25,640.06–37616.52) in the lateral foramen magnum border (ROI 3) (Table 18, Figure 11). Within the late prenatal age group, the condylar limb (ROI 2: Median 24375.80, IQR: 19187.99–32830.13), lateral foramen magnum border (ROI 3: Median 26437.41, IQR: 18777.53–34297.41), and primary ossification site (ROI 5: Median 26349.09, IQR: 20599.14–33275.59) had the highest median MGV values (Table 18, Figure 11). The median MGV for the remaining ROIs in the late prenatal group ranged between 19039.85 and 21236.41 (Table 18, Figure 11). In the postnatal group, the highest median MGV was observed in the lateral foramen magnum border (ROI 3: Median 27358.45, IQR: 22165.36–33014.06), followed by the primary ossification site (ROI 5: Median 25772.04, IQR: 19877.83–33456.44), and the condylar limb (ROI 2: Median 24387.37, IQR: 18961.58–32847.47). The lowest median MGV was found in the mastoid temporal border (ROI 7: Median 18080.65, IQR: 15299.58–23946.72), with the remaining ROIs ranging between 20052.64 and 21242.82 (Table 18, Figure 11).

Table 18: Median values and pairwise comparisons of mean grey value (MGV) between the early prenatal, late prenatal and postnatal pars lateralis for each region of interest (ROI)

		Median (Q_1-Q_3)			Group comparisons ($p<0.05$)	
Variable	ROI	Early prenatal (n=30)	Late prenatal (n=37)	Postnatal (n=29)	Early prenatal vs. late prenatal	Late prenatal vs. postnatal
MGV	1	33830.34 (22901.40-35055.03)	21087.71 (17284.67-29349.69)	20777.88 (16923.92-26981.33)	0.01*	1.00
	2	34458.05 (23443.12-37073.19)	24375.80 (19187.99-32830.13)	24387.37 (18961.58-32847.47)	0.04*	1.00
	3	35448.38 (25640.06-37616.52)	26437.41 (18777.53-34297.41)	27358.45 (22165.36-33014.06)	0.08	1.00
	4	34080.15 (22873.58-35912.42)	19069.33 (16418.84-27625.59)	20052.64 (15281.17-27467.85)	0.01*	1.00
	5	34844.97 (22267.59-36851.36)	26349.09 (20599.14-33275.59)	25772.04 (19877.83-33456.44)	0.20	1.00
	6	33526.67 (20887.89-35894.33)	21236.41 (16630.32-27297.31)	21242.82 (16494.95-26757.10)	0.01*	1.00
	7	32888.22 (18045.37-34504.88)	19039.85 (14649.49-21768.49)	18080.65 (15299.58-23946.72)	0.00*	1.00

Early prenatal: 20–30 gestational weeks. Late prenatal: 30–40 gestational weeks. Postnatal: birth–7.5 months. Pars lateralis regions of interest: (ROI 1): jugular limb. (ROI 2): condylar limb. (ROI 3): lateral foramen magnum border. (ROI 4): posteromedial corner. (ROI 5): primary ossification site. (ROI 6): jugular process. (ROI 7): mastoid temporal border. *Significant value ($p\leq0.05$). Values <0.01 are represented as 0.00.

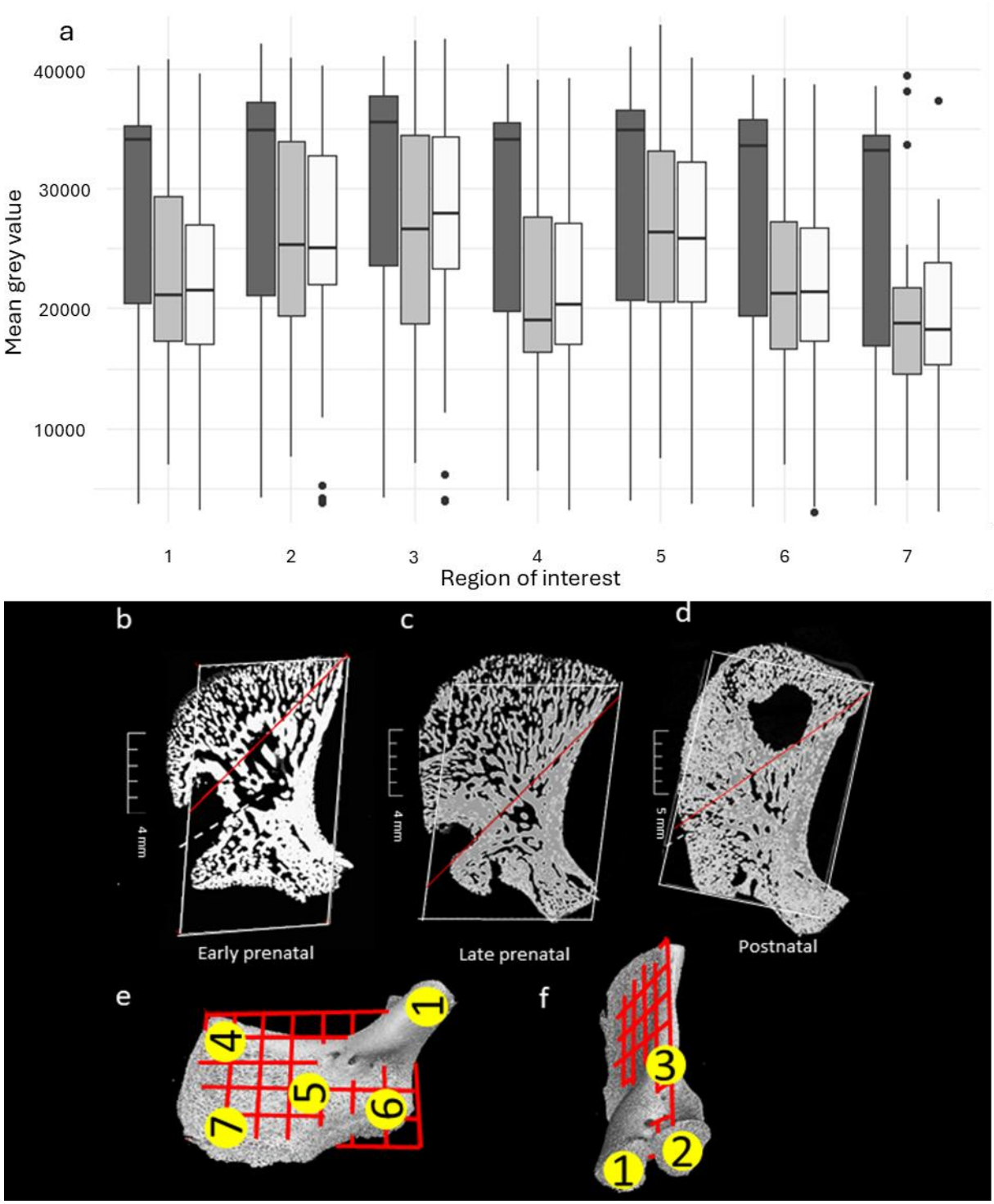


Figure 11: Regional variations of the mean grey value (MGV) in the pars lateralis. (a) Dark grey: early prenatal (20–30 gestational weeks, n=30). Light grey: late prenatal (30–40 gestational weeks, n=37). White: postnatal (birth–7.5 months, n=29). Dots represent outliers. Differences in MGV are illustrated on the (b) early prenatal, (c) late prenatal and (d) postnatal pars lateralis. Brighter areas represent regions of higher MGV. Regions of interest (ROI) are illustrated on (e) 3D reconstruction of the intracranial late prenatal pars lateralis and (f) 3D reconstruction of the hypoglossal region of the late prenatal pars lateralis. Yellow circles represent regions of interest (ROI): (ROI 1): jugular limb. (ROI 2): condylar limb. (ROI 3): lateral foramen magnum border. (ROI 4): posteromedial corner. (ROI 5): primary ossification site. (ROI 6): jugular process. (ROI 7): mastoid temporal border. Graphs were created in RStudio using ggplot2 (Wickham, 2016). Images were generated using VGStudio Max V2.2 software (Volume Graphics GmbH, Heidelberg, Germany).

Comparisons between age groups

The late prenatal pars lateralis had a significantly lower MGV compared to the early prenatal pars lateralis in the jugular limb (ROI 1, $p \leq 0.01$), condylar limb (ROI 2, $p \leq 0.04$), posteromedial corner (ROI 4, $p \leq 0.01$), jugular process (ROI 6, $p \leq 0.01$), and mastoid temporal (ROI 7, $p \leq 0.01$) (Table 18, Figure 11). The MGV of the lateral foramen magnum border (ROI 3) and the primary ossification site (ROI 5) did not differ significantly ($p > 0.05$) between the prenatal groups (Table 18, Figure 11). No significant differences ($p > 0.05$) in MGV were observed between the late prenatal and postnatal pars lateralis across all seven ROIs (Table 18, Figure 11).

Comparisons within age groups

No significant differences in MGV ($p > 0.05$) were observed between any of the ROIs within the early prenatal pars lateralis (Table 19, Figure 11). Within the late prenatal pars lateralis, the mastoid temporal border (ROI 7) exhibited a significantly lower MGV compared to the condylar limb (ROI 2, $p \leq 0.01$), lateral foramen magnum border (ROI 3, $p \leq 0.01$), and primary ossification site (ROI 5, $p \leq 0.01$) (Table 19, Figure 11). The MGV of the mastoid temporal border (ROI 7) did not significantly differ ($p > 0.05$) from the jugular limb (ROI 1), posteromedial corner (ROI 4), and jugular process (ROI 6) (Table 19, Figure 11) within the late prenatal pars lateralis. No further significant differences in MGV ($p > 0.05$) were observed within the late prenatal pars lateralis (Table 19, Figure 11).

Table 19: Pairwise comparisons of mean grey value (MGV) between regions of interest (ROI) within the early prenatal, late prenatal and postnatal pars lateralis

ROI comparisons	MGV		
	Early prenatal (n=30)	Late prenatal (n=37)	Postnatal (n=29)
1 vs 2	1.00	1.00	1.00
1 vs 3	1.00	1.00	0.09
2 vs 3	1.00	1.00	1.00
1 vs 4	1.00	1.00	1.00
2 vs 4	1.00	0.44	0.56
3 vs 4	1.00	0.30	0.02*
1 vs 5	1.00	1.00	1.00
2 vs 5	1.00	1.00	1.00
3 vs 5	1.00	1.00	1.00
4 vs 5	1.00	0.28	0.35
1 vs 6	1.00	1.00	1.00
2 vs 6	1.00	0.68	0.94
3 vs 6	1.00	0.48	0.04*
4 vs 6	1.00	1.00	1.00
5 vs 6	1.00	0.43	0.61
1 vs 7	1.00	0.6	1.00
2 vs 7	0.38	0.01*	0.08
3 vs 7	0.23	0.01*	0.00*
4 vs 7	1.00	1.00	1.00
5 vs 7	0.95	0.01*	0.05*
6 vs 7	1.00	1.00	1.00

Early prenatal: 20–30 gestational weeks. Late prenatal: 30–40 gestational weeks. Postnatal: birth–7.5 months. Pars lateralis regions of interest: (ROI 1): jugular limb. (ROI 2): condylar limb. (ROI 3): lateral foramen magnum border. (ROI 4): posteromedial corner. (ROI 5): primary ossification site. (ROI 6): jugular process. (ROI 7): mastoid temporal border. *Significant value ($p \leq 0.05$). Values <0.01 are represented as 0.00.

Within the postnatal pars lateralis, the lateral foramen magnum border (ROI 3) had a significantly higher MGV compared to the posteromedial corner (ROI 4, $p \leq 0.02$), jugular process (ROI 6, $p \leq 0.04$), and the mastoid temporal border (ROI 7, $p \leq 0.01$) (Table 19, Figure 11). In addition, the mastoid temporal border (ROI 7) exhibited a significantly lower MGV compared to the primary ossification site (ROI 5, $p \leq 0.05$) within the postnatal pars lateralis (Table 19, Figure 11). No significant differences were observed in MGV ($p > 0.05$) between the jugular limb (ROI 1), condylar limb (ROI 2), posteromedial corner (ROI 4), primary ossification site (ROI 5), and jugular process (ROI 6) within the postnatal pars lateralis (Table 19, Figure 11).

Chapter 4: Discussion and conclusions

The current study investigated the internal architecture of the pars basilaris and pars lateralis across the early prenatal, late prenatal, and postnatal stages of growth to ascertain the nature of the internal structure of these bones relative to age and morphological regions associated with muscle attachments, neurovasculature and surrounding bones. The findings of this study contribute to the current foundational work in understanding the ontogeny of the trabecular structure within the cranium during the prenatal and postnatal periods of growth. These results allow for inferences to be made about the normal growth patterns of the immature occipital bone.

The majority of ROIs assessed followed a similar pattern of trabecular development across the three age groups. In general, the late prenatal pars basilaris and pars lateralis tended to have fewer (lower TbN), yet thicker (higher TbTh) trabeculae, a higher bone volume fraction (BV/TV), lower bone surface volume ratio (BS/BV), lower mean grey value (MGV) and minimal differences in trabecular separation (TbSp) and degree of anisotropy (DA) compared to the early prenatal group. This suggests that prenatal development is characterised by bone formation, modelling and delayed mineralisation without significant reorganisation of the bones (Reissis & Abel, 2012; Acquaah et al., 2015; Wiles et al., 2024). The architectural variables tended not to significantly differ between the late prenatal and postnatal age groups, suggesting that the trabecular architecture established during the prenatal period is relatively stable through to the postnatal phase. Select ROIs within the bones followed alternative developmental trajectories that may reflect the specific influence of the associated muscle attachments, neurovasculature and surrounding bones on development. In addition, the

trabecular architecture was not uniform throughout the bones, which may indicate that different regions within the pars basilaris and pars lateralis may have developed specific structural adaptations tailored to their functional roles and local mechanical environments (Richards & Jabbour, 2011).

4.1. Prenatal development

The main differences observed between the early and late prenatal pars basilaris and pars lateralis was that early prenatal bones had a significantly higher BV/TV with thicker yet fewer trabeculae. This suggests that osteoblast deposition is outpacing osteoclast resorption during prenatal development, as there is a net increase in BV/TV (Oftadeh et al., 2015). Modelling involves uncoupled bone formation and resorption where the activity of osteoblasts and osteoclasts do not necessarily act in tandem, leading to changes in bone volume that result in changes in bone shape and size (Frost, 1990; Robling & Turner, 2009). Thus, the higher BV/TV of the late prenatal pars basilaris and pars lateralis compared to the early prenatal bones suggests that modelling is the predominant mechanism behind prenatal development (Frost, 1990; Robling & Turner, 2009). The significant differences in BS/BV between the early and late prenatal groups also likely reflect ongoing bone modelling during the prenatal period (Frost, 1990; Robling & Turner, 2009; Bouxsein et al., 2010). Modelling reshapes the bone by adding or removing bone from the surfaces to better meet mechanical and developmental needs (Frost, 1990; Robling & Turner, 2009). As trabeculae become thicker and bone volume increases, the BS/BV decreases, indicating that bone is being reshaped in a way that reduces unnecessary surface area while increasing overall bone mass (Bouxsein et al., 2010).

Despite the net increase in BV/TV, the significantly lower TbN in the late prenatal age group compared to the early prenatal age group suggests that a significant degree of resorption is occurring (Reid et al., 2024). The process of removing trabeculae is termed “sculpting” and contributes to the shape changes in the bones during development (Reid et al., 2024). Edamoto et al. (2018) demonstrated that the removal of trabeculae appears to be necessary for normal bone maturation, as osteoblasts cannot function properly without osteoclasts. In Tnfsf11−/− mice, which lack osteoclasts, osteoblasts were misaligned and unable to form a distinct osteoblast surface, resulting in impaired bone formation (Edamoto et al., 2018). Thus, the interplay between osteoblasts and osteoclasts is necessary for normal bone development within the occipital bone.

Edamoto et al. (2018) also demonstrated the role of the growing brain in shaping the postnatal pars basilaris, where the compressive stress from brain growth was related to resorption by osteoclasts on the intracranial surface of the murine pars basilaris. The medulla oblongata undergoes a 5.3-fold increase in size between 15 gestational weeks and birth (Dovjak et al., 2020). Thus, the compressive stress caused by the growth of the medulla could influence the activity of the osteoclasts on the pars basilaris and pars lateralis, resulting in a lower TbN in the late prenatal age group compared to the early prenatal group (Edamoto et al., 2018; Dovjak et al., 2020). Notably, the ROIs most closely related to the medulla oblongata, i.e., the anterior foramen magnum border of the pars basilaris (ROI 3) and the lateral foramen magnum border of the pars lateralis (ROI 3) had significantly fewer trabeculae compared to other regions within the early prenatal and late prenatal age groups. Thus, suggesting a relationship between the growth of the medulla oblongata and the foramen magnum borders.

Edamoto et al. (2018) also showed that tensile stress from the muscles of the pars basilaris contributed to bone formation by osteoblasts on its extracranial surface in postnatal mice. However, the prenatal human muscles associated with the pars basilaris and pars lateralis are weak and underdeveloped until the onset of postnatal postural milestones (Krmpotić-Nemanić et al., 2006; Eggington et al., 2024). Thus, it is unlikely that enough tensile stress is being generated to lead to the greater TbTh and BV/TV observed in the late prenatal pars basilaris and pars lateralis compared to the early prenatal bones. Moreover, other indicators of adaptation to mechanical loading from muscles, such as degree of anisotropy (DA) and trabecular separation (TbSp), did not significantly differ between the prenatal age groups, suggesting that factors beyond the tensile stress from muscles have led to the differences in TbTh and BV/TV (Wiles et al., 2024). Similar observations have been made within the postcranial skeleton where TbTh has been shown to increase in the human prenatal vertebrae (Nuzzo et al., 2003; Acquaah et al., 2015), femur (Salle et al., 2002; Reissis & Abel, 2012; Wiles et al., 2024), and humerus (Reissis & Abel, 2012), despite the associated muscular structures being underdeveloped and unlikely to cause increases in TbTh.

The significantly higher TbTh in the late prenatal group compared to the early prenatal group may be attributable to the uterine environment which promotes bone development and facilitates increased vascularisation during pregnancy (Fournier et al., 2021). Vascularisation brings osteoblasts into the avascular hypertrophic chondrocyte zone of the growth plate (Walzer et al., 2014). In addition, the vasculature provides a pathway for the blood vessels that transport nutrients and oxygen to the osteoblasts responsible for bone formation (Filipowska et al., 2017). Thus, promoting bone development and possibly leading to an

increase in TbTh. Moreover, the anterior foramen magnum border (ROI 3) and the lateral foramen magnum border (ROI 3) of the pars lateralis (ROI 5) tended to have significantly thicker trabeculae compared to other regions within the early prenatal and late prenatal age groups. The high concentration of neurovascular structures passing through the foramen magnum necessitates a rich blood supply to support their development and function (Rhoton, 2000). In addition, the presence of the vertebral arteries within the foramen magnum border directly vascularises the bony perimeter of the foramen magnum (Rhoton, 2000). The primary ossification sites of the pars basilaris (ROI 4) and pars lateralis (ROI 5) also tended to have significantly thicker trabeculae compared to other regions within the bones. The primary ossification site of the pars basilaris (ROI 4) is highly vascularised owing to the presence of the basilar plexus on its intracranial surface, and the primary ossification site of the pars lateralis (ROI 5) receives vascularisation from a sigmoid emissary vein that connects the occipital sigmoid and suboccipital venous plexi (Rhoton, 2000). Thus, the high TbTh of the primary ossification sites and foramen magnum borders of the pars basilaris and pars lateralis may be attributed to the high vascularity of these areas.

Maternal oestrogens may also play a role in the significantly higher TbTh and, subsequently, higher BV/TV seen in the late prenatal pars basilaris and pars lateralis compared to the early prenatal bones (Figus et al., 2022). Oestrogen is known to promote bone deposition in the adult skeleton through signalling via oestrogen receptors on osteoblasts (Noirrit-Esclassan et al., 2021). Maternal oestrogen and oestrogen produced by the placenta are elevated during gestation and have been shown to affect the development of the fetal skeleton (Migliaccio et al., 1996). A murine study indicated that fetal trabecular mass increased in the offspring of

pregnant mice injected with synthetic oestrogen (Migliaccio et al., 1996). Moreover, oestrogen stimulates angiogenesis in the placenta by regulating the expression of angioregulatory growth factors (Filipowska et al., 2017). The same factors have been shown to affect angiogenesis in bone development, which would increase vascularisation and promote osteoblast deposition of bone matrix (Noirrit-Esclassan et al., 2021). Thus, it can be hypothesised that the significantly greater TbTh in the late prenatal group may be a function of oestrogen acting on the fetal pars basilaris and pars lateralis.

The length of exposure to the uterine environment may contribute to the regional differences in trabecular architecture observed within the prenatal pars basilaris and pars lateralis. The anterior foramen magnum border (ROI 3) and primary ossification site (ROI 4) of the pars basilaris and the lateral foramen magnum border (ROI 3) and the primary ossification site (ROI 5) of the pars lateralis tended to have significantly thicker, yet fewer trabeculae compared to most of the other ROIs within the early prenatal and late prenatal age group. The primary ossification sites and foramen magnum borders are the first regions to develop in the pars basilaris and pars lateralis and, therefore, are exposed to the intrinsic and extrinsic factors that drive bone modelling for an extended period (Mackie et al., 2008; Badiu et al., 2019; Grzonkowska et al., 2021). The prolonged exposure to these factors leads to more osteoclast activity, causing a lower TbN relative to the other regions, coupled with increased osteoblast activity resulting in thicker trabeculae (Robling & Turner, 2009). Therefore, the differences in trabecular architecture across the bones may reflect the maturity of the different regions of the pars basilaris and pars lateralis.

Less mature regions of the pars lateralis, such as the posteromedial corner (ROI 4) and the mastoid temporal border (ROI 7), were observed to be highly cartilaginous as reflected by the numerous, thin trabeculae that did not exhibit significant differences in BV/TV between the prenatal age groups (Salle et al., 2002; Wiles et al., 2024). Cartilage has a lower density than bone and, therefore, may not have accumulated enough bone volume to register significant changes in BV/TV (Bouxsein et al., 2010; Cendekiawan et al., 2010). Cartilage is also more flexible than bone, thus allowing for flexibility during the expansion of the cranial base (Cendekiawan et al., 2010). The posteromedial corner (ROI 4) is associated with the squamous part of the occipital bone at the posterior interoccipital synchondrosis, which allows for longitudinal growth to accommodate brain expansion and thus requires flexibility (Cendekiawan et al., 2010). The mastoid temporal border (ROI 7) contributes to the mastoid fontanelle, which allows for continued brain growth after birth and, therefore, also requires flexibility during postnatal life (Cendekiawan et al., 2010; Lipsett et al., 2023). Thus, the presence of cartilage as opposed to bone tissue at the posteromedial corner (ROI 4) and the mastoid temporal border (ROI 7) ensures that these regions remain patent and flexible to accommodate prenatal and postnatal brain expansion (Cendekiawan et al., 2010; Lipsett et al., 2023).

4.1.1. Trabecular organisation

Variables that describe the trabecular organisation of bone, such as degree of anisotropy (DA) and trabecular separation (TbSp), tended not to differ significantly between the prenatal age groups. Thus, indicating that the structural organisation of the trabecular bone remains relatively stable across prenatal development (Oftadeh et al., 2015; Wiles et al., 2024). Despite

minimal differences in DA and TbSp found between age groups, regional differences were observed within the pars basilaris and pars lateralis. Within the early prenatal and late prenatal pars basilaris, the more lateral regions, such as the anterolateral maxima (ROI 1 and ROI 2) and lateral angles (ROI 5 and ROI 6), had a higher DA than the midline ROIs, including the anterior foramen magnum border (ROI 3), primary ossification site (ROI 4), and spheno-occipital synchondrosis (ROI 7). The anterolateral maxima (ROI 1 and ROI 2) are the attachment sites for the paired rectus capitis anterior muscles, and the lateral angles (ROI 5 and ROI 6) correspond to the capitis longus muscles (Krmpotić-Nemanić et al., 2006). These muscles are underdeveloped until the onset of postural milestones (Krmpotić-Nemanić et al., 2006; Eggington et al., 2024). Thus, loading from these muscles likely does not play a significant role in the distribution of DA within the pars basilaris.

Developmental factors may contribute to the observed differences in DA (Cunningham & Black, 2009a; 2009b). Cunningham and Black (2009a; 2009b) observed adult-like trabecular patterns in prenatal ilia before the onset of walking and proposed that development may follow a predetermined genetic template. Additionally, variations in isotropy have been observed in the different regions of bones like the immature human talus (Reid et al., 2024), calcaneus (Saers et al., 2020), and the porcine pars basilaris (Sips et al., 2008). As the bone develops outwards from a central ossification centre, the trabeculae are initially laid down in a radiating pattern, leading to a higher degree of anisotropy on the outer regions (Saers et al., 2020). The human pars basilaris also exhibits a radial pattern of ossification (Mackie et al., 2008). Therefore, the radial ossification pattern of the pars basilaris may also contribute to

the differences in DA within the pars basilaris (Mackie et al., 2008; Cunningham & Black, 2009a; 2009b; Saers et al., 2020).

Trabecular separation (TbSp) also contributes to the understanding of the biomechanical requirements of the different regions within the pars basilaris and pars lateralis, as regions with lower TbSp have a denser structure that can better withstand mechanical forces (Bouxsein et al., 2010). The condylar limb (ROI 2) of the pars lateralis exhibited low TbSp and a high BV/TV compared to other ROIs. Likewise, the anterolateral maxima (ROI 1 and ROI 2) of the pars basilaris exhibited low TbSp, indicating a dense trabecular architecture in these regions. Both the condylar limb (ROI 2) and anterolateral maxima (ROI 1 and ROI 2) contribute to the atlanto-occiptial joint (Rhoton, 2000). The dense trabecular network in the condylar limb (ROI 2) and the anterolateral maxima (ROI 1 and ROI 2) likely reflects the need for greater mechanical strength and stability to withstand the forces generated during neck rotation and flexion (Rhoton, 2000). This adaptation in bone architecture suggests a close relationship between trabecular density and the specific biomechanical demands of the regions involved in joint movements.

The spheno-occipital synchondrosis (ROI 7) of the pars basilaris exhibited a unique growth trajectory compared to the rest of the pars basilaris. No significant differences in TbN were observed between the prenatal groups. In addition, the late prenatal spheno-occipital synchondrosis exhibited a significantly lower TbSp compared to the early prenatal group. Thus, suggesting that a dense structure is prioritised in the region. The spheno-occipital synchondrosis (ROI 7) is the interface between the pars basilaris and the sphenoid that allows

for longitudinal growth of the cranial base (Cendekiawan et al., 2010; Hallett et al., 2022). The dense structure of the spheno-occipital-synchondrosis (ROI 7) may contribute to the structural stability of the basicranium while elongation occurs (Cendekiawan et al., 2010). In addition, the dense trabecular structure in this region may be an adaption to resist deformation under the mechanical forces generated during cranial base elongation (Cendekiawan et al., 2010).

4.1.2. Mineralisation and density

Mean grey value (MGV) offers insight into the mineralisation process of the pars basilaris and pars lateralis (Murshed, 2018). The MGV of the pars basilaris and pars lateralis tended to be significantly lower in the late prenatal groups compared to the early prenatal group, seemingly indicating a decrease in BMD during prenatal development. However, as bones grow larger with age, their volume increases, which requires a distribution of minerals (Murshed, 2018). During micro-CT scanning, the densest regions were more attenuating and, therefore, absorbed more X-rays, which is reflected in the higher MGV (Bouxsein et al., 2010; Murshed, 2018). Since the minerals are more dispersed in the late prenatal group, there is less attenuation of X-rays in the bones, which results in a lower MGV (Murshed, 2018). In addition, during rapid bone growth, there is initially a larger proportion of unmineralised osteoid matrix, which is less dense and has a lower mineral content (Bouxsein et al., 2010; Murshed, 2018). Thus, the lower MGV may represent a higher proportion of newly formed, less mineralised bone within the late prenatal pars basilaris and pars lateralis rather than a true decrease in BMD.

The lower MGV coupled with the higher BV/TV in the late prenatal group compared to the early prenatal group suggests that mineral accretion does not occur at the same rate as bone formation during prenatal development. Highly mineralised bone tissue is more rigid and, therefore, less likely to accommodate the morphological shape changes of the bones observed during development (Murshed, 2018; Thornton et al., 2023; 2024). Thus, the delayed mineral accretion may be related to the flexibility required of the bones during development as they rapidly expand to accommodate the brain (Murshed, 2018; Thornton et al., 2023; 2024).

Contrary to the present study's findings, Thornton et al. (2023; 2024) did not observe significant differences in surface BMD between the early and late prenatal pars basilaris and pars lateralis using a similar sample to the present study. Mathematical models suggest that the rate of mineral accretion in bone matrix differs in surface and trabecular bone within the femur (Lerebours et al., 2020). Moreover, animal studies have shown that trabecular elements grow due to the surface apposition of new bone (Mulder et al., 2005; 2006; Sips et al., 2008). Thus, since mineral accretion occurs on the surfaces of the bones, the rate of mineralisation on the surface is likely greater than in the trabecular bone, which could account for the differences observed between Thornton et al. (2023; 2024) and the present study.

4.2. Postnatal development

For the majority of the pars basilaris and pars lateralis, the variables did not significantly differ between the late prenatal and postnatal age groups, which suggests that the trabecular architecture of the pars basilaris and pars lateralis does not change substantially between

birth and seven postnatal months. The transition from the uterine environment may impact the development of the trabeculae post-birth (Land & Schoenau, 2008). Maternal and placental oestrogen is decreased, thus, the bone-promoting factors associated with oestrogen are diminished (Noirrit-Esclassan et al., 2021). In addition, the concentration of calcium provided through lactation is reduced due to the depletion of maternal calcium levels during pregnancy (Land & Schoenau, 2008). Thus, the minerals required for rapid bone formation are depleted compared to the prenatal phase, leading to less pronounced architectural changes.

The trends in trabecular architecture observed between the prenatal and postnatal phases mirror the development of the medulla oblongata (Tate et al., 2015; Dovjak et al., 2020). The prenatal development of the medulla oblongata is characterised by rapid growth and changing proportions, while the postnatal period sees a significant decrease in the rate of growth (Tate et al., 2015; Dovjak et al., 2020). The medulla oblongata is responsible for critical life reflexes such as breathing and, therefore, completes much of its growth prenatally (Tate et al., 2015). Compressive stress from the medulla oblongata may contribute to the modelling of the pars basilaris and pars lateralis by stimulating the activity of osteoclasts during prenatal development (Edamoto et al., 2018). However, as the growth rate of the medulla oblongata slows down postnatally, the reduction in compressive stress may lead to a stabilisation of cranial bone modelling, resulting in the fewer structural changes observed in the pars basilaris and pars lateralis.

In addition, the role of the muscles in the development of the pars basilaris and pars lateralis are likely not apparent in the age range assessed. In the postcranial skeleton, variations in

trabecular architecture are often observed only after the onset of major biomechanical milestones such as walking or crawling (Ryan & Krovitz, 2006; Gosman & Ketcham, 2009; Colombo et al., 2019). Motor milestones that impact the pars basilaris and pars lateralis mostly involve the cervical muscles independently supporting the head on the neck (Scharf et al., 2016; Eggington et al., 2024). The cervical muscles are weak at birth as neonatal infants cannot support their own heads for the first month of life (Scharf et al., 2016; Eggington et al., 2024). The head can be held up independently for very brief periods of time after the first month, and sustained independent control of the head is usually achieved between six and seven months (Scharf et al., 2016; Eggington et al., 2024). The current study assessed postnatal individuals between birth and 7.5 months. Thus, the lack of differences in trabecular architecture may be attributable to the limited mechanical loading and muscle activity in the cervical region during this period.

Despite minimal differences in trabecular architecture observed between the late prenatal and postnatal age groups, there are still variations observed between the ROIs within the postnatal age group that were established in the prenatal pars basilaris and pars lateralis. For example, the anterior and lateral foramen magnum borders (ROI 3 for both the pars basilaris and pars lateralis) had the highest BV/TV and TbTh of all the regions assessed, which contributes to its function of protecting and transmitting neurovasculature (Rhoton, 2000; Oftadeh et al., 2015). Moreover, areas that require greater plasticity to allow for basicranial expansion during brain growth, such as the posteromedial corner (ROI 4) and mastoid temporal border (ROI 7) of the pars lateralis, were observed to have a low BV/TV and many numerous thinner trabeculae which allows for greater flexibility (Cendekiawan et al., 2010;

Lipsett et al., 2023). In addition, the anterolateral maxima (ROI 1 and ROI 2) and lateral angles (ROI 5 and ROI 6), which are the sites of muscle attachment on the pars basilaris, had a relatively high DA, which helps in facilitating more efficient force transmission of the rectus capitis anterior and capitis longus muscles (Krmpotić-Nemanić et al., 2006; Oftadeh et al., 2015). Furthermore, the anterolateral maxima (ROI 1 and ROI 2) of the pars basilaris and condylar limb (ROI 2) of the pars lateralis had relatively low TbSp, which likely contributes to the enhanced stability and strength required for articulation with the atlas (Rhoton, 2000; Oftadeh et al., 2015). The lack of changes between the late prenatal and postnatal age groups suggests that the key structural adaptations of the pars basilaris and pars lateralis are mostly completed by the end of prenatal development, highlighting the importance of prenatal bone development in establishing a foundation for effective mechanical function during the postnatal period.

While the majority of the pars basilaris and pars lateralis did not exhibit significant differences between the late prenatal and postnatal bones, the primary ossification site (ROI 4) and the left lateral angle (ROI 6) of the pars basilaris, as well as the jugular process (ROI 6) of the pars lateralis did show significant differences that highlight the impact of the transition to postnatal life in shaping bone structure during postnatal development. The transition from a mostly uniform to a differential ossification pattern postnatally suggests active bone adaptation is occurring in these select regions (Delteil et al., 2021).

The primary ossification of the pars basilaris (ROI 4) was the only region to show a significant difference in the degree of anisotropy (DA), where the late prenatal group had a significantly

higher DA than the postnatal age group. While changes in DA usually indicate increased or decreased biomechanical stresses in a specific direction, a decrease in DA might also suggest that mechanical loads are becoming more evenly distributed, with the trabeculae orienting to manage stressors from multiple directions (Oftadeh et al., 2015). The decrease in DA at the primary ossification site of the pars basilaris may be due to the need for more balanced mechanical load distribution postnatally (Oftadeh et al., 2015). The primary ossification site of the pars basilaris (ROI 4) is the location of the pharyngeal tubercle, which serves as the insertion site for the pharyngeal raphe and the superior constrictor muscles (Shimada & Gasser, 1987). The pharyngeal raphe and superior constrictor muscles are involved in swallowing (Shimada & Gasser, 1987; Krmpotić-Nemanić et al., 2006). Swallowing of amniotic fluid occurs prenatally, and swallowing for oral feeding occurs postnatally (Delaney & Arvedson, 2008). However, the mechanical demands for prenatal and postnatal swallowing are different, as oral feeding after birth requires the integration and coordination of sucking, swallowing, and breathing (Delaney & Arvedson, 2008). This activity may subject the region to a variety of mechanical stresses, which may contribute to a more even distribution of forces, thus leading to the decreased DA observed in the prenatal age group (Oftadeh et al., 2015).

In addition, the left lateral angle (ROI 6) of the postnatal pars basilaris had a significantly higher TbSp compared to the late prenatal age group. The lateral angles (ROI 5 and ROI 6) correspond to the petro-occipital fissure between the pars basilaris and the petrous part of the temporal bone (Balboni et al., 2005). In the earliest stage of ossification between the pars basilaris and the petrous part of the temporal bone, numerous projections extend into the fissure from

lateral angles (Balboni et al., 2005). The significantly higher TbSp in the postnatal age group may contribute to the modelling process of the bony projections, as a higher TbSp allows for greater flexibility to allow for continued ossification (Balboni et al., 2005). Notably, the right lateral angle (ROI 5) was not observed to significantly differ between the late prenatal and postnatal age groups. The lack of symmetry observed may reflect that the ossification and morphology of the petro-occipital fissure are also often asymmetrical (Balboni et al., 2005)

The jugular process of the pars lateralis (ROI 6) exhibited a unique growth trajectory compared to the other ROIs. The late prenatal jugular process (ROI 6) had significantly fewer trabeculae compared to both the early prenatal group and the postnatal group. This suggests that the number of trabeculae decreased during gestation but increased after birth in this region. The jugular process forms the lateral border of the jugular foramen, which transmits the jugular vein and the glossopharyngeal (cranial nerve IX), vagus (cranial nerve X), and accessory (cranial nerve XI) nerves (Ma et al., 2020; Thornton et al., 2023). It can be hypothesised that compressive stress due to the growth of these structure may result in the modelling of the prenatal jugular process prenatally causing the removal of trabeculae during prenatal development (Edamoto et al., 2018; Ma et al., 2020). In addition, the jugular process (ROI 6) is the attachment site of the rectus capitis lateralis muscle (Murakami et al., 2023). Cervical muscles are generally weak and underdeveloped during the early postnatal phase (Scharf et al., 2016; Eggington et al., 2024). However, the pull of rectus capitis lateralis during development is thought to contribute to the elongation of the jugular process (Murakami et al., 2023). The strain caused from the pull of the rectus capitis lateralis may lead to increased

bone production, through the creation of new trabeculae, thus resulting in a higher TbN in the postnatal age group (Frost, 2003; Robling & Turner, 2009).

4.3. Limitations

The use of cross-sectional data in the present study made it challenging to determine the specific factors contributing to the observed patterns in the pars basilaris and pars lateralis development (Wang & Cheng, 2020). Finite element analysis could be used to model the forces acting on the muscles of the pars basilaris and pars lateralis both in utero and postnatally (Verbruggen et al., 2018). Finite element analysis could help to elucidate the relationship between muscle forces and bone development in these regions (Verbruggen et al., 2018). In addition, the reliance on estimated ages for the individuals in the sample presents and additional limitation (Cunningham et al., 2016). While established methods were used to approximate gestational and postnatal ages, these estimates inherently carry a degree of uncertainty, which may affect the precision of age-related comparisons (Cunningham et al., 2016).

Furthermore, the role of loading from muscles would likely be made more apparent in older infants, who have begun to develop more advanced independent head control and movement (Scharf et al., 2016). Milestones beyond 7.5 months include sitting independently, crawling, pulling to stand, and cruising, which would increase the frequency and magnitude of loads on the cranial base due to greater head and neck movements (Scharf et al., 2016). These movements would place additional stresses on the neck musculature, transmitting forces to the cranial base (Scharf et al., 2016). Future trabecular architecture studies should include

pars basilaris and pars lateralis skeletal elements in individuals older than 7.5 months to elucidate the role of mechanical loading from muscles in the development of the head and neck in the context of these developmental milestones.

The forensic nature of the sample introduces additional limitations. The absence of maternal or fetal clinical histories makes it impossible to control for confounding variables like nutrition, maternal health, and socioeconomic status, all of which can influence bone development (Masztalerz-Kozubek et al., 2021; Thornton et al., 2023; 2024).

4.4. Conclusions

The results of this study suggest that the prenatal stage is a period of rapid trabecular development and modelling to accommodate the growth of the brain and prepare the cranial base for the mechanical requirements of postnatal life (Richards & Jabbour, 2011; Edamoto et al., 2018). However, a delay in mineralisation suggests that the pliability and flexibility of the cranial elements are prioritised. A balance of hormonal, vascular, biomechanical and genetic factors drive the prenatal development of the pars basilaris and pars lateralis. Minimal differences observed between the late prenatal and postnatal age groups suggest that the trabecular architecture established during the prenatal period is relatively stable through to the postnatal phase. This stability suggests that the critical adaptations to mechanical stresses and structural support are largely completed by the end of prenatal development. The transition from a mostly uniform to a differential ossification pattern postnatally suggests active bone adaptation is occurring specific regions of the pars basilaris and pars lateralis (Delteil et al., 2021). Variations in the trabecular architecture within and between the specific

regions of the pars basilaris and pars lateralis reflect the localised functional demands and growth patterns of these cranial elements. Overall, this study underscores the importance of prenatal bone development in establishing a foundation for effective mechanical function during the postnatal period of development.

Chapter 5: References

Abel, R., & Macho, G. A. (2011). Ontogenetic changes in the internal and external morphology of the ilium in modern humans. *Journal of Anatomy*, 218(3), 324-335.

Acquaah, F., Robson Brown, K. A., Ahmed, F., Jeffery, N., & Abel, R. L. (2015). Early trabecular development in human vertebrae: Overproduction, constructive regression, and refinement. *Frontiers in Endocrinology*, 6(67).

Akbareian, S. E., Pitsillides, A. A., Macharia, R. G., & McGonnell, I. M. (2015). Occipital foramina development involves localised regulation of mesenchyme proliferation and is independent of apoptosis. *Journal of Anatomy*, 226(6), 560-574.

Allan, J. (1982). *Learning About Statistics: A Primer in Simple Statistical Methods for Students of the Medical, Biological, Paramedical, Social and Behavioural Sciences* (1st ed.). Johannesburg: Macmillan.

AlQahtani, S., Hector, M., & Liversidge, H. (2010). Brief communication: The London Atlas of human tooth development and eruption. *American Journal of Physical Anthropology*, 142(3), 481-490.

Altafulla, J., Bordes, S., Jenkins, S., Litvack, Z., Iwanaga, J., Loukas, M., & Tubbs, R. S. (2019). The basal subarachnoid cisterns: Surgical and anatomical considerations. *World Neurosurgery*, 129, 190-199.

Badiu, G. A., Tarţa-Arsene, E., Ispas, A. T., Niculae, A., Baciu, A., & Stroică, L. (2019). Estimation of the age from fetal occipital bone. *Revista Romana de Anatomie*, 18(3), 165-168.

Balboni, A. L., Estenson, T. L., Reidenberg, J. S., Bergemann, A. D., & Laitman, J. T. (2005). Assessing age-related ossification of the petro-occipital fissure: Laying the foundation for

understanding the clinicopathologies of the cranial base. *The Anatomical Record*, 282(1), 38-48.

Beltrand, J., Alison, M., Nicolescu, R., Verkauskiene, R., Deghmoun, S., Sibony, O., Sebag, G., & Lévy-Marchal, C. (2008). Bone mineral content at birth is determined both by birth weight and fetal growth pattern. *Pediatric Research*, 64(1), 86-90.

Bernard, S., Loukas, M., Rizk, E., & Oskouian, R. J. (2015). The human occipital bone: Review and update on its embryology and molecular development. *Child's Nervous System*, 31, 2217-2223.

Bouxsein, M., Boyd, S., Christiansen, B., Guldberg, R., Jepsen, K., & Müller, R. (2010). Guidelines for assessment of bone microstructure in rodents using micro-computed tomography. *Journal of Bone and Mineral Research*, 25(7), 1468-1486.

Cardoso, H. F., Gomes, J., Campanacho, V., & Marinho, L. (2013). Age estimation of immature human skeletal remains using the postnatal development of the occipital bone. *International Journal of Legal Medicine*, 127, 997-1004.

Cendekiawan, T., Wong, R. W., & Rabie, A. B. M. (2010). Relationships between cranial base synchondroses and craniofacial development: A review. *The Open Anatomy Journal*, 2, 67-75

Charbonneau, L., Watanabe, K., Chaalala, C., Bojanowski, M. W., Lavigne, P., & Labidi, M. (2024). Anatomy of the craniocervical junction: A review. *Neurochirurgie*, 70(3), 101511.

Colombo, A., Stephens, N. B., Tsegai, Z. J., Bettuzzi, M., Morigi, M. P., Belcastro, M. G., & Hublin, J. J. (2019). Trabecular analysis of the distal radial metaphysis during the acquisition of crawling and bipedal walking in childhood: A preliminary study. *Bulletins et Mémoires de la Société d'Anthropologie de Paris*, 31(1-2), 43.

Coqueugniot, H., & Le Minor, J. M. (2002). Intra-occipital synchondroses closure: Implication for the foramen magnum shape. *Comptes Rendus Palevol*, 1(1), 35-42.

Cunningham, C. A., & Black, S. M. (2009a). Development of the fetal ilium - Challenging concepts of bipedality. *Journal of Anatomy*, 214(1), 91-99.

Cunningham, C. A., & Black, S. M. (2009b). Anticipating bipedalism: Trabecular organization in the newborn ilium. *Journal of Anatomy*, 214(6), 817-829.

Cunningham, C., Scheuer, L., & Black, S. (2016). *Developmental Juvenile Osteology* (2nd ed.). London: Elsevier.

Delaney, A. L., & Arvedson, J. C. (2008). Development of swallowing and feeding: Prenatal through first year of life. *Developmental Disabilities Research Reviews*, 14(2), 105-117.

Delteil, C., Lesieur, E., Tuchtan, L., Alvarez, A. C., Chaumoitre, K., Saliba, B., Adalian, P., & Piercecchi-Marti, M. D. (2021). Study of the growth and shape of the brain and cranial base during the first two years of life. *Morphologie*, 105(348), 45-53.

Di Ieva, A., Bruner, E., Haider, T., Rodella, L. F., Lee, J. M., Cusimano, M. D., & Tschabitscher, M. (2014). Skull base embryology: A multidisciplinary review. *Child's Nervous System*, 30, 991-1000.

Dovjak, G. O., Schmidbauer, V., Brugger, P. C., Gruber, G. M., Diogo, M., Glatter, S., Weber, M., Ulm, B., Prayer, D., & Kasprian, G. J. (2020). Normal human brainstem development in vivo: A quantitative fetal MRI study. *Ultrasound in Obstetrics & Gynecology*, 58(2), 254-263.

du Plessis, A., Broeckhoven, C., Guelpa, A., & le Roux, S. (2017). Laboratory X-ray micro-computed tomography: A user guideline for biological samples. *GigaScience*, 6(6), 1-11.

Dunn, O. J. (1964). Multiple comparisons using rank sums. *Technometrics*, 6(3), 241–252.

Ecarot-Charrier, B., Shepard, N., Charette, G., Grynpas, M., & Glorieux, F. H. (1988). Mineralization in osteoblast cultures: A light and electron microscopic study. *Bone*, 9(3), 147-154.

Edamoto, M., Kuroda, Y., Yoda, M., Kawaai, K., & Matsuo, K. (2018). Trans-pairing between osteoclasts and osteoblasts shapes the cranial base during development. *Scientific reports*, 9(1), 1956.

Eggington, J., Pitt, R., & Hodson, C. (2024). A macroscopic assessment of porosity and new bone formation on the inferior pars basilaris: Normal growth or an indicator of scurvy? *International Journal of Paleopathology*, 45, 62-72.

Emecen, A. N., Ertekin, R., Baysal, B., Arslan, F., & Vahaboglu, H. (2019). Clival defect in the pathogenesis of recurrent meningitis: A case report and literature review. *Egyptian Journal of Neurosurgery*, 34, 36.

Fazekas, I. G., & Kosa, F. (1978). *Forensic Fetal Osteology*. Budapest: Akadémiai Kiadó.

Fiester, P., Rao, D., Soule, E., Orallo, P., & Rahmathulla, G. (2021). Anatomic, functional, and radiographic review of the ligaments of the craniocervical junction. *Journal of the Craniovertebral Junction & Spine*, 12(1), 4-9.

Figueiro, G., Olivares, I. J., & Aguilera, A. I. (2022). Age estimation in infant skeletal remains by measurements of the pars lateralis. *International Journal of Legal Medicine*, 136(6), 1675-1684.

Figus, C., Stephens, N. B., Sorrentino, R., Bortolini, E., Arrighi, S., Higgins, O. A., Lugli, F., Marciani, G., Oxilia, G., Romandini, M., Silvestrini, S., Baruffaldi, F., Belcastro, M. G., Bernardini,

F., Festa, A., Hajdu, T., Mateovics-László, O., Pap, I., & Szeniczey, T. (2022). Morphologies in-between: The impact of the first steps on the human talus. *The Anatomical Record*, 306(1), 124-142.

Filipowska, J., Tomaszewski, K. A., Niedźwiedzki, Ł., Walocha, J. A., & Niedźwiedzki, T. (2017). The role of vasculature in bone development, regeneration and proper systemic functioning. *Angiogenesis*, 20(3), 291-302.

Flynn, W. P., Ntuli, Y., Zhang, H., & Tiberi, S. (2021). A case of clival tuberculosis and associated meningitis. *Journal of Clinical Tuberculosis and Other Mycobacterial Diseases*, 25, 100273.

Fournier, S. B., D'Errico, J. N., & Stapleton, P. A. (2021). Uterine vascular control preconception and during pregnancy. *Comprehensive Physiology*, 11(3), 1871–1893.

Frost, H. M. (1987). Bone “mass” and the “mechanostat”: A proposal. *The Anatomical Record*, 219(1), 1-9.

Frost, H. M. (1990). Skeletal structural adaptations to mechanical usage (SATMU): 2. Redefining Wolff's law: The remodeling problem. *Anatomical Record*, 226(4), 414-422

Frost, H. M. (2003). Bone's mechanostat: a 2003 update. *The Anatomical Record*, 275(2), 1081-1101.

Frost, H. M. (2004). A 2003 update of bone physiology and Wolff's Law for clinicians. *The Angle Orthodontist*, 74(1), 3-15.

Gkiatas, I., Lykissas, M., Kostas-Agnantis, I., Korompilias, A., Batistatou, A., & Beris, A. (2015). Factors affecting bone growth. *American Journal of Orthopaedics*, 44(2), 61-67.

Gosman, J. H., & Ketcham, R. A. (2009). Patterns in ontogeny of human trabecular bone from SunWatch Village in the prehistoric Ohio Valley: General features of microarchitectural change. *American Journal of Physical Anthropology*, 138(3), 318-332.

Grzonkowska, M., Baumgart, M., Badura, M., Wiśniewski, M., Lisiecki, J., & Szpinda, M. (2021). Quantitative anatomy of primary ossification centres of the lateral and basilar parts of the occipital bone in the human foetus. *Folia Morphologica*, 80(4), 895-903.

Hallett, S. A., Ono, W., Franceschi, R. T., & Ono, N. (2022). Cranial base synchondrosis: Chondrocytes at the hub. *International Journal of Molecular Sciences*, 23(14), 7817.

Henze, N., & Zirkler, B. (1990). A class of invariant consistent tests for multivariate normality. *Communications in Statistics: Theory and Methods*, 19(10), 3595-3617.

Hutchinson, E. F., Farella, M., Hoffman, J., & Kramer, B. (2017). Variations in bone density across the body of the immature human mandible. *Journal of Anatomy*, 230(5), 679-688.

Jeffery, N. (2003). Brain expansion and comparative prenatal ontogeny of the non-hominoid primate cranial base. *Journal of Human Evolution*, 45(4), 263-284.

Jeffery, N. (2005). Cranial base angulation and growth of the human fetal pharynx. *The Anatomical Record*, 284(1), 491-499.

Kaur, G., Kumari, G., & Sharma, S. (2021). Functional matrix hypothesis: A review of literature. *Surface Plasmon Resonance*, 1(2), 33-42.

Kavitha, S., & Anand, A. (2013). A study of the condylar canal and its incidence, morphology and clinical significance. *International Journal of Current Research and Review*, 5(2), 66.

Kennedy, E., Albert, M., & Nicholson, H. (2017). Do longus capitis and colli really stabilise the cervical spine? A study of their fascicular anatomy and peak force capabilities. *Musculoskeletal Science and Practice*, 32, 104-113.

Kivell, T. L. (2016). A review of trabecular bone functional adaptation: What have we learned from trabecular analyses in extant hominoids and what can we apply to fossils? *Journal of Anatomy*, 228(4), 569-594.

Kovacs, C. S. (2014). Bone development and mineral homeostasis in the fetus and neonate: roles of the calciotropic and phosphotropic hormones. *Physiological Reviews*, 94(4), 1143-1218.

Kranioti, E. F., Rosas, A., García-Vargas, S., Estalrrich, A., Bastir, M., & Peña-melián, Á. (2009). Remodeling patterns of occipital growth: A preliminary report. *The Anatomical Record*, 292(11), 1764-1770.

Krmpotić-Nemanić, J., Vinter, I., Ehrenfreund, T., & Marušić, A. (2006). Age-related changes in the anatomical landmarks of the osseous epipharynx. *Annals of Anatomy*, 188(5), 459-467.

Land, C., & Schoenau, E. (2008). Fetal and postnatal bone development: Reviewing the role of mechanical stimuli and nutrition. *Best Practice & Research Clinical Endocrinology & Metabolism*, 22(1), 107-118.

Lerebours, C., Weinkamer, R., Roschger, A., & Buenzli, P. R. (2020). Mineral density differences between femoral cortical bone and trabecular bone are not explained by turnover rate alone. *Bone Reports*, 13, 100731.

Lieberman, D. E., Pearson, O. M., & Mowbray, K. M. (2000). Basicranial influence on overall cranial shape. *Journal of Human Evolution*, 38(2), 291-315.

Lipsett, B. J., Reddy, V., & Steanson, K. (2023). *Anatomy, Head and Neck: Fontanelles*. Treasure Island (FL): StatPearls

Ma, S. C., Liu, S., Agazzi, S., & Jia, W. (2020). The jugular process: A key anatomical landmark for approaches to the jugular foramen. *World Neurosurgery*, 135, e686-e694.

Mackie, E. J., Ahmed, Y. A., Tatarczuch, L., Chen, K. S., & Mirams, M. (2008). Endochondral ossification: How cartilage is converted into bone in the developing skeleton. *The International Journal of Biochemistry & Cell Biology*, 40(1), 46-62.

Maclean, S. J., Black, S. M., & Cunningham, C. A. (2014). The developing juvenile ischium: Macro-radiographic insights. *Clinical Anatomy*, 27(6), 906-914.

Malakhov, S., Shmarhalov, A., El Falougy, H., Lukacikova, P., Polovinshchykov, A., El Hassoun, O., & Polak, S. (2024). Canalis basilaris medianus: An anatomical study. *Translational Research in Anatomy* (37), 100345.

Masztalerz-Kozubek, D., Zielinska-Pukos, M. A., & Hamulka, J. (2021). Maternal diet, nutritional status, and birth-related factors influencing offspring's bone mineral density: a narrative review of observational, cohort, and randomized controlled trials. *Nutrients*, 13(7), 2302.

Menezes, A. H. (1997). Craniovertebral junction anomalies: Diagnosis and management. *Seminars in Pediatric Neurology*, 4(3), 209-223.

Migliaccio, S. I., Newbold, R. R., Bullock, B. C., Jefferson, W. J., Sutton, F. G., McLachlan, J. A., & Korach, K. S. (1996). Alterations of maternal estrogen levels during gestation affect the skeleton of female offspring. *Endocrinology*, 137(5), 2118-2125.

Moss, M. L. (1962). The functional matrix. *Vistas in Orthodontics*. 1, 85-98

Mowbray, K. (2005). Surface bone histology of the occipital bone in humans and chimpanzees. *The Anatomical Record*, 283(1), 14-22.

Muhleman, M., Charran, O., Matusz, P., Shoja, M. M., Tubbs, R. S., & Loukas, M. (2012). The proatlas: A comprehensive review with clinical implications. *Child's Nervous System*, 28, 349-356.

Mulder, L., Koolstra, J. H., de Jonge, H. W., & van Eijden, T. M. (2006). Architecture and mineralization of developing cortical and trabecular bone of the mandible. *Anatomy and Embryology*, 211, 71-78.

Mulder, L., Koolstra, J. H., Weijs, W. A., & Van Eijden, T. M. (2005). Architecture and mineralization of developing trabecular bone in the pig mandibular condyle. *The Anatomical Record*, 285(1), 659-666.

Müller, F., & O'Rahilly, R. (1994). Occipitocervical segmentation in staged human embryos. *Journal of Anatomy*, 185(Pt 2), 251.

Müller, F., & O'Rahilly, R. (2003). Segmentation in staged human embryos: The occipitocervical region revisited. *Journal of Anatomy*, 203(3), 297-315.

Murakami, G., Cho, K. H., Kitamura, K., Rodríguez-Vázquez, J. F., & Sato, T. (2023). Rectus capitis lateralis muscle revisited: A histological study using human fetuses. *Surgical and Radiologic Anatomy*, 45(11), 1483-1491.

Murshed, M. (2018). Mechanism of bone mineralization. *Cold Spring Harbor Perspectives in Medicine*, 8(12), a031229.

Nagaoka, T., Kawakubo, Y., & Hirata, K. (2012). Estimation of fetal age at death from the basilar part of the occipital bone. *International Journal of Legal Medicine*, 126, 703-711.

Nemzek, W. R., Brodie, H. A., Hecht, S. T., Chong, B. W., Babcook, C. J., & Seibert, J. A. (2000). MR, CT, and plain film imaging of the developing skull base in fetal specimens. *American Journal of Neuroradiology*, 21(9), 1699-1706.

Nie, X. (2005). Cranial base in craniofacial development: Developmental features, influence on facial growth, anomaly, and molecular basis. *Acta Odontologica Scandinavica*, 63(3), 127-135.

Niel, M., Chaumoître, K., Corny, J., Lalys, L., & Adalian, P. (2019). Maturation of the human foetal basioccipital: Quantifying shape changes in second and third trimesters using elliptic Fourier analysis. *Journal of Anatomy*, 235(1), 34-44.

Noirrit-Esclassan, E., Valera, M. C., Tremollieres, F., Arnal, J. F., Lenfant, F., Fontaine, C., & Vinel, A. (2021). Critical role of estrogens on bone homeostasis in both male and female: from physiology to medical implications. *International Journal of Molecular Sciences*, 22(4), 1568.

Nuzzo, S., Meneghini, C., Braillon, P., Bouvier, R., Mobilio, S., & Peyrin, F. (2003). Microarchitectural and physical changes during fetal growth in human vertebral bone. *Journal of Bone and Mineral Research*, 18(4), 760-768.

Oftadeh, R., Perez-Viloria, M., Villa-Camacho, J. C., Vaziri, A., & Nazarian, A. (2015). Biomechanics and mechanobiology of trabecular bone: A review. *Journal of Biomechanical Engineering*, 137(1), 0108021–01080215.

Olivares, I. J., & Aguilera, A. I. (2017). Proposal of new regression formulae for the estimation of age in infant skeletal remains from the metric study of the pars basilaris. *International Journal of Legal Medicine*, 131, 781-788.

Pang, D., & Thompson, D. N. (2011). Embryology and bony malformations of the craniovertebral junction. *Child's Nervous System*, 27, 523-564.

Rai, R., Iwanaga, J., Shokouhi, G., Loukas, M., Mortazavi, M. M., Oskouian, R. J., & Tubbs, R. S. (2018). A comprehensive review of the clivus: Anatomy, embryology, variants, pathology, and surgical approaches. *Child's Nervous System*, 34, 1451-1458.

Redfield, A. (1970). A new aid to aging immature skeletons: Development of the occipital bone. *American Journal of Physical Anthropology*, 33(2), 207-220.

Reid, R. A., Davies, C., & Cunningham, C. (2023). The developing juvenile distal tibia: Radiographic identification of distinct ontogenetic phases and structural trajectories. *Journal of Anatomy*, 242(2), 191-212.

Reid, R. A., Davies, C., & Cunningham, C. (2024). The developing juvenile talus: Radiographic identification of distinct ontogenetic phases and structural trajectories. *Journal of Anatomy*, 244(1), 75-95.

Reissis, D., & Abel, R. L. (2012). Development of fetal trabecular micro-architecture in the humerus and femur. *Journal of Anatomy*, 220(5), 496-503.

Rhoton, A. L. (2000). The Foramen Magnum. *Neurosurgery*, 47(3), S155-S193.

Richards, G. D., & Jabbour, R. S. (2011). Foramen magnum ontogeny in Homo sapiens: A functional matrix perspective. *The Anatomical Record*, 294(2), 199-216.

Robling, A. G., & Turner, C. H. (2009). Mechanical signaling for bone modeling and remodeling. *Critical Reviews in Eukaryotic Gene Expression*, 19(4).

Rubinstein, D., Burton, B. S., & Walker, A. L. (1995). The anatomy of the inferior petrosal sinus, glossopharyngeal nerve, vagus nerve, and accessory nerve in the jugular foramen. *American Journal of Neuroradiology*, 16(1), 185-194.

Ryan, T. M., & Krovitz, G. E. (2006). Trabecular bone ontogeny in the human proximal femur. *Journal of Human Evolution*, 51(6), 591-602.

Saers, J. P., Ryan, T. M., & Stock, J. T. (2020). Baby steps towards linking calcaneal trabecular bone ontogeny and the development of bipedal human gait. *Journal of Anatomy*, 236(3), 474-492.

Salle, B. L., Rauch, F., Travers, R., Bouvier, R., & Glorieux, F. H. (2002). Human fetal bone development: Histomorphometric evaluation of the proximal femoral metaphysis. *Bone*, 30(6), 823-828.

Schaefer, M., Black, S., & Scheuer, L. (2009). *Juvenile Osteology: A Lab and Field Manual*. San Diego: Academic Press.

Scharf, R. J., Scharf, G. J., & Stroustrup, A. (2016). Developmental milestones. *Pediatrics in Review*, 37(1), 25-38.

Scheuer, L., & MacLaughlin-Black, S. (1994). Age estimation from the pars basilaris of the fetal and juvenile occipital bone. *International Journal of Osteoarchaeology*, 4(4), 377-380.

Shimada, K., & Gasser, R. F. (1987). Variations of the pharyngeal raphe. *Clinical Anatomy*, 1(4), 285-294.

Singh, R., Thorwarth, R. M., Bendok, B. R., Rath, T. J., Bhuskute, A. A., Gnagi, S. H., & Lal, D. (2022). Association of meningitis and clival canal defect: Case illustration, management, and systematic review of the literature. *Journal of Neurosurgery. Pediatrics*, 29(4), 379-386.

Sips, R. J., Mulder, L., Koolstra, J. H., & van Eijden, T. M. (2008). Development of the micro architecture and mineralization of the basilar part of the pig occipital bone. *Connective Tissue Research*, 49(1), 22-29.

Smith, D. E., Humphrey, L. T., & Cardoso, H. F. (2021). Age estimation of immature human skeletal remains from mandibular and cranial bone dimensions in the postnatal period. *Forensic Science International*, 327, 110943.

Smith, W. L., Pękala, P. A., Iwanaga, J., Loukas, M., Dumont, A. S., Walocha, J., & Tubbs, R. S. (2022). The forgotten intermediate condylar canal: Anatomic study with application to skull base surgery. *World Neurosurgery*, 161, 75-79.

South Africa. (1977). *Criminal Procedure Act No. 57 of 1977, section 239*. [Accessed: 04.04.23]. Available: https://www.justice.gov.za/legislation/acts/1977-051.pdf

South Africa. (1992). *Births and Deaths Registration Act No. 51 of 1992, section 12*. [Accessed: 4.04.23]. Available: https://www.gov.za/sites/default/files/gcis_document/201409/a511992.pdf

South Africa. (2003). *National Health Act No. 61 of 2003, section 64*. [Accessed: 4.04.23]. Available: https://www.gov.za/sites/default/files/gcis_document/201409/a61-03.pdf

Swan, A. K., & Dunn, R. N. (2019). 'Out with the old and in with the new'- a retrospective review of paediatric craniocervical junction fixation: Indications, techniques and outcomes. *South African Orthopaedic Journal*, 18(4), 28-34.

Tate, M. C., Lindquist, R. A., Nguyen, T., Sanai, N., Barkovich, A. J., Huang, E. J., Rowitch, D. H., & Alvarez-Buylla, A. (2015). Postnatal growth of the human pons: A morphometric and immunohistochemical analysis. *Journal of Comparative Neurology*, 523(3), 449-462.

Thornton, R. (2018). *Towards a biological profile for South African perinatal remains: Osteological and genetic perspectives*. PhD thesis. Rhodes University: Grahamstown.

Thornton, R., Edkins, A. L., & Hutchinson, E. F. (2020). Contributions of the pars lateralis, pars basilaris and femur to age estimations of the immature skeleton within a South African forensic setting. *International Journal of Legal Medicine*, 134(3), 11.

Thornton, R., Mendelow, M. G., & Hutchinson, E. F. (2023). Assessing the morphology and bone mineral density of the immature pars lateralis as an indicator of age. *International Journal of Legal Medicine*, 138(2), 467-486.

Thornton, R., Mendelow, M. G., & Hutchinson, E. F. (2024). Bone mineral density and geometric morphometrics: Indicators of growth in the immature pars basilaris. *Forensic Science International*, 361(112111).

Tocheri, M. W., & Molto, J. E. (2002). Aging fetal and juvenile skeletons from roman period Egypt using basiocciput osteometrics. *International Journal of Osteoarchaeology*, 12(5), 356-363.

Tubbs, R. S., Hansasuta, A., Loukas, M., Louis, R. G., Shoja, M. M., Salter, E. G., & Oakes, W. J. (2007b). The basilar venous plexus. *Clinical Anatomy*, 20(7), 755-759.

Tubbs, R. S., Kelly, D. R., Humphrey, E. R., Chua, G. D., Shoja, M. M., Salter, E. G., Acakpo-Satchivi, L., Wellons, J. C., Blount, J. P., & Oakes, W. J. (2007a). The tectorial membrane: Anatomical, biomechanical, and histological analysis. *Clinical Anatomy*, 20(4), 382–386.

Tuli, A., Mangal, A., Dixit, S. G., Choudhry, R., & Sanghwan, S. (2008). Incidence, morphology and clinical relevance of bony canals and vascular grooves in the paracondylar region of adult human skulls. *Journal of Clinical Neuroscience*, 15(6), 689-692.

Verbruggen, S. W., Kainz, B., Shelmerdine, S. C., Hajnal, J. V., Rutherford, M. A., Arthurs, O. J., Phillips, A. T., & Nowlan, N. C. (2018). Stresses and strains on the human fetal skeleton during development. *Journal of the Royal Society, Interface*, 15(138), 20170593.

Volume Graphics GmbH. (2013). *VGstudio Max: Reference Manual*. Heidelberg: Volume Graphics GmbH

Walzer, S. M., Cetin, E., Grübl-Barabas, R., Sulzbacher, I., Rueger, B., Girsch, W., Toegel, S., Windhager, R., & Fischer, M. B. (2014). Vascularization of primary and secondary ossification centres in the human growth plate. *BMC Developmental Biology*, 14, 1-12.

Wang, X., & Cheng, Z. (2020). Cross-sectional studies: Strengths, weaknesses, and recommendations. *Chest*, 158(1), S65-S71.

Weiss-Bilka, H. E., Brill, J. A., & Ravosa, M. J. (2018). Non-sutural basicranium-derived cells undergo a unique mineralization pathway via a cartilage intermediate in vitro. *PeerJ*, 6, e5757.

Wickham, H. (2016). *ggplot2: Elegant Graphics for Data Analysis*. New York: Springer-Verlag.

Wiles, C. C., Suh, S. H., Brown, K. R., & Abel, R. L. (2024). The ontogeny of human fetal trabecular bone architecture occurs in a limb-specific manner. *Nature*, 14 (1), 1-13.

Wolff, J. (1892). *The law of bone transformation*. Berlin: Hirschwald.

Wysocki, J., Kobryń, H., Bubrowski, M., Kwiatkowski, J., Reymond, J., & Skarżyńska, B. (2004). The morphology of the hypoglossal canal and its size in relation to skull capacity in man and other mammal species. *Folia Morphologica*, 63(1), 11-17.

Zdilla, M. J. (2017). Clival canal and clival foramen development in the fetal and infant basioccipital. *Child's Nervous System*, 33(7), 1209-1216.

Zdilla, M. J., Pancake, J. P., Russell, M. L., & Koons, A. W. (2022). Ontogeny of the human fetal, neonatal, and infantile basioccipital bone: Traditional and extended eigenshape geometric morphometric analysis. *The Anatomical Record*, 305(11), 3230-3242.

Appendix A: Ethics certificate

UNIVERSITY OF THE WITWATERSRAND, JOHANNESBURG	HUMAN RESEARCH ETHICS COMMITTEE (MEDICAL)

Office of the Deputy Vice-Chancellor (Research and Innovation)

TO: Ms M Mendelow
School of Anatomical Sciences
Medical School
University

E-mail: 1847379@students.wits.ac.za

CC: Supervisor: Drs E Hutchinson and R Thornton
Erin.Hutchinson@wits.ac.za
and <HREC-Medical Research Office@wits.ac.za>

FROM: Mr Iain Burns
Human Research Ethics Committee (Medical)
Tel: 011 717 1252

E-mail: Iain.Burns@wits.ac.za

DATE: 21 December 2023

REF: R14/49

PROTOCOL NO: **M230943** (This is your ethics application reference number. Please quote it in all enquiries, oral or written, relating to this study.)

PROJECT TITLE: *Assessing changes in internal bone architecture of the immature human pars basilaris and pars lateralis, during the pre-natal and post-natal stages of growth*

Please find attached the Clearance Certificate for the above project. I hope it goes well and that an article in a recognized publication comes out of it. This will reflect well on your professional standing and contribute to Government funding of the University.

MSWorks2000/Iain0007/Clearscan.wps

UNIVERSITY OF THE WITWATERSRAND, JOHANNESBURG

R49 Ms M Mendelow

HUMAN RESEARCH ETHICS COMMITTEE (MEDICAL)
CLEARANCE CERTIFICATE NO. M230943

NAME: Ms M Mendelow **DEGREE:** MSc (Med)
(Principal and Co-Investigators)

DEPARTMENT: School of Anatomical Sciences
Medical School
University

PROJECT TITLE: *Assessing changes in internal bone architecture of the immature human pars basilaris and pars lateralis, during the pre-natal and post-natal stages of growth*

DATE CONSIDERED: 29 September 2023

DECISION: Approved unconditionally

CONDITIONS:

NOTE: If contact information regarding student study participants is required, please contact the Registrar's office <Nicoleen.Potgieter@wits.ac.za>

SUPERVISOR: Drs E Hutchinson and R Thornton

APPROVED BY:
Ms M van Niekerk, Co-Chairperson, HREC (Medical)

DATE OF APPROVAL: 21 December 2023 **EXPIRY DATE:** 20 December 2028

This Clearance Certificate is valid for 5 years from the date of approval. An extension may be applied for.

DECLARATION OF INVESTIGATORS

To be completed in duplicate and **ONE COPY** returned to the Research Office secretariat on the 3rd floor, Phillip Tobias Building, Parktown, University of the Witwatersrand, Johannesburg.

I/we fully understand the conditions under which I am/we are authorized to carry out the above-mentioned research and I/we undertake to ensure compliance with these conditions. Should any departure be contemplated from the research protocol as approved, I/we undertake to submit details to the Committee. **I agree to submit a yearly progress report** in the format available at https://wits.ac.za/research/researcher-support/research-ethics/ethics-committees/. This report is due annually, for the duration of the Clearance Certificate, beginning on the first anniversary of Date of Approval above. Unreported changes to the study may invalidate the clearance given by the HREC (Medical).

Signature of Principal Investigator

15/01/2024
Date

Appendix B: Observer error

Pars basilaris observer error results of the Lin's concordance test

Intra-observer error						
ROI	BV/TV	BS/BV	TbTh	TbN	TbSp	MGV
1	0.9471411	0.9179037	0.9480690	0.9167558	0.9093014	0.9945332
2	0.9283441	0.9371784	0.9068173	0.9282681	0.8926474	0.9970755
3	0.9538064	0.9253952	0.9757309	0.9525901	0.9513861	0.9997554
4	0.8894093	0.8496056	0.7963911	0.9578666	0.8807443	0.9975568
5	0.9856227	0.9488436	0.7640349	0.9126759	0.8301875	0.9946665
6	0.9793567	0.9362338	0.8960925	0.9207425	0.9407945	0.9966648
7	0.9757803	0.9033531	0.8683548	0.8466598	0.8661396	0.9976477
Inter-observer error						
ROI	BV/TV	BS/BV	TbTh	TbN	TbSp	MGV
1	0.8919718	0.9339013	0.8263947	0.9161837	0.8519012	0.9940432
2	0.8658444	0.9015306	0.8125976	0.9115374	0.9007391	0.9940855
3	0.8662275	0.9095658	0.9144314	0.9027499	0.6996374	0.9994654
4	0.8832131	0.8929881	0.8555821	0.9039237	0.7425201	0.9975678
5	0.9771246	0.9286075	0.7522163	0.8892746	0.8800234	0.9945895
6	0.8856760	0.8928641	0.8410015	0.8740211	0.7782458	0.9945768
7	0.9826944	0.8637588	0.8649563	0.9057514	0.9419021	0.9976174

Pars basilaris regions of interest: (ROI 1): right anterolateral maxima of the foramen magnum. (ROI 2): left anterolateral maxima of the foramen magnum. (ROI 3): anterior foramen magnum border. (ROI 4): primary ossification site. (ROI 5): right lateral angle. (ROI 6): left lateral angle. (ROI 7): spheno-occipital synchondrosis. Variables assessed included bone volume fraction (BV/TV), bone surface area fraction (BS/BV), trabecular thickness (TbTh), trabecular number (TbN), trabecular separation (TbSp) and mean grey value (MGV)

Pars lateralis observer error results of the Lin's concordance test

Intra-observer error						
ROI	BV/TV	BS/BV	TbTh	TbN	TbSp	MGV
1	0.9193031	0.8220124	0.8914134	0.8062555	0.8781157	0.9952431
2	0.7489606	0.7158823	0.7322466	0.6994366	0.7535885	0.9968724
3	0.9121879	0.8830097	0.9465148	0.8655764	0.7822343	0.9989246
4	0.9848643	0.9803664	0.9785061	0.9971471	0.9932018	0.9973185
5	0.8263102	0.8703718	0.8045878	0.9217682	0.7656813	0.9957812
6	0.9281189	0.8477578	0.8127008	0.9268822	0.8858376	0.9964399
7	0.9100377	0.8276657	0.8333025	0.9717171	0.9692923	0.9952431
Interobserver error						
ROI	BV/TV	BS/BV	TbTh	TbN	TbSp	MGV
1	0.9666696	0.9029479	0.9046412	0.9592039	0.9518552	0.9948123
2	0.9668112	0.9273482	0.9442355	0.9493312	0.9243972	0.9965017
3	0.9393384	0.9630559	0.9367813	0.9536811	0.7254904	0.9991348
4	0.9699912	0.9314002	0.8787641	0.8614544	0.8118399	0.9977294
5	0.9550365	0.9640569	0.9590811	0.9028772	0.9023918	0.9956082
6	0.8711413	0.8468075	0.7128522	0.8141030	0.7746483	0.9969831
7	0.9821089	0.8346798	0.9101721	0.8967364	0.8952472	0.9982215

Pars lateralis regions of interest: (ROI 1): jugular limb. (ROI 2): condylar limb. (ROI 3): lateral foramen magnum border. (ROI 4): posteromedial corner. (ROI 5): primary ossification site. (ROI 6): jugular process. (ROI 7): mastoid temporal border. Variables assessed included bone volume fraction (BV/TV), bone surface area fraction (BS/BV), trabecular thickness (TbTh), trabecular number (TbN), trabecular separation (TbSp) and mean grey value (MGV)

Appendix C: AI Statement

Wits University Faculty of Science post-graduate student AI declaration

I understand that the use of generative AI tools (such as ChatGPT or similar) without explicitly declaring such use constitutes a form of plagiarism and is classified by Wits University as academic misconduct.

I declare that in the course of conducting the research towards my degree or in the preparation of this thesis/dissertation/research report (select one by marking with an X):

I **did not** make use of generative AI tools ☐

I **did** make use of generative AI tools for the following (tick all that apply):

1. Idea Generation (research problem/design, hypothesis)	
2. Sourcing Related Work (summarising, identifying sources)	x
3. Methods and Experiment Design (experiment setup, model tuning)	
4. Data Analysis (presentation, coding, interpretation)	x
5. Theoretical Development (theorem proving, conceptual analysis)	
6. Code Development (generating algorithms, writing scripts)	
7. Presentation (rendering graphics, formatting)	
8. Editing (grammar, readability)	x
9. Writing (text generation, document structuring)	
10. Citation Formatting (structuring, organising)	

If other uses were involved, please specify below:

Generative AI tool used (list all)	**Used for?**
Notebooklm	Sourcing Related Work (summarising, identifying sources)
ChatGPT	Data Analysis (coding)
Grammarly	Editing (grammar, readability)

If generative AI tools were used as an integral part of the experimental design or in the direct execution of my research, I confirm that details of this use are clearly outlined in the relevant experimental/methodology chapters of my thesis/dissertation/research report.

Student number: 1847379

Candidate signature:



Appendix D: Turnitin report

MMendelow_masterssubmission_02.03.2025.docx

ORIGINALITY REPORT

25%	21%	19%	5%
SIMILARITY INDEX	INTERNET SOURCES	PUBLICATIONS	STUDENT PAPERS

PRIMARY SOURCES

1	hdl.handle.net Internet Source	3%
2	wiredspace.wits.ac.za Internet Source	2%
3	www.ncbi.nlm.nih.gov Internet Source	2%
4	discovery.dundee.ac.uk Internet Source	1%
5	Roxanne Thornton, A. L. Edkins, E. F. Hutchinson. "Contributions of the pars lateralis, pars basilaris and femur to age estimations of the immature skeleton within a South African forensic setting", International Journal of Legal Medicine, 2019 Publication	1%
6	Roxanne Thornton, Mira G. Mendelow, Erin F. Hutchinson. "Bone mineral density and geometric morphometrics: Indicators of growth in the immature pars basilaris", Forensic Science International, 2024	1%